1. LITERATURE REVIEW & AIMS

1.1. Metallic Nanoparticles

One of the most widely reseached areas in the field of nanotechnology is that of nanoparticles, due to the broad range of unique and useful properties that they possess. Metallic nanoparticles have been of particular interest owing to these particles having the widest range of available properties.

1.1.1. Basic Principles

Perhaps the most important attribute of metallic nanoparticles that gives rise to their unique properties is the fact that these nanoparticles effectively span the size regime between bulk materials and atomic or molecular structures, which results in the emergence of properties due to quantum mechanical effects [1].

Electronic Properties

One prominent example of this is the effect of nanoparticle dimensions upon the electronic structure, which can best be described by first considering the case of a free electron. A free electron is defined as an electron that is not bound or affected by any external potential. As such, these electrons can have any value of energy. However, if an electron is bound to an atomic nucleus, it can only possess discrete energies due to confinement of the electron wavefunction within the potential well of the positively charged nucleus. [2]

Now, consider a situation where two metal atoms, such as lithium, combine via the exchange of their $2s^1$ electrons to form a diatomic species. The electronic structure of the resulting dilithium species in its ground state (at 0K), as determined by molecular orbital theory, consists of a doubly occupied molecular bonding orbital, σ, and an unoccupied anti-bonding orbital, σ^*

(figure 1.1a). In principle, this idea can be extended to larger numbers of bound atoms, such as a cluster of 6 lithium atoms (fig 1.1b). As more and more atoms are bound together, new non-degenerate energy levels become available for the electrons to occupy. Furthermore, these energy levels differ in energy by concurrently smaller values, as the electrons are increasingly less confined. If this process is repeated until a near infinite number of atoms have been bound together (as is the case for a bulk solid), then the spacing between energy levels is so infinitesimally small that there is now effectively a *band* of allowed electron energies, half originating from the bonding molecular orbitals and the other half from the anti-bonding orbitals (fig 1.1c). [1-2]

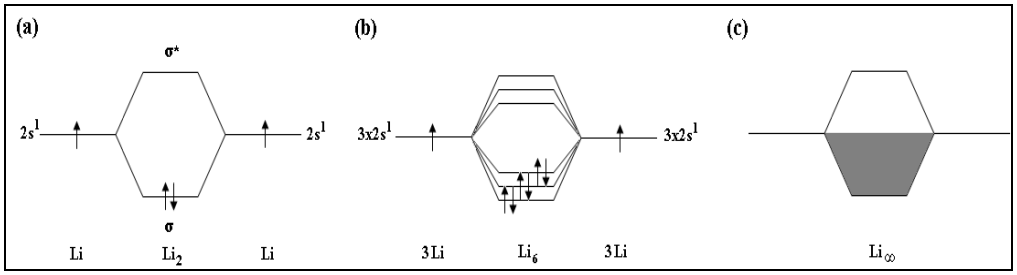

Fig 1.1: Diagram showing the electronic structure of (a) diatomic lithium (b) a cluster of 6 lithium atoms and (c) bulk lithium.

In the case of lithium at 0K, the lower half of this band is occupied by electrons (known as the valence band), with the highest occupied electron energy known as the fermi energy. Electrons at this energy are very weakly bound to the atomic nuclei that make up the bulk metal, such that the gain of a very small amount of energy is sufficient to promote these electrons into the unoccupied part of the band (known as the conduction band). Electrons at these energies are considered to act as essentially free electrons (within the confines of the material), and give rise to electrical conductivity i.e. application of an electric field across the material will incite movement of these electrons. Note that this model is not limited exclusively to lithium, but can be applied to all metals with partially filled bands. In cases where the entire band is filled with electrons, conductivity can only occur if electrons can be promoted to an unoccupied higher energy band. Typically, different bands are separated by an energy known as the band gap energy, and when

this energy barrier is significant, electrical conduction cannot easily occur (and the material acts as an insulator) [1-2]

In the case of a metallic nanoparticle, the number of constituent atoms is much smaller than that of the bulk, such that there begins to be a departure from the bulk band structure towards quantised energy levels (as in fig 1.1b). In this situation, the amount of energy required to promote an electron from the fermi level to an unoccupied energy level is no longer necessarily trivial. The energy level spacing, known as the kubo gap, is given by the following equation:

$$\delta = \frac{4E_f}{3n}$$

where n is the number of nanoparticle valence electrons and E_f is the fermi energy. [3] If the thermal energy (k_bT) available to promote electrons at the fermi level to unoccupied conduction levels is smaller than the kubo gap, then electron conduction cannot occur, and the metal becomes an insulator. Furthermore, this metal-insulator transition is size dependant, as smaller nanoparticles will obviously consist of fewer atoms (and hence valence electrons) than much larger nanoparticles of the same composition, and therefore have larger kubo gaps.

Interestingly, the kubo gap for electrons in a nanoparticle is not only affected by the total number of constituent atoms, but also by the dimensionality of the nanoparticle. Confinement of the valence electrons in one or more dimensions results in increased kubo gaps in those spatial axes, while the bulk band structure remains for the unconfined dimensions. This can be represented by a density of states diagram, which depicts the number of available electron states at different energies (figure 1.2). [1] As can be seen, particles with no confinement in any dimension (a) and confinement in all three dimensions (d) yield density of states diagrams showing a continuous band structure and quantised energy states respectively. However, when only one or two spatial

dimensions are confined, the resulting density of states is a combination of the two aforementioned cases.

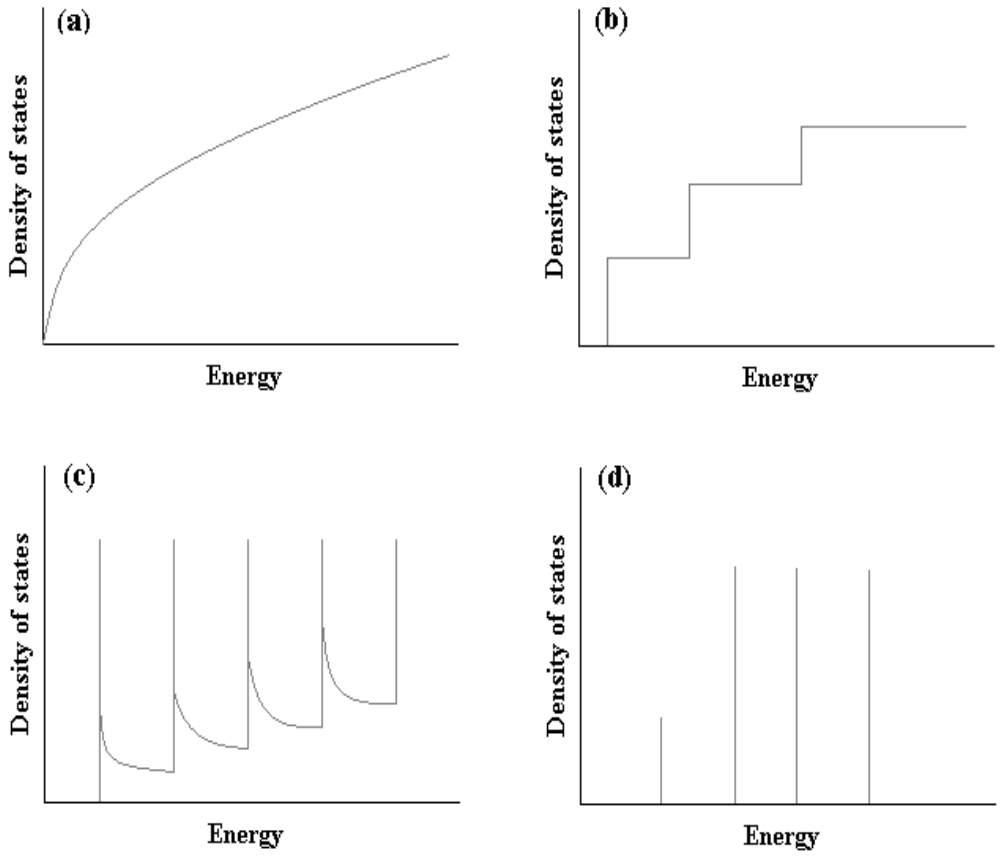

Fig 1.2: Diagram showing the density of states for a metal with (a) no spatial confinement (b) confinement in one dimension (c) confinement in two dimensions and (d) confinement in all three dimensions.

Another electronic property that comes about due to the small size of a metal nanoparticle is quantisation of charge, which occurs due to a phenomenon known as the coulomb blockade. This effect comes about due to the fact that, upon the addition or removal of an electron to/from a metal particle, the metal becomes more charged, which results in an energy barrier that must be overcome if additional electrons are to be added to the particle. [4-7] The energy requirement to add such a charge, Q, to a metal particle (known as the charging energy) is given by;

$$\frac{Q^2}{2C}$$

where C is the effective capacitance of the metal particle, which is proportional to the particle size. [4] Particles large enough to be considered a bulk metal will have very small charging energies, whereas in the case of nanoparticles, this charging energy becomes quite large. Thus, if the charging energy is much greater than the available thermal energy (k_bT), charging of the nanoparticle is suppressed (the coulomb blockade). This in turn leads to charge quantisation when a potential difference is applied across the metal nanoparticle in order to supply the required energy to add electrons. As the potential is increased, no charge is added until the charging energy barrier is overcome, allowing a single electron to be added and discharged from the metal particle. No further charge can be added until the potential is increased by another increment equivalent to the charging energy, whereupon a second electron can be added to and discharged from the nanoparticle. The end result is a stepwise graph of current vs potential, which is in stark contrast to that of a bulk metal that has a linear current vs potential relation (fig 1.3).

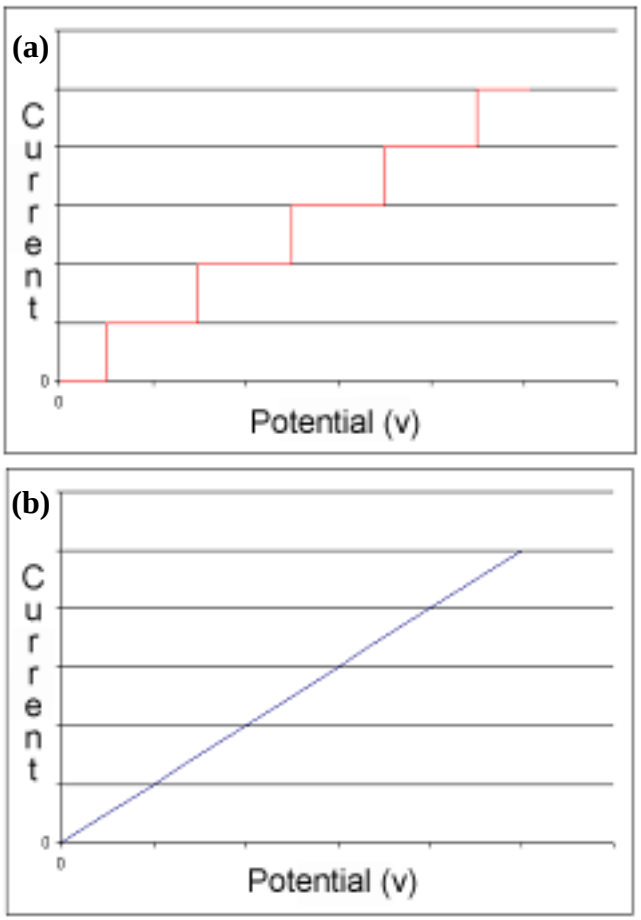

Fig 1.3: Current vs applied potential for (a) a metal nanoparticle exhibiting a coulomb blockade and (b) bulk metal.

Magnetic Properties

The influence of nanoparticle size on the electronic structure of metal nanoparticles is significant in that its effects are not limited exclusively to properties such as conductivity, but also extend to other electron derived phenomena, such as magnetism.

Magnetism is broadly defined as an intrinsic property of materials with a net magnetic dipole moment, which involves a force being exerted when in the presence of a magnetic field, the field itself being the product of a magnetic dipole moment. In the case of a stationary magnetic field, a torque is exerted on the material, creating a potential energy that depends upon the alignment of the materials magnetic dipole moment with the field. The tendency is to reduce the potential energy by aligning with the magnetic field.

The magnetic dipole moment can be thought of as being analogous to the electric dipole moment that results from two closely separated, but opposing, electric charges. However, although related, a magnetic dipole moment comes about not from closely separated charges, but from what can be described as a closed loop of current, with the dipole moment being perpendicular to the plane of the current loop (fig 1.4) [8]

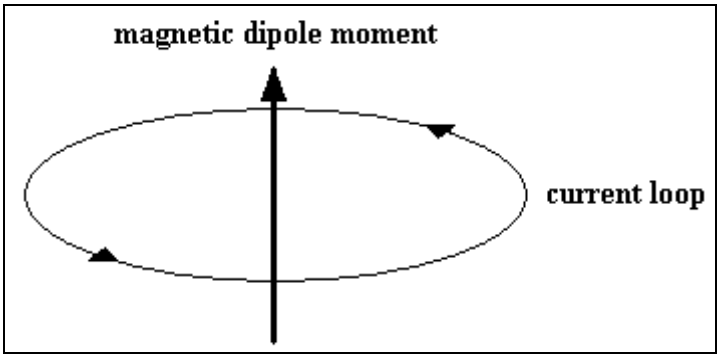

Fig 1.4: Depiction of a magnetic dipole moment arising from a "current loop".

There are two principal forms of "current loop" that contribute to the magnetic dipole moment of a material. Firstly, the orbit of a localised electron around the nucleus of an atom can be considered to be a closed current loop, and as such, induces a magnetic dipole moment. Secondly, electrons and protons possess an intrinsic angular momentum, which means that they can be effectively treated as if they are rotating (this property being referred to as spin). [8] A spinning charged particle can be considered to be a very small radius current loop, and hence, electrons and protons also contribute to the magnetic dipole moment of an atom, although typically, the magnetic dipole moment associated with a proton is much smaller than that of an electron (as a result of its much smaller charge to mass ratio), and so can be effectively ignored in this case.

The total magnetic dipole moment, and hence magnetic properties of a material, can be determined by taking the vector sum of all contributing moments. In the case of electrons that are closely bound to the atomic nuclei, one of two different situations can arise. In the instance where all bound electrons are paired in their respective orbitals with electrons of opposing spin

(due to Pauli exclusion principle), the total magnetic dipole moment is zero, as contributions due to electron orbit and spin are matched by an equal magnitude, opposing magnetic dipole moment from the other electron in the same orbital. Application of a magnetic field causes a net decrease in the field strength, as the applied magnetic field perturbs the orbits of the electrons around the nucleus in such a way that a net magnetic dipole moment that opposes the field which induced it results (Lenz's law). [8] This response to an applied magnetic field is called diamagnetism.

The alternative scenario is where at least one unpaired electron is bound to each of the nuclei. In this case, the magnetic moments are not cancelled out, and therefore an overall magnetic dipole moment exists. Typically, the orientation of the magnetic moments for an ensemble of such nuclei is random, and fluctuates due to energy imparted from thermal vibration, resulting in a net zero magnetic moment. However, upon the application of a magnetic field of sufficient strength to overcome thermal fluctuations, the magnetic moments align with the magnetic field, resulting in an increase in the magnetic field strength due to the magnetic field induced by the aligned magnetic dipole moments. This response to an applied magnetic field is referred to as Curie type (or localised) paramagnetism. [8]

In the case of solids, one must also consider the contribution from electrons that are delocalised (conduction electrons in a metallic solid at temperatures above 0K). As is the case for unpaired, nuclei-bound electrons, these electrons do not yield a net magnetic dipole moment due to thermal fluctuations causing the electron spin magnetic dipole moment to change orientation randomly. Upon application of a sufficiently strong magnetic field, these dipole moments align to yield an increase in the overall magnetic field strength. This response is referred to as Pauli type (or itinerant) paramagnetism. Note that this form of paramagnetism is weaker than Curie paramagnetism, due to fewer contributing electrons and the lack of an orbital magnetic moment.

In a bulk metal of a given composition, the form of magnetism exhibited is constant. Upon reduction of the metal to nanoparticle dimensions however,

the type of magnetism exhibited is strongly dependant upon whether there is an odd or even number of conduction electrons present, known as the odd-even effect. This is due to the quantisation of electron energy levels that occurs in a small nanoparticle, where if the available thermal energy is small enough relative to the kubo gap, electrons are confined to energy levels, and so curie type paramagnetism is exhibited if an odd number of valence electrons are present (unpaired spin), and diamagnetism is exhibited for even numbers of electrons (all electrons are spin paired), with an increase in temperature yielding pauli type paramagnetism. [9]

At this point, it is important to point out that the magnetic properties discussed so far involve magnetic moments that interact exclusively with an external magnetic field and that there are no interactions between the magnetic moments themselves. In some materials however, the electron magnetic moments from unpaired electrons interact with one another by overlap of their respective wavefunctions (known as an exchange interaction) to form magnetically ordered states. In the instance where the interaction is such that the electron magnetic moments are aligned parallel to one another, a permanent magnetic dipole moment is established. This is known as ferromagnetism. If however, the exchange interaction is such that the electron magnetic moments are aligned antiparallel with one another, then no overall magnetic dipole moment exists (unless perturbed by an external magnetic field). This is known as antiferromagnetism. At raised temperatures, thermal fluctuations of the electron magnetic moments can be sufficient to overcome the exchange interaction, and paramagnetism results. [8]

It is important to note that even though the exchange interaction in a ferromagnetic metal results in the formation of permanent magnetic dipole moments, the whole metal does not necessary possess a net magnetic dipole moment. The exchange interaction between neighbouring electrons, although quite strong, is only effective at short range (< 100nm). Outside of this range, another interaction called the magnetostatic (dipole-dipole) interaction dominates, which (depending on the metals crystal structure) typically drives the interacting magnetic dipoles to orient anti-parallel with one another. [10]

The balance between these two interactions results in the formation of magnetic domains, regions wherein the individual magnetic dipole moments are aligned with one another. Unless a magnetic field has been applied, the net magnetic dipole moments of the domains are not necessarily aligned with one another, typically resulting in a weak or even zero magnetic dipole moment for the entire ferromagnet. Application of a magnetic field causes each domains magnetic dipole moment to align parallel to the field direction, and due to the exchange interaction between many individual dipole moments in any given domain, they remain aligned even after the applied magnetic field is removed (fig 1.5), as the thermal energy requirement to change the direction of all of the individual dipole moments in a domain is very high. [8]

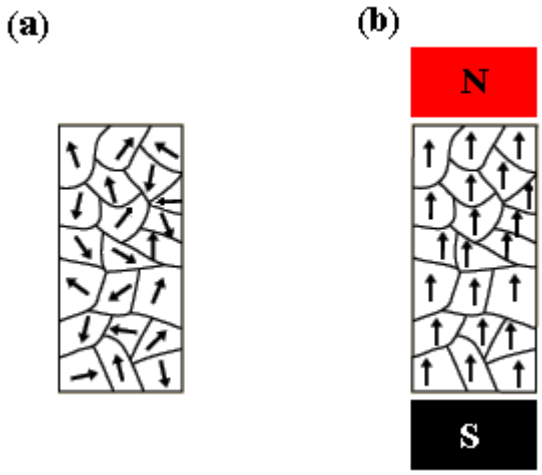

Fig 1.5: Ferromagnetic domain structure in (a) zero field and (b) in an applied magnetic field.

If a ferromagnetic metal is reduced to nanoparticulate dimensions, which is significantly smaller than the typical size of a ferromagnetic domain (>1μm diameter) [11], then the nanoparticle acts as a single magnetic domain, as the short distance between all contributing magnetic dipole moments in the nanoparticle results in exchange interactions dominanting. However, collections of such particles do not exhibit typical bulk ferromagnetic behaviour i.e. application of a magnetic field does not result in a permanent magnetic dipole moment over the entire ensemble of nanoparticles. Instead, due to the much smaller number of interacting magnetic dipole moments in nanoparticles compared to a typical magnetic domain, thermal fluctuations in the direction of each magnetic dipole moment occurs, even at temperatures

where the exchange interactions between individual magnetic dipole moments are maintained i.e. the alignment of the individual magnetic moments relative to one another is unchanged. This phenomenon is called superparamagnetism. [12] Ferromagnetic properties only arise in ensembles of such nanoparticles when the temperature is reduced below a temperature equivalent to the so called crystalline anisotropy energy, which is the minimum energy required for the ensemble of interacting magnetic dipole moments in the nanoparticle to collectively change direction. Below this temperature, the direction of the nanoparticles magnetic dipole moment is static. Application of a magnetic field provides the energy for the dipole moments to align, and after the field is removed, the low available thermal energy only allows a slow relaxation into a state where the net dipole moments are randomly oriented between all of the nanoparticles. Typically, the larger the nanoparticle, the higher the crystalline anisotropy energy, and hence the longer the relaxation time. [13]

Optical properties

The optical properties of metallic nanoparticles are also influenced by nanoparticle size, principally through an effect known as the localised surface plasmon resonance. When electromagnetic radiation is incident on a bulk metal, the conduction electrons oscillate with a frequency equal to that of the driving electric field. The oscillating electrons then transform this energy in one of two ways. Firstly, the resistance to the electron motion (due to electron scattering from other electrons, phonons, lattice defects etc) causes the energy to be lost as heat (absorption). [14] Secondly the acceleration of the electrons by the electric field causes the consequent re-radiation of electromagnetic radiation (reflection and scattering). [15] In the case of metallic nanoparticles, the dimensions are typically smaller than the wavelengths of visible electromagnetic radiation. As a consequence, the conduction electrons in the nanoparticle experience an effectively homogeneous electric field when illuminated by visible light (known as the quasi-static approximation). [16] This field causes the entire ensemble of nanoparticle conduction electrons to oscillate coherently relative to the positive nuclei comprising the nanoparticle (which are assumed to be immobile due to their much greater mass). This is

known as a localised surface plasmon oscillation (the conduction electrons are located principally at the surface of the nanoparticle as the nanoparticle is smaller than the magnitude of the oscillation). Due to electrostatic attraction between the nuclei and the displaced electrons, there exists a restoring force in this driven oscillation. [16] This driven 'harmonic oscillation' is characterised by resonance frequencies, or driving frequencies at which the oscillation experiences a maximum amplitude. Therefore, at certain frequencies of incident electromagnetic radiation corresponding to these resonances, the electron oscillation experiences an amplitude maxima, and consequently considerable dampening of the electron motion (energy absorption) occurs due principally to resistance to electron motion (if the nanoparticle is larger than the electron mean free path) or due to dispersion (electron scattering) from the nanoparticle surface (if the nanoparticle is smaller than the electron mean free path). [15] Note that the mean free path of an electron at room temperature is ~10 - 100 nm [17] and that light scattering is not effective for particles smaller than the light wavelength.[18]

The end result is that colloids of such nanoparticles appear strongly colored due to particularly strong absorption of visible light (oscillation of the conduction electrons is dampened so very little re-radiation occurs). The precise resonance frequency is very sensitive to the size of the nanoparticle, as the harmonic oscillation of the electrons is restricted by the nanoparticles dimensions and the nanoparticle experiences a less homogeneous electromagnetic field with increasing particle size. [14-15, 18] Likewise, resonance frequencies are also modified by the nanoparticle shape, composition and surrounding media, so small modifications in these parameters also cause a dramatic shift in the light absorption frequency. [14, 18-20]

Mechanical properties

Another example of where the properties of metallic nanoparticles deviate from bulk metal due to their size is mechanical properties. Metallic solids typically consist of atoms arranged into a regular crystalline lattice, and when

this atomic ordering extends throughout the whole solid, it is referred to as being monocrystalline. If a stress is applied to such a material, dislocations (defects in the ordering of the constituent atoms into a regular crystalline lattice) emerge, and propagate throughout the structure. The propagation of such dislocations leads to plastic flow and thus deformation (failure) of a metal. [21] However, in many metals, the regular arrangement of atoms does not extend throughout the entire solid. Instead, these (polycrystalline) metals are composed of regions known as crystal grains, each of which consists of atoms arranged into a regular crystalline structure that is mismatched with the arrangement of atoms in adjacent grains (a region known as the grain boundary). In this case, when a stress is applied, dislocations within a grain propagate until they reach a grain boundary, upon which they are impeded from propagating further. As more stress is applied, more dislocations propagate to the grain boundary (known as a "pile up"). This results in an increased driving force for dislocation propagation across the grain boundary, until a point is reached where propagation of the dislocations can continue into the adjacent grain. As a result of this inhibition of dislocation propagation, polycrystalline metals can withstand a higher applied stress before yielding compared to their monocrystalline counterparts.

Typically, decreasing the grain size increases the hardness and level of stress that can be endured before deformation occurs, a phenomenon known as the Hall-Petch effect. [22-23] This results from the fact that smaller grains result in smaller grain boundaries, and therefore, less dislocations that can potentially pile up against the grain boundary. This means that a smaller driving force due to dislocation pile up is present, and thus, a greater stress needs to be applied to allow propagation of the dislocations. When the grain size is reduced to nanoscale dimensions (as is the case for metallic nanoparticles) the size of the dislocations is about the same as the size of the grains, and so, very few dislocations can fit into any given grain. This effectively prevents dislocation pile up, and so would be expected to yield extraordinarily high yield stresses. However, the grain boundaries are now small enough that sliding of the grains past one another can occur at smaller stresses than that for dislocation propagation. The stress required for such

grain sliding is smaller for smaller grain sizes, and so a decrease in the hardness and yield strength of nanoparticulate metals is observed. [12, 24-25]

Chemical reactivity

As the particle size approaches the nanoscale, the percentage of atoms at the particle surface becomes significant compared to that of the bulk material (fig 1.6). For example, in the case of a spherical iron nanoparticle, ~50% of the atoms are at the surface when the diameter is 3nm compared to only 5% at a diameter of 30nm. This results in the surface properties of the material dominating in lieu of the bulk properties. [1]

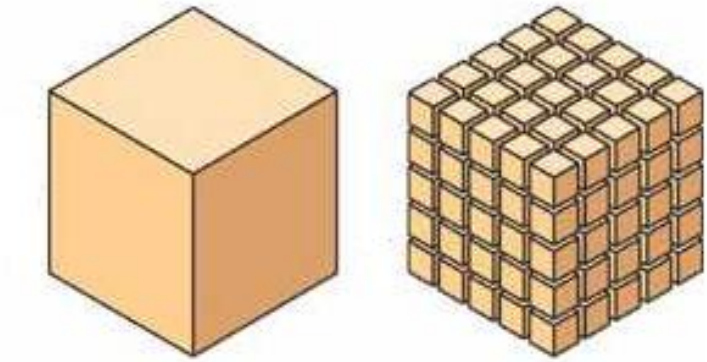

Fig 1.6: Diagram showing the increase in surface area when a bulk solid is divided into an equal volume of smaller particles.

An example of this is the marked increase in the free surface energy of nanoparticles compared to the bulk material. [26] The free surface energy of a metal is defined as the work required to increase the surface area by a given unit area. Physically, it is derived from the energy input required for cleavage of interatomic bonds during the formation of a surface, or equivalently, the unsatisfied bonding of atoms at the surface of a material due to these atoms having a smaller coordination number than atoms in the interior. Given the increased proportion of surface atoms in a nanoparticle compared to the bulk material, it is clear that an increase in free surface energy (for a given volume of metal) results. Furthermore, as the nanoparticles decrease in size, there is an increase in the number of surface atoms at edges and corners of surface faces, which have even smaller coordination numbers and hence contribute to the free surface energy even more. [27]

One of the consequences of an increased free surface energy is that metallic nanoparticles typically exhibit enhanced reactivity compared to their bulk equivalents. This can be understood by first considering the fact that there is a thermodynamically driven tendency toward minimisation of the free surface energy, and that although rearrangement of the surface occurs in an attempt to better satisfy the bonding requirements of the surface atoms, this is typically insufficient. [28-29] As a result, interactions with other chemical species (as well as aggregation of nanoparticles) take place in order to fulfil the surface atom's bonding requirements, such as chemical reactions leading to the formation of a new, unreactive surface layer of lower free surface energy (such as an oxide layer); a process known as passivation. [28] In the case of nanoparticles, the high free surface energy results both in reactions that have a lower energy barrier to overcome than is the case for the bulk solid (due to the high number of corner and edge surface atoms which readily bond with other species) and that occur to a much larger extent than in the bulk solid (due to the larger surface area to volume ratio). [28-29] As a result, nanoparticles can exhibit a significant increase in the rate and extent of chemical reactions. An example of this is iron nanoparticles, which react with oxygen much more readily and completely than bulk iron. [30]

Similarly, metallic nanoparticles can also exhibit enhanced catalytic activity. An alternate way by which surface free energy can be minimised is by the reversible binding of species to the surface of a solid (adsorption) instead of the permanent formation of a new surface layer. Bonding between the adsorbate and the surface can weaken other bonds within the adsorbate molecule, making them more susceptible to scission and thus lowering the energy requirement for subsequent chemical reactions (dissociative adsorption). [28] As before, the high surface area to volume ratio results in more species being involved in catalysed reactions at a given time, while the large number of low coordination number surface atoms yields many sites at which binding to the surface requires less energy than elsewhere on the surface, leading to a further reduced energy requirement for the catalysed reaction. An important example of the enhanced catalytic activity is exhibited

by gold nanoparticles. Bulk gold is known to be a relatively unreactive metal, owing to its full d-sub shell and high ionisation potential, resulting in adsorption occurring only to a relatively small extent. However, when reduced to dimensions of ~3nm diameter, gold becomes very reactive for many reactions such as CO oxidation, at temperatures as low as 40K. [31], [32], [33] This has been ascribed to the fact that such small nanoparticles have many low coordination surface atoms (edge and corner atoms), where adsorption occurs much more readily. [34-35]

Importantly, the enhanced reactivity of nanoparticles can also impact upon other properties. For example, small nanoparticles that undergo passivation by forming an oxide layer are comprised of a greater volume of metal oxide compared to a larger nanoparticle, meaning that more of the properties are associated with the oxide in a smaller nanoparticle than in a larger nanoparticle. For particularly small particles, this volume fraction becomes significant, to the extent that the properties are dominated by that of the metal oxide. [12, 36]

Thermal properties

Another example of the dominance of surface aspects for particles at the nanoscale is the reduction in melting point that occurs with decreasing particle size. The melting point is defined as the temperature at which thermal motion is sufficient to destroy the order of a lattice. Due to the fact that surface atoms have a smaller coordination number than those in the bulk, they are more easily rearranged than the interior atoms. [37] [38], [39] [40] Given that nanoparticles have a significant percentage of their constituent atoms at the surface, with the proportion increasing as the nanoparticle size decreases, the end result is that the onset of melting of a nanoparticle occurs at lower temperatures than that of the bulk material. One example of this is the decline of the melting point of gold nanoparticles as they are reduced below 20nm in diameter. [41]

1.1.2. Synthesis

Clearly, metal nanoparticles possess a wide range of desirable properties that can be accessed by finely tuning the nanoparticle dimensions. However, it is important to note that all of the properties discussed so far are not only size dependant, but are also modulated by changes in other nanoparticle characteristics such as composition and morphology (shape and number of confined dimensions). [21, 42-43] These aspects of nanoparticles, and their associated properties, are determined by the way that the nanoparticles are made. As such, a vast amount of research has been conducted on exploring and understanding various methods of nanoparticle synthesis so that these physical characteristics can be tailored and controlled.

Current nanoparticle synthesis methods can be classified into one of three broad categories; mechanical attrition, vapour condensation and chemical synthesis.

Mechanical Attrition

Nanoparticle synthesis by mechanical attrition involves breaking down macroscopic metal or metallic particulates to such an extent that smaller nanoscale particles form. This is known as a "top down" approach towards nanoparticle formation. The most common method of mechanical attrition is the high energy ball mill, which involves the use of a cylindrical chamber (drum) filled with the mass to be broken down and a number of hard spheres. The drum is rotated, creating multiple impacts between the hard spheres and the solid mass. [12]

Depending upon the arrangement of the mill, particles on the order of 100's of nanometers can be formed. Ball milling is an advantageous technique in that very large volumes of nanoparticles can be formed, the formation process is relatively fast and easy and many types of metals can be used. [44-51] Mechanically alloyed nanoparticles can also be formed by attrition of a

mixture of compounds/metals. [52] However, access to smaller nanoparticles is not possible using this technique, with control over particle size and particularly size distribution being very difficult to achieve (the only factors that can be varied is the energy involved in the impacts, milling time and milling/milled material) and little to no control over the particle morphology. There is also typically a large amount of impurities mixed with the nanoparticles from the mill.

An alternative form of mechanical attrition is ion milling, which involves the use of a beam of ions to etch away metallic material from a surface in order to form the desired nanoparticles. [53-54] This method results in the formation of nanoparticles of very well defined morphology (compared to ball milling), but has numerous disadvantages, not the least of which is the time associated with forming any reasonably large number of nanoparticles, the restriction of nanoparticle morphologies that can be formed and the confinement to the substrate they were etched from.

Vapor condensation

Vapor condensation methods involve the formation of nanoparticles through the nucleation of vaporised metal atoms into small clusters followed by growth of these nuclei into larger metallic nanoparticles, a process that first involves diffusion of the growth species towards the surface of the nuclei followed by adsorption to the surface, with subsequent incorporation into the nanoparticle through the formation of additional chemical bonds in such a way that the crystal structure of the nanoparticle results in the lowest possible surface free energy facets. [55] This is known as a “bottom up” approach to nanoparticle synthesis. Nucleation can be initiated by either heterogeneous (using a foreign molecule, ion or surface) or homogeneous (absence of foreign material) means, but in either case requires supersaturation of the metal vapor for both spontaneous nucleation and growth to occur, as these conditions yield a decrease in overall energy of the system with the formation of nanoparticles (the reduction in energy due to the bulk phase change outweighing that required to form a surface). [12]

Specific techniques for forming nanoparticles based on this method revolve around achieving supersaturation. One way by which supersaturation may be achieved is to reduce the vapor temperature. The primary means by which a low temperature supersaturated vapour may be formed is through supersonic expansion, which involves the use of a high pressure vapor source that is suddenly expanded into a much larger volume to attain low pressure. Such expansion cools the vapor, resulting in supersaturation (despite the "dilution" of the vapour). [56-59] Vapor formation for supersonic expansion can occur through a number of means, the simplest being evaporation of low boiling point metallic precursors in a furnace or oven (typically mixed with an inert carrier gas which is used as a means of absorbing heat and therefore assisting the formation of the nanoparticles). [60-66] An alternative method uses laser pulses to heat a metal target (~10^4 K), with the metal vapor then being drawn away using a carrier gas jet before being expanded to cool and condense. This method overcomes the main problem with the oven source method, in that it can achieve the much higher temperatures which are required to vaporise some metals. [67-79] Lasers can also be used to form a metal vapour by initiating photolysis of organometallic compounds, with the consequential dissociation of organometallic precursors producing a metal vapour. [80]

Supersaturation can also be achieved using a vapour with a high concentration of metal species, [81-82] which may be formed by (i) thermal evaporation of the metal [36, 83-89], (ii) sputtering (where metal atoms are ejected from a solid target due to bombardment with energetic ions) [90-97] , (iii) electron beam evaporation and laser ablation [98-99], (iv) spark erosion [100-102], (v) flames [103-105] and (vi) thermal decomposition of metal-organic precursors. [106] All of these techniques use a high pressure inert gas, as this controls the vapor temperature and inhibits diffusion away from the source via a high level of collisions. Otherwise, this would prevent supersaturation as the concentration would never be sufficiently high.

Nanoparticle size is controlled in the vapor condensation method by controlling the temperature during nucleation and growth stages, with higher temperatures resulting in faster growth and hence larger nanoparticles for a

given reaction time. Furthermore, if a narrow particle size distribution is to be obtained, reaction conditions (principally temperature and pressure) must be selected such that the nucleation process is fast (i.e. not diffusion limited) while the growth process is slow as this allows the nuclei to all form essentially at the same time and then allows them to grow at the same rate.

Although vapor condensation methods provide a means for rapidly forming large quantities of very small, narrow size distribution nanoparticles from a wide variety of metals, these methods suffer from a lack of versatility, in that they are essentially limited to forming spherical nanoparticles. In order to form non-spherical nanoparticles (particles with confinement in only one or two dimensions) one of two approaches are typically used. In the first approach, nanoscale features are used a nucleus for nanoparticle growth. One such example of this is the use of step-edge defects on an otherwise flat surface, which act as sites of nucleation for the formation of wire shaped nanoparticles as the defects higher surface energy (free bonds) causes accumulation of metallic growth species at these sites. [107-110] Another example is the use of pre-existing nanoparticles, such as carbon nanotubes. [111]

The second approach uses a template to physically direct where the vapor condenses and hence where nanoparticles form. One example of this is the use of grooves in a solid substrate, where the vapor condenses at the bottom of the grooves and thereby forms metallic nanoparticles that replicate the shape of the groove (fig 1.7a). [112-113] A modified form of this method is the use of grooves to restrict where the vapor can condense by creating “shadows” in the stream of vapor projected onto the surface (fig 1.7b). [114-115] Porous substrates, like zeolite, have also been used as templates to form more complex nanoparticles due to its regular cage like nanostructure [116], in addition to structures formed through the use of photo- or electron beam lithography. [117]

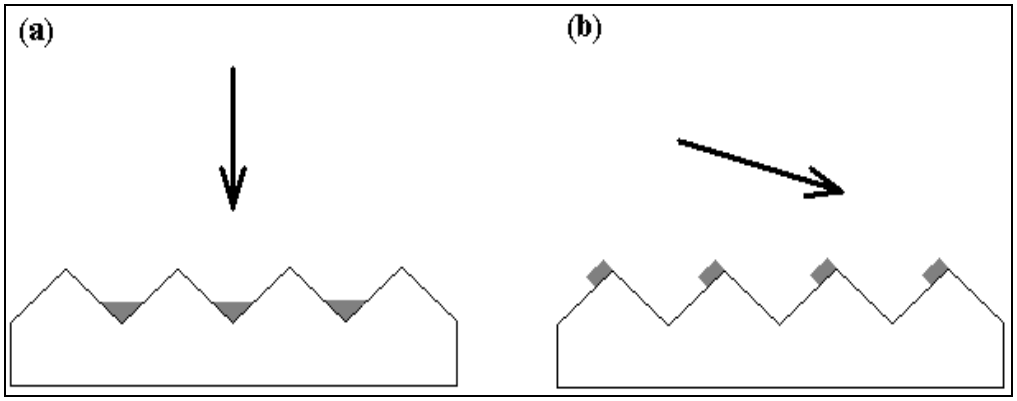

Fig 1.7: Diagram showing the use of grooves as a template in vapour synthesis of nanoparticles (a) direct replication of the grooves by directing the vapour at the substrate through the use a gas stream (b) utilising the groove shape and angle of vapour approach to form particles outside the "shadow" created by the grooves.

Another limitation to the synthesis of nanoparticles using this method is in the composition of the nanoparticles. Only metals and metal compounds that can be vaporized to form a superatuarated vapor are applicable, and the formation of complex ordered compositions (such as multiple shell nanoparticles and hollow nanoparticles) is relatively difficult. This method remains relatively expensive compared to other two methods and is not readily amenable to large scale production of commercial nanoparticles.

Chemical synthesis

Chemical synthesis techniques, like vapor condensation, involve the formation of a supersaturated solution (high *initial* concentration) of the growth species, with subsequent nuclei formation and growth of the nuclei by adsorption of growth species to form metallic nanoparticles. [118] The main difference is that the nuclei and growth species are formed by the reduction of a metal precursor (typically salts or complexes), and that the whole process occurs in solution.

Chemical synthesis methods can be differentiated by the means by which the metal precursor is reduced to the growth species that contribute to the growth of the metallic nanoparticles. By far the most common means is the use of a chemical reducing agent. [119-129] Electrochemical reduction at the surface

of an electrode is also used [130-131] along with electroless reduction on catalytically active metal surfaces.[132] Sonochemical synthesis is another more recent strategy for reduction of the growth species. Here the high vapor pressure of a metal carbonyl compound in the bubbles formed during sonication, with the subsequent heating upon cavitation and collapse of the bubble, results in the reduction of the metal complex to metal (0), through the intermediate generation of highly reactive radical species. [133-134] Thermolysis of organometallic precursors is yet another method for forming a reducible species, and involves the thermal decomposition of a metal complex. [135-136] Similarly, light induced degradation of metal species into a reduced form can also be used to form metallic nanoparticles. [137]

Control over nanoparticle size and size distribution, as with vapor condensation methods, requires fast nucleation, with subsequent slower growth. Unlike vapor condensation however, chemical synthesis techniques are considerably more versatile, as these synthesis methods only require initial supersaturation, and as such do not suffer from the constraints of maintaining vapor supersaturation (extremes in temperature and pressure). Furthermore, as the synthesis is in solution, a wider range of parameters can be adjusted to change the nucleation and growth rates of the nanoparticles, and thus control the size of the nanoparticles. For example, growth and nucleation rates can be controlled thermodynamically (the energy of formation) or kinetically by adjusting the reaction medium (viscosity and involvement in the growth process), the concentration of the growth species (which in itself can be controlled by the temperature, pH, reducing agent, rate of decomposition of the growth species), the temperature, the concentration of other species in solution (through influencing the diffusion of the growth species, for instance by sequestering the metal precursor species in a polymer so that upon reduction only adjacent metal species can aggregate to form nanoparticles [138]) and the order of addition of the reagents. Chemical synthesis of nanoparticles is also versatile in that a wide range of nanoparticle compositions can be accessed, such as a plethora of different metals, [42, 120, 139-151] intermixed alloys [152-153] and even core-shell alloy arrangements. [154]

Chemical synthesis does possess a few disadvantages however. For one, the synthesis is typically slower than in vapor condensation methods due to the lower temperatures, concentrations and diffusion rates of metal growth species involved. Secondly, the chemical synthesis method, as with vapor condensation methods, principally forms spherical structures. The formation of nanoparticles with a different morphology (number of confined dimensions and shape) requires the use of one of a number of strategies during the nanoparticle synthesis. In this regard, chemical synthesis is again more versatile than other means of nanoparticle synthesis, in that there is a wide range of methods available that allow control of nanoparticle morphology, partly owing to the gentler reaction conditions and that such nanoparticle synthesis occurs in solution. [155-158] One of the most common methods is the use of a template, which directs the growth of the nanoparticles by serving as a scaffold within or around which the nanoparticles are formed. Templates can be classified as either "hard" or "soft" depending upon the nature of the template medium.

A soft template typically involves the use of media that self assemble into permeable nanoscale structures, with the surfaces of these structures possessing the necessary chemical functionality or charge to direct the desired metal complex to concentrate in the desired region (generally the interior of the structure). The metal species are then reduced to form the desired nanoparticles. Micelles are the most commonly used template of this type, with numerous examples of surfactant micelles in an oil/water emulsion being used to form metal nanoparticles. [159-160] Similarly, block copolymers (which will be discussed in more detail later) form micelles in solution, and consequently have also been used as templates in the synthesis of metal nanoparticles. [161-164] Other forms of structured soft templates used in metal nanoparticle synthesis include liposomes (phospholipid bilayers), vesicles (surfactant bilayer) [165], DNA [166], protein microtubes (such as α,β-tubilin) [167-168] and dendrimers. [169-172]

In contrast, hard templates typically consist of macroscopic solids with regular nano-scale features. The growth of nanoparticles here is directed by physical

confinement of the growth species to these nanoscale features. One of the most prevalent forms of hard templates are membranes which contain parallel nanochannels. Examples of this type of template include; anodic alumina [173-175], nanochannel glass [176-177], track etched polycarbonate [178-180] and etched mica films. [181] Another common form of hard template is zeolite, which possesses a regular nanoscale cage like structure. [182-185] Some forms of hard template are formed in situ with a mixture of metal growth species and template forming species, thereby encapsulating the growth species in void spaces prior to reduction to solid metal. On example of this is the use of a lyotropic liquid crystal, which is crosslinked to form channels. [186] Another prevalent example is the use of silicate [187] and titanate [188] sols, where the metal precursor species is introduced into the colloidal solution, followed by gelation of the sol to form a porous solid. The metal precursor is subsequently reduced in situ. Another form of hard template arises from the features present on the surface of a bulk solid. One example of such a template is the step edges that are present on such a surface, which are used as nucleation centres in the reduction of metal precursors. [189] Another method involves the use of a multilayer structure which has been cleaved to expose the cross sections of different layers. The different properties of each layer can then be utilized for the selective reduction of metal precursor at the desired layer i.e. electrochemical deposition at the electrically conducting layers. [190-191]

In contrast to the types of hard template mentioned thus far, some hard templates are based on existing nanostructures. For example, carbon nanotubes have been used as a template for the formation of nanowires comprised of metals. [192-193] Nanowires have also been used as templates for the formation of metallic nanotubes, where the nanowire template is itself a material that is used to initiate reduction of the metal growth species. [194-196]

An alternative method of directing nanoparticle growth is through the use of capping agents. This method involves the adsorption of any one of a range of molecules to the specific crystal faces of the nanoparticle, which then results

in a reduction in the surface free energy of these faces, and therefore slower or even halted growth at these locations, while such growth continues unabated at the other crystal faces. [19-20, 42, 197-200] The most prevalent form of capping agent is a short chain polymer [42, 201-204], although organic molecules (such as those typically used in the synthesis of semiconductor quantum dots) are also applied as capping agents in the directed growth of metal nanoparticles. [197, 205-207]

Importantly, although the use of such measures to direct nanoparticle growth into different morphologies allows for a great deal of control, it is often necessary to remove the template or capping agent after nanoparticle synthesis in order to facilitate collection of the nanoparticles and to retain control over their surface properties.

1.1.3. Functionalisation

One of the principal challenges when working with nanoparticles is that there is typically a very strong tendency towards both aggregation of the nanoparticles and Ostwald ripening, a process whereby large particles grow at the expense of smaller particles via dissolution of the smaller particles and migration of the constituent atoms. [208-209] Although different, both of these processes are driven by a reduction in the total surface free energy. The result is clearly undesirable, as it effectively eliminates any control over nanoparticle size, size distribution, shape and dimensionality, and therefore properties. In order to stabilise the nanoparticles against aggregation and Ostwald ripening, the nanoparticles need to be effectively isolated from their environment. This can be achieved by modifying the surface of the nanoparticles through coating with a layer of material that either (a) introduces an opposing force to particle aggregation and Ostwald ripening or (b) reduces the surface free energy. [12] This process is known as functionalisation.

Functionalisation can introduce an opposing force by either introducing steric interactions (the approach of two nanoparticles involves a local increase in the concentration of the species that the nanoparticle is functionalised with, resulting in an osmotic and steric force that drives the nanoparticles away from one another) or by creating a net surface charge on the nanoparticle (electrostatic repulsion). [210] There exists a number of ways to do this; the most common is the covalent attachment of individual molecules (ligands) to the surface, through a specific functional group, to form a monolayer. For example, functionalising a nanoparticle with long alkyl chain ligands allows the functionalised nanoparticle to be highly soluble in aprotic non-polar solvents, whilst functionalisation with polar ligands makes the nanoparticles soluble in polar solvents. [211] The most prevalent ligands used to stabilise metallic nanoparticles are Lewis bases such as amines [212], phosphines [152, 213-214] and thiols [211, 215-223] as these functional groups bind strongly to metals. An alternative method for functionalisation involves coating the

nanoparticles with polymers [224-229] or dendrimers [230-231]. Reduction in the surface free energy of a nanoparticle can also be achieved by simply coating the nanoparticle with a layer of material that has less surface free energy i.e. less electrons available for bond formation. Both silica [232-234] and polymer coatings can be used to stabilise nanoparticles by lowering their surface free energy. [210]

The motivation behind nanoparticle functionalisation is not limited solely to stabilisation; functionalisation also provides a means for fine tuning the surface properties of the nanoparticles, as this surface layer dominates the interactions of the nanoparticle with its surroundings. [1, 216, 235] Firstly, this allows the nanoparticles solubility properties to be modulated, which is useful handling of such nanoparticles. Secondly, the surface layer mediates interactions with other chemical species in solution, allowing for a virtually unlimited range of chemical reactions to occur at the surface of the nanoparticles provided the chemistry of the surface layer (accessible functional groups) is selected to promote the desired reaction. For example, polymerisation reactions can occur at the surface of a nanoparticle functionalised with a surface layer of polymerisable groups. [236-239] Importantly, the nanoparticle substrate will influence these reactions due to its influence on the electron density and hence the energy levels inherent to the surface layer's functional groups. [240-243]

In addition to modification of a nanoparticles surface properties, functionalisation is also expected to influence many of its other properties, as the formation of many new chemical bonds will invariably influence the electronic energy levels of the nanoparticle (the high surface to volume ratio means that functionalisation affects a large percentage of the nanoparticles constituent atoms). One marked example of this is the modification of the surface plasmon resonance wavelength upon functionalisation of a nanoparticle with ligands. [244-245] Another example is the reduction in the saturation magnetisation of magnetic nanoparticles upon functionalisation with carbon monoxide. [246]

1.2. Nanoparticle Assemblies

Clearly, a vast amount of research in the field of nanoparticles has been performed over the last few decades, which has resulted in the development of synthesis and functionalisation methods that allow control over virtually any nanoparticle attribute. As a consequence, nanoparticles have been employed in a wide range of applications. [247-249] More recently however, the focus of research has begun to shift towards the incorporation of nanoparticles into ordered assemblies; a trend which has been driven by the need for precise placement of nanosized components in devices [250-252] (the formation of complex 3D nanostructures using well established "top-down" methods such as lithography being remarkably difficult and expensive [253]) in addition to the interesting set of properties that are inherent to such structures. Such properties can be classified based on whether they originate from the collective behaviour of nanoparticle interactions, which occur when nanoparticles are in close proximity, or from external interactions with the specific structural arrangement.

1.2.1. Properties

Nanoparticle Interactions

The properties that result from interactions between nanoparticles in an assembly typically exhibit features that fall between those of isolated nanoparticles and those of bulk metals. When the particles are well separated such that no interactions occur, the nanoparticles correspondingly act as isolated particles. As the interparticle separation is reduced, interactions between the nanoparticles may begin to take place, leading to a shift in the properties exhibited by the individual nanoparticles. Further decreases in separation often result in a strengthening of these interactions and hence, the change in properties that emerges from these interactions becomes more extensive.

One of the foremost examples of this is the variation in electrical conductivity that occurs with changes in the interparticle spacing. As an example, consider the case of an ordered array of identical spherical metallic nanoparticles at low temperature ($T \rightarrow 0K$). When the nanoparticles are well separated from one another, charge transfer between nanoparticles (which under these conditions occurs by electron tunnelling[*]) is almost non-existent (the assembly is electrically insulated) (fig 1.8a). As the nanoparticles in the assembly are brought closer together, the tunnelling probability would typically increase, but as a result of the coulomb blockade, tunnelling between nanoparticles in such an assembly is still strongly inhibited, effectively resulting in no charge transport between the nanoparticles unless the charging energy is overcome (fig 1.8b). [254-256] At the same time however, reduction in the interparticle spacing allow the wavefunctions of the neighbouring nanoparticles to begin to overlap, upon which an interaction known as exchange coupling occurs. [254, 256-258] Exchange coupling can be viewed conceptually as a partial sharing of the charge carriers between the nanoparticles, much in the same way as when a chemical bond is formed, and effectively results in a reduction of the charging energy that needs to be overcome in order for charge carriers to tunnel from one nanoparticle to another. As the interparticle spacing is decreased, the strength of the coupling increases, until a point is reached where the exchange coupling overcomes the charging energy entirely. In this situation, the electrons in the assembly are effectively delocalised over the interacting nanoparticles i.e. the assembly is electrically conducting, although the current at a given applied potential is typically smaller than that for the bulk metal (fig 1.8c). [254-255, 259-260]

[*] Charge transfer by thermally activated nearest neighbour hopping is the dominant mechanism at relatively high temperatures (300K), but this mechanism is quenched at low temperatures, with charge tunnelling becoming dominant.

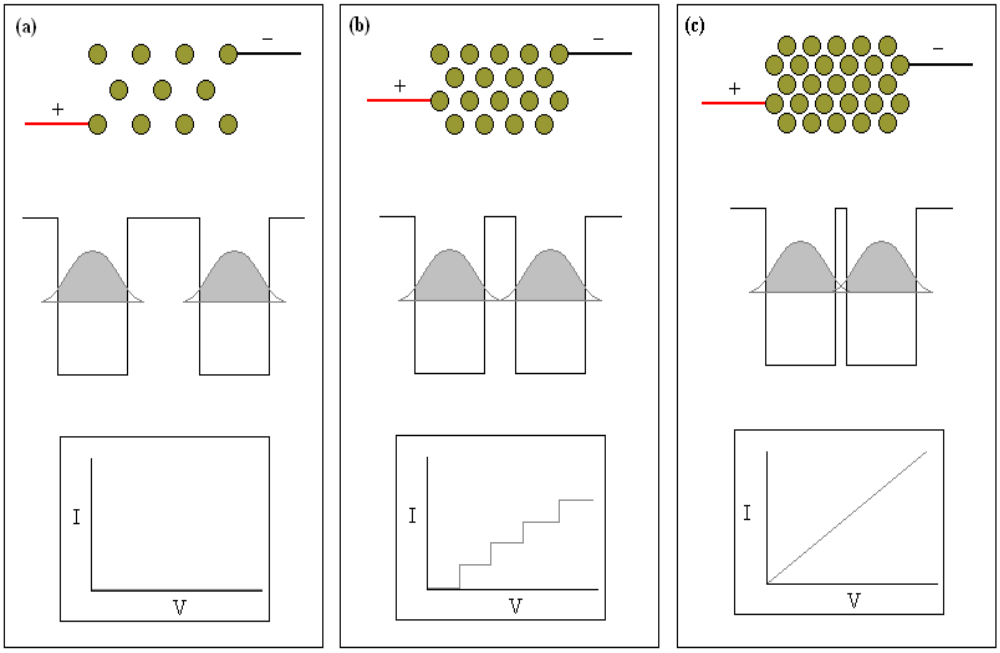

Fig 1.8: Depiction of an assembly of spherical nanoparticles on a surface (top), ground state wavefunctions for charge carriers localised in two adjacent nanoparticles i.e. finite potential wells (middle) and graphs of current due to an applied voltage (bottom) where (a) the interparticle spacing is "large" such that no charge transport by tunnelling occurs (b) the interparticle spacing is "moderate" such that tunnelling can occur but is inhibited by the coulomb blockade (c) the interparticle spacing is "small" such that exchange coupling is strong enough to delocalise the charge carriers over the whole assembly.

Another example of the shift in properties that results from interactions between nanoparticles in an assembly is the change that occurs in the localised surface plasmon resonance. When metal nanoparticles in an assembly are well separated from one another and the assembly is illuminated with light, the electrons in each nanoparticle are acted upon by the incident light, and form a localised surface plasmon oscillation as would occur for an isolated nanoparticle (fig 1.9a). However, one of the consequences of a localised surface plasmon oscillation is the concomitant formation of an oscillating evanescent electric field (near field Mie scattering) on the surface of the nanoparticles, often much stronger than the incident electromagnetic field that induced the oscillation. [18] Thus, as the nanoparticles are brought closer together (separation less than 5 times the nanoparticle radius for identical spherical nanoparticles), they not only experience the oscillating electric field from the incident light, but also begin to experience the electric

field due to the localised surface plasmon oscillations of the neighbouring nanoparticles. This interaction (known as electromagnetic coupling) leads to a *collective* surface plasmon oscillation among the particles (any changes in the surface plasmon oscillation of one particle will affect the surface plasmon oscillation of all other coupled particles); with a resonant frequency that is red shifted relative to that of the isolated nanoparticles (fig 1.9b). [18, 256, 261-262]

Continued reduction in the interparticle spacing leads to an increasing electric field strength arising from the neighbouring nanoparticles, and hence to stronger coupling (more pronounced red shift) (fig 1.9c). Importantly, this red-shift also reveals other, weaker localised surface plasmon resonances (such as those attributed to quadrupole surface plasmon oscillations rather than the dipole surface plasmon oscillations that are dominant for particles satisfying the quasi-static approximation) which are not strongly affected by the electromagnetic coupling, and are normally obscured by the main plasmon oscillation. [263] Eventually, a point is reached where the nanoparticles in the assembly are so closely spaced that exchange coupling begins to occur. At this point, the electrons start to become delocalised over multiple nanoparticles, and the assembly begins to behave as a single particle (albeit a larger non-spherical particle). This results in the localised surface plasmon resonance frequency blue shifting back towards that of a single isolated particle rather than an assembly (fig 1.9d). [256]

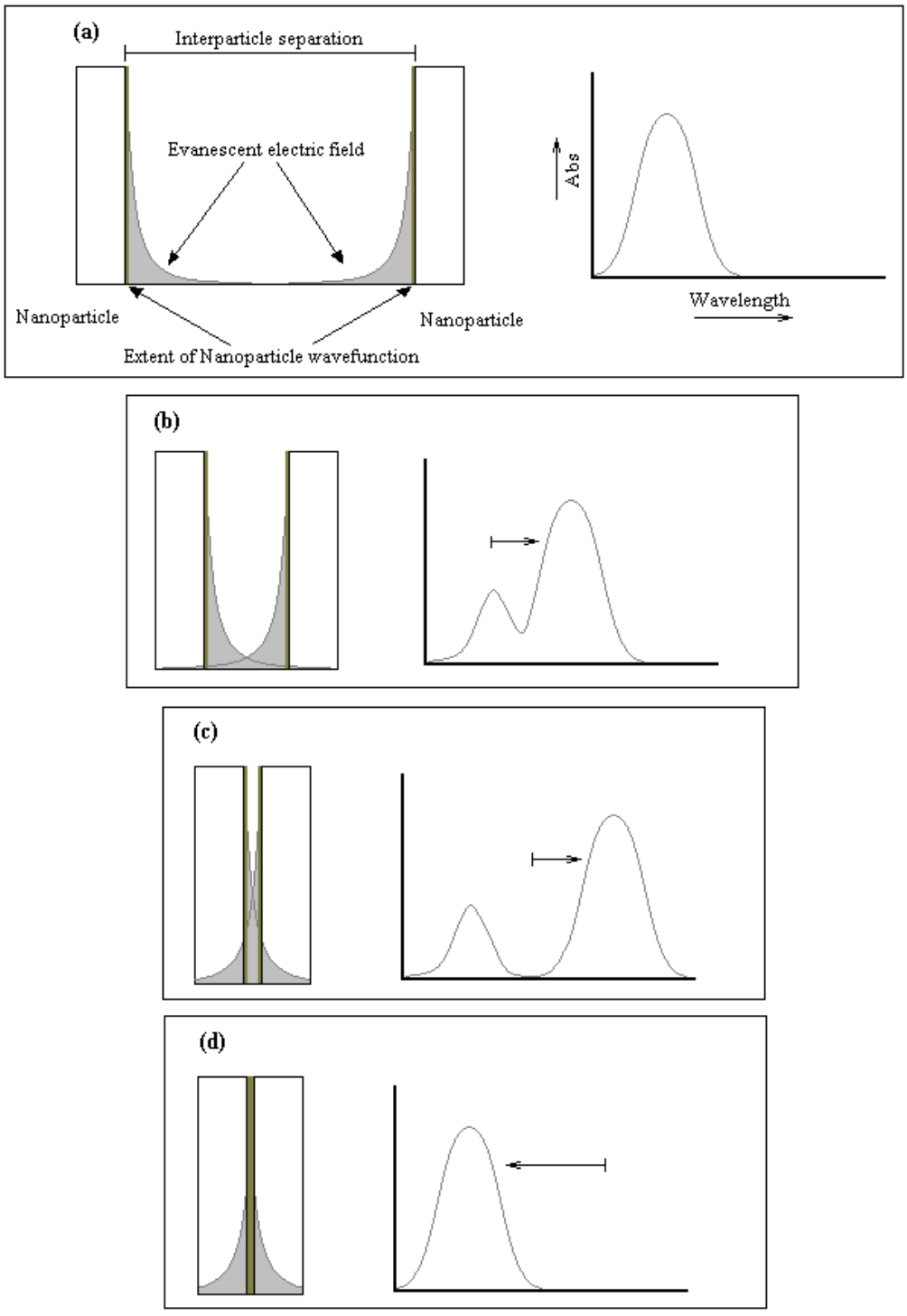

Fig 1.9: Depiction of the electric field strength and extent of the nanoparticle wavefunction away from the surface of two identical spherical nanoparticles or radius r together with the corresponding light absorption spectrum due to localised surface plasmon resonance in the case of (a) interparticle spacing >> 5r (no electromagnetic coupling) (b) interparticle spacing = 5r (weak electromagnetic coupling) (c) interparticle spacing < 5r (strong electromagnetic coupling) and (d) interparticle spacing << 5r (strong electromagnetic and exchange coupling).

The magnetic properties of interacting metallic nanoparticle assemblies also exhibit properties between that of a bulk metal and those of isolated nanoparticles. Consider a collection of superparamagnetic nanoparticles that are placed into an ordered assembly. At large interparticle separations, the nanoparticles can be considered to be non-interacting, and so the entire ensemble of nanoparticles behaves in a superparamagnetic fashion. Now, given that each nanoparticle can be considered to be a single magnetic dipole (due to the strong exchange interactions occurring between the individual magnetic moments of atoms within the nanoparticles), as the interparticle spacing is reduced, magnetostatic (dipole-dipole) interactions begin to occur. Just as with the magnetic dipole moments of atoms in a bulk magnet, this magnetostatic interaction typically drives the nanoparticles net magnetic dipole moments to preferentially align antiparallel with one another, resulting in an antiferromagnetic assembly. [10] However, it is important to note that, just as the nature of this interaction can vary with crystal structure in bulk magnets, different structural arrangement of the nanoparticles in the assembly can also modulate such interaction. Thus, for certain structural arrangements (such as 2D triangular and square lattices) this interaction can in fact result in parallel alignment of neighbouring nanoparticles net magnetic moments i.e. a ferromagnetic assembly. As the interparticle spacing is further reduced, the strength of these interactions increases, leading to progressively greater ferro/antiferromagnetic behaviour, such as a net magnetisation being held for longer after the application of a magnetic field (a longer relaxation time). [264-265] This is further modulated by the collective long range orientation of the nanoparticles (in the case of non-spherical nanoparticles) within the assembly. [266]

Structural Arrangement

Perhaps the most distinguishing property of metal nanoparticle assemblies that originate from external interactions with a precise structural arrangement, is the so called photonic band gap.

The photonic band gap is a range of wavelengths of light that cannot propagate through a material, and comes about in an analogous way to the formation of an electronic band gap in a semi conductor. To understand this, consider the example of an infinite *periodic* array of spherical metal nanoparticles. Light that enters such an arrangement will scatter off of the interfaces between the metal nanoparticles and surrounding medium. Normally, such scattering will result in only slight attenuation of the light as it passes through the assembly. However, light with wavelengths corresponding to approximately twice the interparticle spacing will scatter such that it destructively interferes with the light scattered from other interfaces in the assembly. [267] This results in no propagation of these wavelengths. Thus, by tuning the interparticle spacing, the wavelength range that is forbidden can be selected. Furthermore, photonic band gaps are not limited to just such structures; alternative structural arrangements can yield photonic band gaps that are selective for different ranges of wavelengths, light propagating in a specific direction or even give different photonic band gaps for different light propagation directions.

It is also important to note that this phenomenon is not unique to metal nanoparticle assemblies; non-metallic materials can be used as long as there is a periodic difference in the dielectric permittivity, and the range of forbidden wavelengths can be tuned for any length scale, not just nanoscale separations. Having said that, the use of metallic nanoparticles is particularly advantageous, because metals have a negative dielectric permittivity, and as such, yield a very large difference in the dielectric permittivity between the metal and surrounding medium, which results in much stronger scattering (than with a smaller dielectric permittivity difference), meaning that the required volume to achieve a photonic band gap is smaller. [268]

1.2.2. Methods of Assembly

As a result of the significant interest in forming ordered nanoparticle assemblies, a large volume of research has been conducted into the methods allowing such assembly. The requirements for a given assembly method will of course vary with the desired application, but ultimately, the ideal assembly method would satisfy the following criteria: short assembly time, simple to apply, a high level of order over macroscopic sized regions, a wide range of possible structures (both 2D and 3D) and a high maximum structural density. Given these stringent requirements, a wide range of approaches have been examined, all of which can be classified based on the *modus operandi*.

Before reviewing these methods however, it is important to note that the morphology of the nanoparticles to be assembled has a significant influence on the assembly process and as such, should be viewed as an additional parameter. One should also bear in mind that in reality, combinations of different assembly methods are sometimes utilised in order to overcome disadvantages inherent to any one particular assembly method. However, the additional complexity involved in the use of multiple assembly techniques generally makes this undesirable.

External Forces

One category of assembly methods involves the use of external forces to arrange the nanoparticles. Perhaps the simplest example of such external ordering forces is the use of solvent evaporation on a colloidal suspension of nanoparticles. [225, 269-277] This involves the suspension of the target nanoparticles into a volatile solvent, and the placement of this suspension onto a clean substrate (fig 1.10a). As the solvent volume is reduced via evaporation, the concentration of the nanoparticles in the suspension is increased (fig 1.10b) until a point is reached where a highly concentrated surface layer has formed at the surface. The particles in this layer adopt a

close packed structure on the substrate surface owing to capillary forces at the solvent meniscus (fig 1.10c)

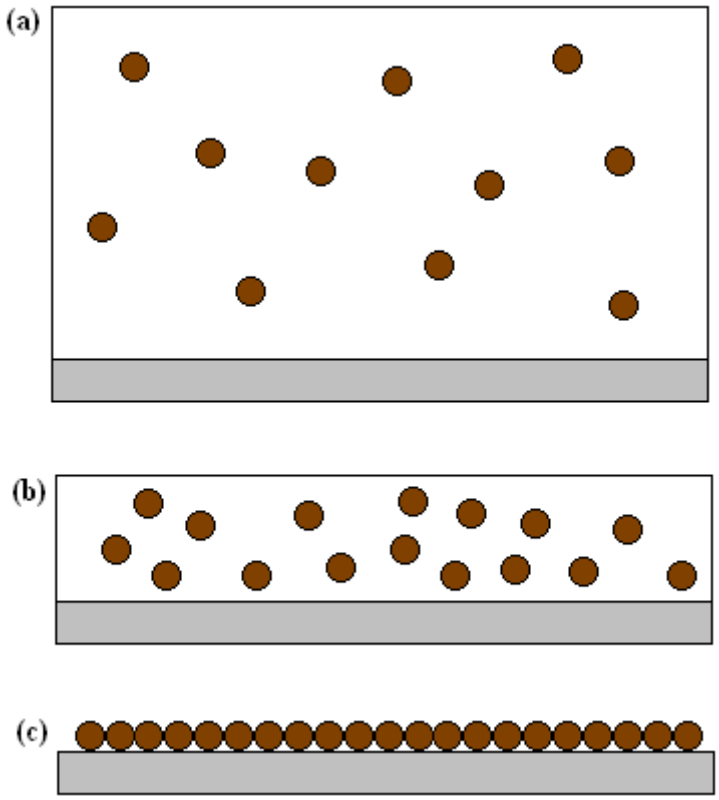

Fig 1.10: A suspension of spherical nanoparticles on a solid substrate (a) immediately after deposition (b) after most solvent has been evaporated (c) after all solvent has evaporated.

This method of forming nanoparticle assemblies possesses a number of advantages; the ordering of the nanoparticles occurs over macroscopic sized regions, such ordering occurs relatively fast and that this method is simple to implement. The principal disadvantage of this method is that it can only be used to form ordered structures from approximately spherical nanoparticles (spheres and other isotropic morphologies), and the structures that can be formed are limited to only close packed sphere structures (known as a superlattice). Control over the exact close packed structure that is formed is also rather limited, as the only parameters that can be modified are the nanoparticle functionalisation (which is principally used to modulate the interparticle spacing and interaction with the substrate) and the composition of the nanoparticle assembly, as the use of two or more nanoparticle types

changes the close packed structure based on the relative sizes and shapes of the various nanoparticles.

Some of the disadvantages of nanoparticle assembly by solvent evaporation can be overcome through the use of another external force, such as an electric field. Electric fields can be used in one of two ways. [278-281] Firstly, an electric field can be used to drive the close packed assembly of *charged* nanoparticles onto the substrate (in this case an electrode) from suspension to form structures in much the same way as solvent evaporation (fig 1.11a,b), but with more control over which regions of the substrate the nanoparticles deposit on (only those regions that are acting as an electrode will attract nanoparticles). This means that the deposition of non-spherical nanoparticles into ordered structures is possible (fig 1.11c). [282] Alternatively, electric fields can be used in combination with solvent evaporation as a means of enhancing control over structure formation. For example, charged nanowires in a suspension may be aligned through the use of an electric field parallel to a substrate, and the solvent then evaporated to deposit the nanowires onto this substrate (fig 1.11d). [283] In a similar way, the application of external magnetic fields can be used to accelerate the deposition process, or influence the ordering of deposited magnetic nanoparticles. [284-287]

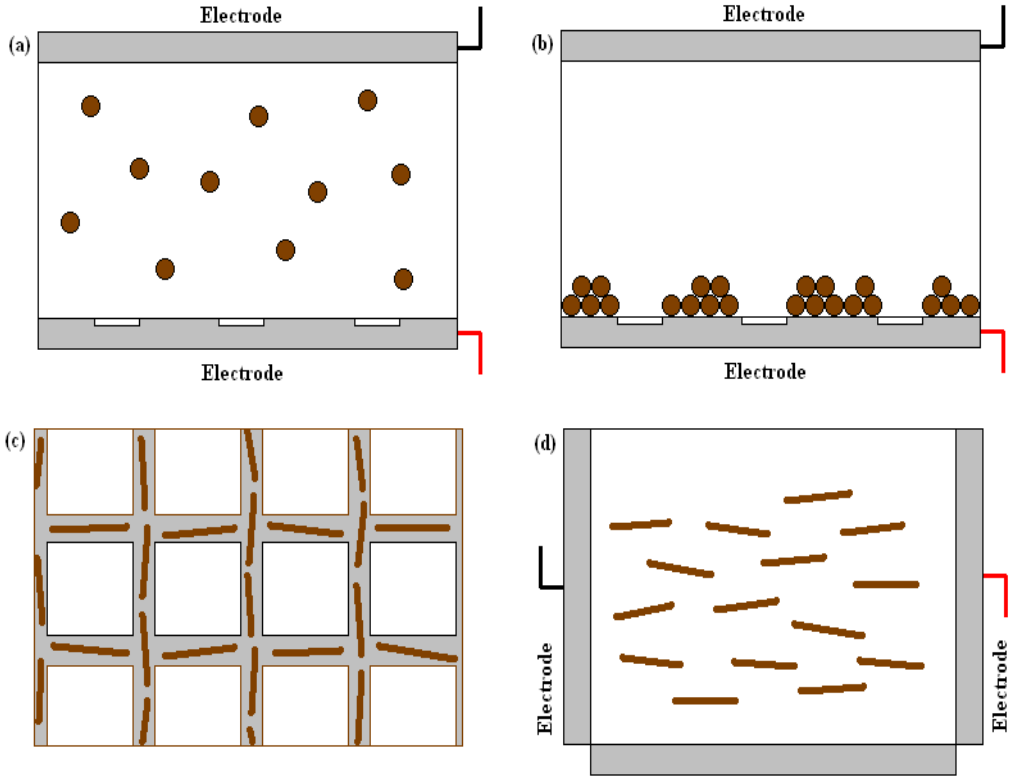

Fig 1.11: A suspension of spherical nanoparticles between a patterned substrate electrode and counter electrode (a) before the electric field is applied and (b) when the electric field is applied. (c) shows an example top-down view of the deposition of nanowires onto a patterned electrode substrate. (d) depicts alignment of nanowires in solution by an electric field prior to deposition onto a substrate by solvent evaporation.

Clearly, the application of electric fields to nanoparticle assembly is advantageous as it extends the range of structures accessible by the solvent evaporation assembly method. However, the use of electric fields introduces a number of complications, such as the fact that particles with high dielectric constants (or alternatively surface charges) are now required and substrate composition is limited to electrically conducting media. In addition, the formation of truly complex structures using this method principally comes about due to the use of a patterned electrode substrate, which in itself needs to be formed prior to deposition. Forming nanoscale patterns with high structural density and complexity is quite difficult in practice, thereby limiting the usefulness of this method of nanoparticle assembly. Methods by which such nanoscale patterns are formed are examined later in this review.

Another way of forming nanoparticle assemblies through the application of an external force is the use of Langmuir-Blodgett (LB) assembly. [254, 260, 288-291] LB assembly initially involves the sequestration of nanoparticles at a liquid-air interface by selecting the functionalisation on the nanoparticles and solution such that they are immiscible (fig 1.12a). This is then followed by reduction of the surface area of this interface (known as compression), which leads to a commensurate reduction in the interparticle separation (fig 1.12b). Depending on the nanoparticle morphology, this packing can result in close packed structures (spherical or approximately spherical) [292] or parallel nanowire arrays. [293] The nanoparticle assembly at the interface is then transferred to the surface of a solid substrate, and the process can be repeated to form a multilayer structure. [294] Due to their similarity to solvent evaporation based assembly (both methods involve the increase in concentration of the nanoparticles) these two techniques share many of the same advantages and disadvantages. However, the LB assembly is a quicker technique for the formation of 2D assemblies, though slower for the assembly of 3D assemblies, and significantly, LB assembly can be used to order anisotropic nanoparticles into simple structural arrangements. [288]

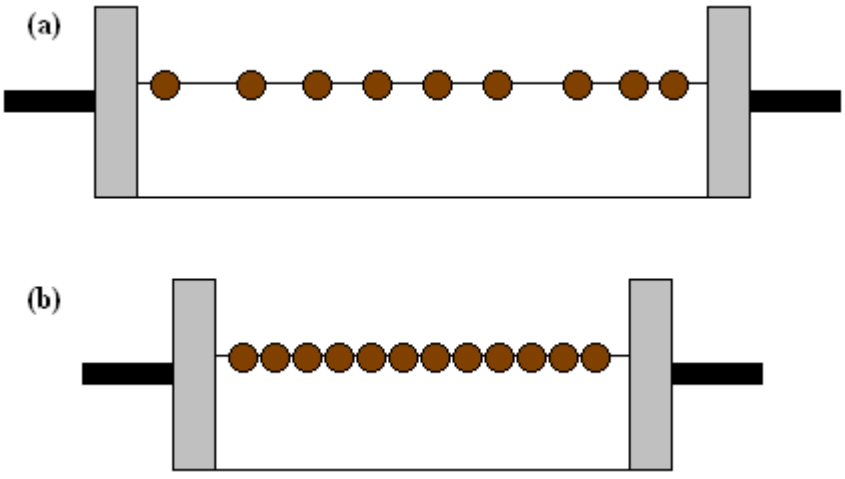

Fig 1.12: (a) functionalised nanoparticles at the liquid-air interface (b) close packed nanoparticles when the interfacial area is compressed.

A very different way of forming nanoparticle assemblies through the use of external forces is by the direct placement of nanoparticles. This is typically enacted by the use of Scanning Tunnelling Microscope (STM) probes to apply

an attractive force to a nanoparticle, and to utilise this force to place the nanoparticle in a specific location on a solid substrate. [295-296] Unlike the other external force based assembly techniques, this method allows for the assembly of nanoparticles of widely varying morphologies into a broad range of complex, densely packed structures with very precise placement. However, as the nanoparticles need to be addressed individually, this method in not feasible for large scale assembly.

Interparticle Interactions

The second category of nanoparticle assembly methods encompasses techniques that utilise interparticle interactions which promote their *self-assembly* into ordered structures.

One of the most prevalent examples of this is the use of electrostatic attraction. This method involves creating a surface charge on the nanoparticles, which then leads to attraction between oppositely charged nanoparticles, resulting in self assembly into close packed structures, with an interparticle spacing that is determined by the size of the molecules that the nanoparticles are functionalized with. [297] Control over the exact structure that is formed can be achieved in a number of ways. One approach involves incorporating a range of nanoparticle types (distinguished by different composition, size, morphology and surface charge) into the structure, where the collective interaction results in different forms of close packing. [298-300] An extension of this is the use of molecules with charged functional groups, such as polyelectrolytes, to attract oppositely charged nanoparticles, and thereby form alternating multilayered structures. [301-302] Structural control can also entail selectively functionalizing different sections of the individual nanoparticles with different charges. One example of the latter is the use of so called segmented nanorods, which consist of discrete segments of differing composition. By carefully selecting the segment's compositions to each yield a unique surface chemistry, selective functionalisation can be achieved. [303-305] The use of electrostatic interactions between the nanoparticles for assembly possesses many of the same advantages that are inherent to

assembly by solvent evaporation, with the additional benefits of not requiring a solid substrate for the assembly to occur, the resulting structures being more mechanically stable (owing to the strong interparticle interactions) and a greater variety of structures being accessible. Having said that, the range of structures that can be formed, although greatly expanded compared to the methods discussed so far, are still limited, and disordered structures can result if the charges on the particles change.

In a similar way, magnetostatic interactions can also be used to form nanoparticle assemblies. This form of interparticle interaction is advantageous in that it not only allows for the formation of close packed structures [306], but other structural morphologies as well (such as nanoparticle chains). [285] Although, in contrast to electrostatic interactions, less structural diversity and control is available due to the nature of the magnetic interaction (each nanoparticle is a magnetic dipole) and the fact that the magnetic interaction is dominated by the nanoparticles composition, and so other parameters such as nanoparticle morphology and functionality cannot be readily used to alter the interparticle interactions.

Another example of an interparticle interaction that has been utilised in the formation of nanoparticle assemblies is chemical bonding. Functionalisation of the nanoparticles with molecular species possessing functional groups that, under the right conditions, form chemical bonds with molecules on the surface of other nanoparticles enables the particles to link together. Such bonding can take the form of covalent bonds [88, 307-310] or utilise secondary bonding forces. [311-313]

As with other interparticle interaction based assembly techniques, this form of assembly typically results in close packed structures. Explicit control over the assembly structure is also afforded in much the same way; through the inclusion of multiple nanoparticle types and selective functionalisation of the nanoparticle surfaces e.g. striped nanorods. However, owing to the wide range of possible chemical functionalities, and hence the many types of bond that can be formed, these interactions are explicitly controlled by the nanoparticles

functionality, affording an extra dimension of structural control. Furthermore, the fact that the chemical bonding (particularly in the case of secondary bonding) is controlled by the reaction conditions (such as the presence of other chemical agents and the temperature) allows for even greater control over the assembly process and resulting structure. The use of chemical bonding also lends itself to a very high degree of specificity i.e. only nanoparticles (or sections of nanoparticles such as is the case for striped nanorods) with the corresponding functionalities will interact and link up, thereby allowing additional structural complexity. Such specificity is exemplified in the use of biological molecules in the assembly of nanoparticles. For example, the use of single helices of DNA which only bond with helices that exhibit the exact combination of corresponding base pairs. [314-317] Similarly, antibody-antigen interactions [318] and protein interactions such as biotin-streptavidin also carry high specificity. [319-321]

Given that this method of nanoparticle assembly is essentially the same as other interparticle interaction based assembly methods, it shares many of the same advantages. The higher number of parameters involved in the use of this form of interaction greatly expands the range of nanoparticle assembly structures that can be formed. Yet, for the most part, this method is still limited to the formation of close packed assemblies

Template Patterning

This third group of nanoparticle assembly methods involves the use of a patterned template (a pre-existing nanostructure or scaffold) to confine and direct the nanoparticle placement into ordered structures, with the assembly itself typically being driven by the use of either interactions between the particles and the template or through the application of external forces. As such, these methods allow for the widest range of assembly configurations, while retaining many of the advantages offered by other techniques for nanoparticle assembly.

There exists a number of ways by which a template may be applied to direct nanoparticle assembly. One example uses the interactions between functionalised nanoparticles and a surface consisting of discrete regions that have been selectively functionalised. The attractive interactions between the nanoparticles and the correspondingly functionalised regions of the surface lead to confinement of the nanoparticles to these areas, thereby directing the nanoparticle assemblies' structure. Common interactions employed in this way include the use of electrostatic attraction [88, 219, 322-327] covalent bonding [88, 328-330] and secondary bonding, particularly that which occurs between associated biological molecules, such as DNA [331-332] and proteins [333] as the high specificity of their interaction allows for the very precise and exclusive placement of nanoparticles in surface regions functionalised with the corresponding conjugate biological molecule. The use of such interactions can also be extended to 3D matrices. For example, the use of complex fluids consisting of polymer/lipid mixtures which form nanoscale compartments of hydrophilic and hydrophobic fluids, where appropriately functionalised nanoparticles are confined to either phase. [334]

An alternative way by which templates can be used to direct the assembly of nanoparticles is to use the void spaces that are present in some forms of template to physically confine pre-made nanoparticles. This is done by drawing the nanoparticles into the void spaces (typically through the use of an external force) whereupon the location and orientation in the case of anisotropic nanoparticles is dictated by the template void structure. Common examples of this is the use of porous membranes such as alumina [335-336] and microfluidic channels. [337]

A further way by which templates can be used to direct nanoparticle assembly is through the in situ growth of the nanoparticles, through the confinement of the growth species within the template, followed by reduction of the growth species. The subsequent growth of the nanoparticles is restricted by the template and thus, control is afforded over the nanoparticles structural arrangement. There are two main types of template that are used in this way; porous substrates and matrices. Porous substrates confine the growth species

to void spaces within the template, and thus the assembly structure replicates that of the templates void spaces. Examples of the use of this form of template include; porous membranes made from alumina and track-etched polycarbonate, [147, 177, 338] lithographically etched substrates [117, 339], bacterial S-layers (two-dimensionally ordered self-assembled films of proteins that feature in many bacterial cell walls) [340-343] and the step edges of atomic planes on surfaces such as highly oriented pyrolytic graphite (HOPG). [344]

Matrices, on the other hand, involve the initial dispersion of the growth species throughout a matrix, followed by selective reduction of the growth species at particular spatial locations (such as by the photoreduction of metal precursors in a matrix by a laser). In this way, growth occurs only at the desired locations, and the structural arrangement of the resulting nanoparticles can thus be controlled. The principle example of this method is the use of lasers to “write” patterns of nanoparticles in an optically transparent matrix (such as an organic polymer or sol-gel), either through reduction by laser pyrolysis [345] or by photoreduction using laser pulses. [346-348] Note that this method typically results in lines of small spherical nanoparticles rather than single continuous nanoparticles. As such, electroless reduction of surrounding metal growth species is required to join the nanoparticles into a larger structure. [166]

1.2.3. Template Formation

Although the use of a template to direct nanoparticle assembly allows for the precise placement of nanoparticles into a very wide range of assembly structures, where interactions or external forces drive the assembly process (fast assembly over large regions), the reliance on a template to direct the assembly of the nanoparticles can also serve as a weakness. Complex templates can only be formed by either using top-down nanostructure fabrication methods (principally lithography) or by combining a multitude of simpler (and easier to form) template materials.

Lithography

Lithography involves the etching or deposition of material onto a surface to form nanoscale patterns. The most common, photolithography, involves a photosensitive material being exposed to EM radiation (of wavelengths ranging from visible to ultra-violet to X-rays) in order to introduce some latent image into the material (usually some change in the solubility or chemical reactivity of the substrate). These regions (or alternatively the unchanged substrate) are then selectively etched using appropriate chemicals in order to develop a one or two-dimensional patterned structure. [253] Although this technique by itself is relatively simple and quick to implement, it has a number of disadvantages. Firstly, it requires some sort of pre-made patterned mask through which the radiation is shone, to ensure that only the selected regions of the substrate are exposed to the radiation and are thus etched to give the desired topology and periodicity. The fabrication of these masks is often a time consuming process. [349-350] Secondly, the use of EM radiation means that there is an intrinsic limit to the resolution of the structures that can be formed due to the diffraction limit of light. [350-351] Although shorter wavelength light can be used to improve the pattern resolution, photolithography typically uses a lens to focus the image from the light passing through the mask, so that masks much larger than the patterned structure can be used. Short wavelengths (such as extreme UV and x-rays) are

more difficult to work with as they cannot be easily focussed using conventional optics. In addition, the high-energy nature of such radiation is damaging for many materials that are used as masks and substrates, [350-351] and so the formation of 3D structures is quite difficult.

An alternative is electron/ion lithography, where etching is performed directly using beams of electrons or charged ions that are scanned across the substrate to etch the desired nanostructure patterns. [349] As beams of particles are used as opposed to EM radiation, the inherent size limit of features that can be formed is significantly smaller (as electrons and atoms diffract at atomic length scales) and a mask is not required. [350-351] However, this technique is a very time consuming as a single beam forms the nanostructures.

As opposed to the aforementioned techniques where selective etching is used to form the desired template structures, deposition lithography involves material being deposited upon a substrate in a controlled manner to form 2D patterns. There currently exist a number of deposition lithography techniques, such as micro contact molding, micro contact printing and dip-pen nanolithography that can be used to form 2D surface structures. [350-351] In micro contact molding, a pre-patterned stamp consisting of a surface with etched trenches is placed in contact with a substrate, and the open trenches are filled with some liquid (usually a liquid polymer) using capillary action. Subsequent UV or thermal curing hardens or cures the polymer and then the stamp is removed, leaving the surface pattern. [350-352] In the case of micro contact printing, this same type of stamp is “inked” with a layer of molecules that bind to a given substrate. The stamp is then placed into contact with the substrate, such that the molecules on the non-etched areas are transferred to the substrate surface. [350-351] Both of these methods allow for simple and fast patterning of large surface areas. However, creation of the stamp itself can be difficult (it requires the use of high resolution lithography) and the formation of 3D structures is very difficult. Dip-pen nanolithography involves the transfer of molecules to a substrate via a solvent meniscus at the contact point between a substrate and an AFM tip. [350-351] The tip is scanned over the substrate, with the molecules being deposited only in the specific written

areas. Such tips are extremely sharp (several atoms wide at the end contacting the subtrate) and so allow for very high resolution patterning. However, as with all scanning based methods, it is very time consuming when applied to large areas.

Chemical Synthesis / Self-assembly

The difficulties associated with the formation of templates using lithography (at least one step that takes a long time to implement or low structure resolution) mean that templates that require these methods are not ideal for use in nanoparticle assembly. However, there are a number of other template formation methods which do not possess such limitations. For example, many nanoporous templates (such as porous alumina and track etched polycarbonate) are formed using bulk chemical etching techniques that are fast, easy to apply over very large length scales and allow the formation of controlled, nano-sized void spaces. Likewise, template formation using self-assembly, where the material that comprises the template spontaneously assembles into an ordered configuration due to attractive and/or repulsive interactions, possesses the same advantages. [353] Although these templates are much more easily formed, and often form 3D structures, the trade off is that there is less direct control over structure formation, and for many of these templates, only one possible structure. The range of templates available means that a wide range of structures may be formed. However, a different type of template is needed for each nanoparticle assembly, and typically, a multitude of template materials need to be combined to form complex 3D structures.

Exceptions

Most available template materials fall into either of the aforementioned categories. There do exist, however, a few exceptional materials that can form multiple, complex structures through rapid, simple processes. One of the most promising of these template materials are block copolymers.

1.3. Block Copolymers

1.3.1. Definition

Block copolymers are polymers whose chains consist of two or more chemically different macromolecules (or blocks) that are covalently linked together at their ends to form a single chain. [354] There are many different chain architectures for block copolymers, the complexity and diversity of which depends upon the number of distinct species in the chain. When two monomers A and B are present, the architectures include simple diblock (AB), triblock (ABA), pentablock (ABABA), segmented (multiblock) $(AB)_n$ and star copolymers (AB)X. If additional chemically distinct monomers are added, the number of possibilities increases dramatically. [355] Some examples of block copolymer architectures are depicted in fig 1.13.

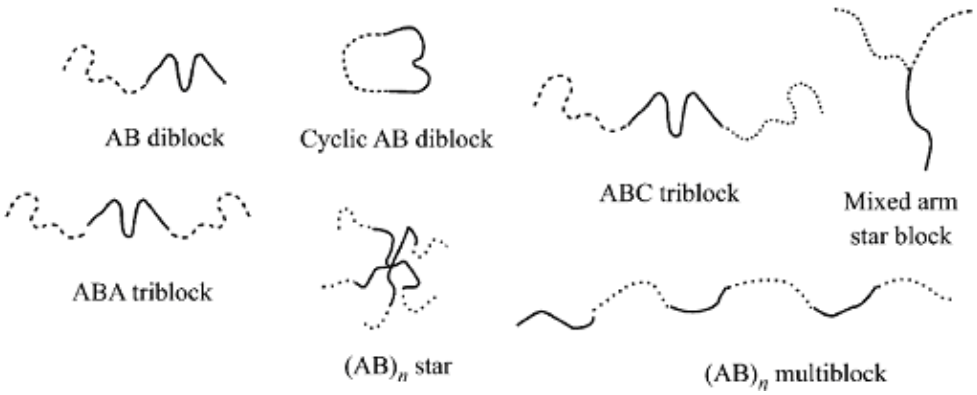

Fig 1.13: Examples of block copolymer chain architectures. [356]

The fact that such materials are composed of more than one type of polymer means that they can possess unique hybrid properties that result from their different chemical and physical natures. One of the most characteristic features of block copolymers that is useful for nanoparticle assembly templating is microphase separation.

1.3.2. Microphase Separation

Microphase separation arises in block copolymers due to the repulsion that occurs between chemically distinct polymer chains even when the repulsion between the respective constituent monomers is relatively weak. [354, 357] Such repulsion tends to lead to segregation (phase separation), but as the different blocks are restricted in their connectivity, this doesn't lead to macrophase separation as would be the case for a mixture of two homopolymers. Instead, the blocks segregate into chemically distinct microdomains that are periodically spaced throughout the solid. [357-358] Such microphase separated materials can assume a number of different morphologies depending upon the polymer architecture, the thermodynamics of the system and the blocks' relative volume fractions. The work covered in this thesis involves the use of amorphous (that is non-crystalline) AB diblock copolymers, so the following discussion will focus on this class of block copolymer. In order to see how these factors affect the microphase separation, one must consider the forces at play during the phase separation process.

Microphase separation is driven by mutual repulsion between dissimilar blocks, meaning that the system tends towards minimising the surface area of the interface between the microphases (the intermaterial dividing surface or IMDS) in order to achieve the smallest degree of contact between dissimilar blocks, thereby minimising this enthalpic contribution to the free energy. [357] However, from an entropic standpoint, the chains prefer to adopt a randomly coiled arrangement as this increases the entropy (and hence reduces the free energy). Thus, the overall chain configuration (morphology) is determined by the interplay between these competing forces, with a stable configuration occurring when thermodynamic equilibrium is achieved. One way in which this competition can be quantified is through the Flory-Huggins parameter χ. [357]

χ is a measure of the effective interaction that occurs between individual monomer units that comprise the block copolymer. [357] For sufficiently

large positive χ values, the repulsion force between the copolymers blocks is strong enough to overcome the entropy considerations and so microphase separation results. If χ is zero or very small, entropy is the dominant force and the polymer blocks mix amorphously. Furthermore, the degree of influence of χ on the microphase separation is moderated by the number of monomer units N in (or molecular weight of) the copolymer chain. [357] A large number of monomer units support segregation more so than smaller chains as there is a greater overall repulsion between the dissimilar blocks. So, when considering the mutual repulsion between the copolymer blocks, it is χN that is used. This parameter allows us to define three microphase separation regimes; the disordered regime ($\chi N<10$) where the entropic forces dominate and the polymer blocks amorphously mix [359], the weak segregation regime ($\chi N\sim10$) where the energetic and entropic forces are balanced such that limited segregation occurs but the individual copolymer chains are relatively unperturbed, and the strong segregation regime ($\chi N>50$) where repulsion forces dominate and a high level of segregation occurs. [360] † The segregated regimes may be further characterised by the relationship between the size of the microphases (larger for stronger repulsion) and the thickness of the interfacial region (IMDS) between microphases (larger for weaker repulsion). The periodicity of the microphases (and hence the microphase dimensions) is quantified by the following relationship: [359, 361]

$$d = a\chi^{\delta} N^{\delta+0.5}$$

Where a is the monomers statistical segment length, δ is a factor that scales with χN ($1/6$ for strong segregation and up to 0.45 for weak segregation) and d is the microphase periodicity [362-363], while the interfacial thickness is entirely dependant on the factor $\chi^{-1/2}$. [364-365]

As such, strong segregation is characterised by thin interfacial regions relative to the microphase dimensions i.e. the domains consist almost purely of one

† Note that the quoted values are for symmetric diblock copolymers; in the case of an asymmetric block copolymer (one block comprises the majority of the polymer volume), these limits are higher, as the total interaction that can effectively occur between the two blocks is reduced.

block or the other. In the weak segregation regime, interfacial thickness is of commensurate size to that of the microphases, such that a sinusoidally varying composition profile between the microphases results (fig 1.14).

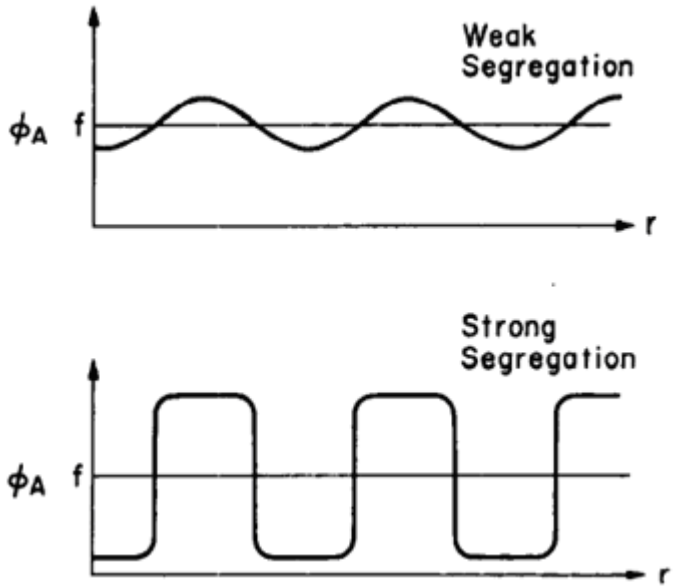

Fig 1.14: Composition profile for the cross section of a diblock in the weak segregation and strong segregation regime. [359]

While χ and N determine if phase separation occurs, these parameters do not control the exact structure that the phase separated domains will assume when the system reaches thermodynamic equilibrium. This is determined by the relative volume fractions of the copolymer blocks, as this dictates the form of the smallest surface area IMDS. To conceptualise this, consider a linear AB diblock copolymer where each block occupies an equal volume fraction in the material (50% A and 50% B). In this case, the IMDS that gives the smallest interfacial surface area (and hence lowest free energy) is a lamellar arrangement; all other configurations result in a greater interfacial surface area. If however the volume ratio of A and B changes, for example such that A is now the minority phase, then the lowest surface area IMDS (equilibrium morphology) that the system will tend towards will also change by increasing the radius of curvature of the interface (as this results in the lowest possible surface area). [358]

By taking the above factors into consideration, a phase diagram can be constructed that describes the state of a block copolymer at thermodynamic equilibrium for a given composition and chain length. Fig 1.15 shows a typical phase diagram for a symmetric diblock copolymer as computed using self consistent mean field theory, which depicts the phase morphology that results for a particular combination of chain interactions (χN) and composition (volume fraction of one of the blocks) denoted by f. The region labelled by *dis* is the disordered state that results when the repulsion between the blocks is small enough that entropy is the dominant force. Above a certain critical value of χN (the order-disorder transition) inter-block repulsion dominates, resulting in one of seven periodic phase separated morphologies. For volume filling fractions $0 < f < 0.21$, a body centred cubic (*bcc*) array of the minority block in the majority block is the resulting phase morphology. If the volume filling fraction of the minority block is $0.21 < f < 0.33$, a hexagonally packed array of parallel cylinders (*hex*) of the minority block is the result. For volume fractions $0.33 < f < 0.37$, a double gyroid or double diamond network structure (*gyr*) is formed. For volume fractions of $0.37 < f < 0.5$, a lamellar phase morphology (*lam*) is achieved. At higher volume fractions, the same morphologies are achieved (in reverse order) but with the other block in the diblock copolymer becoming the minority block. [253]

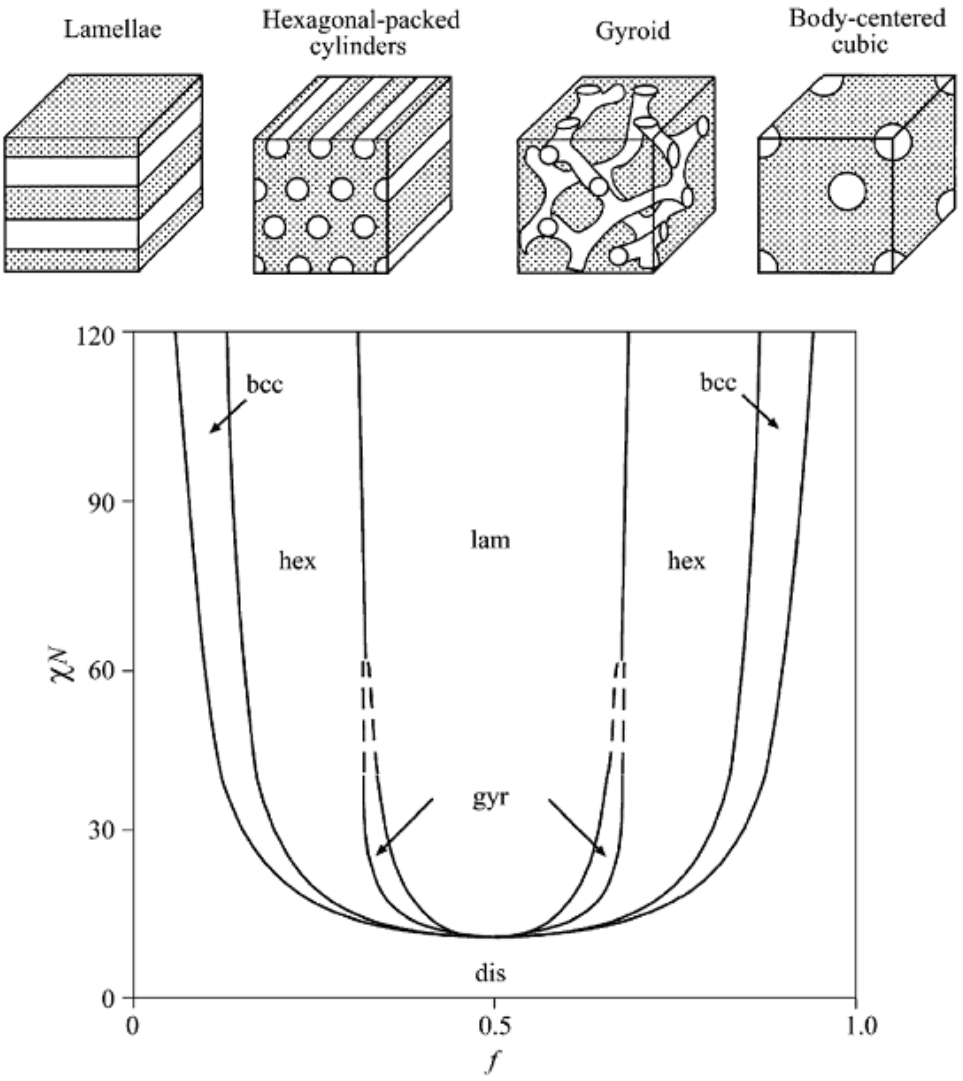

Fig 1.15: Phase diagram depicting the morphology of a diblock copolymer at thermodynamic equilibrium as a function of volume fraction of one of the blocks (f) and the strength of inter-block repulsion (χN). [356]

The phase behaviour of more complex architectures such as three component ABC triblock copolymers is much richer than two component block copolymers, as expected due to the multiple interactions that take place (χ_{AB}, χ_{AC} and χ_{BC}) that result from the increased number of chemically distinct components. [356] As a consequence of this increased complexity, a phase diagram for such a block copolymer has yet to be devised. Some examples of microphase separated morphologies for a three component triblock copolymer at thermodynamic equilibrium are given in fig 1.16.

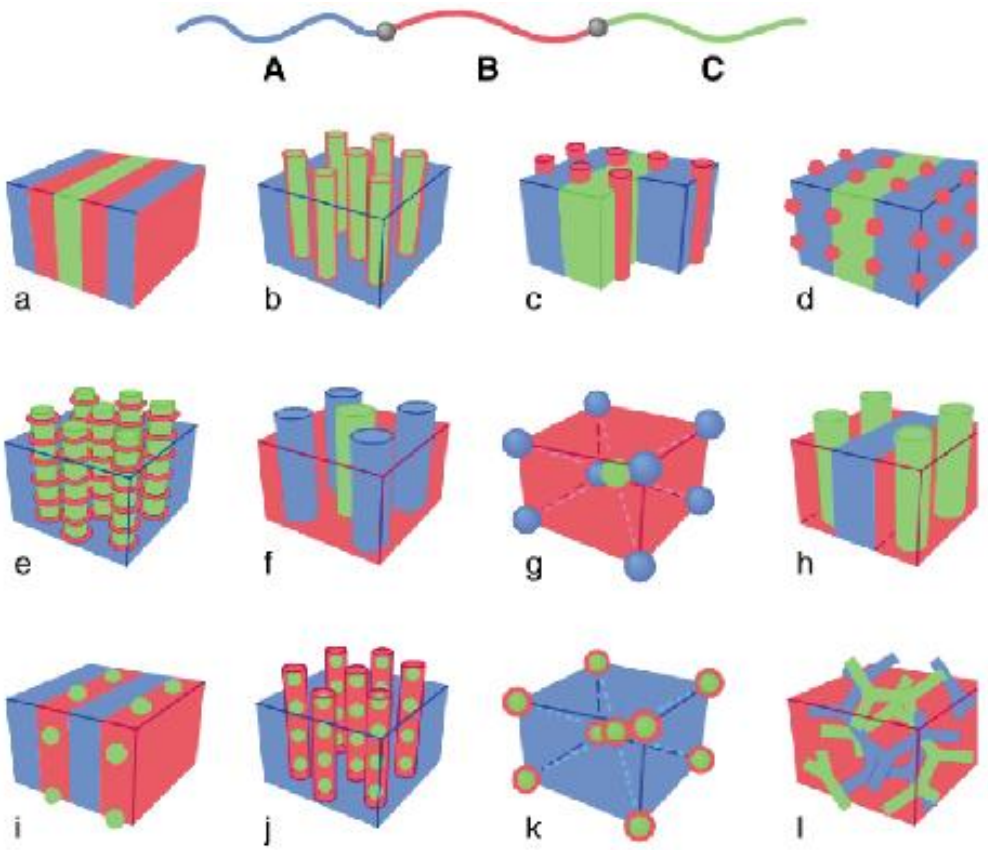

Fig 1.16: Microphase separated morphologies for a triblock copolymer containing three chemically distinct blocks of varying volume fraction at thermodynamic equilibrium. [253]

Thermodynamic Equilibrium

In order for a block copolymer to assume one of these microphase separated morphologies, the polymer must be able to approach thermodynamic equilibrium. However, when a block copolymer is first synthesised and collected, it is typically in a disordered form, and is unable to reach thermodynamic equilibrium as the chains are kinetically inhibited from rearranging their configuration. This constraint may be lifted by improving polymer chain mobility, which can be performed by either raising the polymers temperature or by dissolving in a suitable solvent. However, such approaches also lead to a decrease in the effective repulsion between the copolymer blocks, either due to the increased kinetic energy from heating overcoming this repulsion, or due to the solvent shielding the repulsion. Therefore, in order to achieve thermodynamic equilibrium, a compromise between these two factors is required: an increase in chain mobility, but not to

the extent that the repulsion between blocks is overcome. The block copolymer is then left under these conditions for a period of time (the required time being greater for progressively more asymmetric block volume fractions) to achieve a state close to thermodynamic equilibrium (as the interaction between the blocks is still partially reduced). [366] The required time period is typically shorter for higher χN, but high N can also lead to a greater extent of chain entanglement and thus lower chain mobility. [367] The block copolymer is then slowly returned to a solid, room temperature state in order to subject the blocks to a steadily increasing repulsion force, while allowing the chains to reconfigure in response, until thermodynamic equilibrium is essentially obtained and "locked in" due to the now relatively immobile polymer chains.

Microphase Orientation

It is important to note that during a typical microphase separation process, the microphase structure forms by nucleation at various locations throughout the polymer, with subsequent growth of the microphase structure from these points. As a result, the block copolymer does not exhibit globally ordered structures. Rather, the microphase structure can be envisioned as consisting of randomly oriented "grains" within which there is excellent short range ordering between the microdomains. The "grain size" of these regions is typically on the sub micron scale (figure 1.17). [368-369]

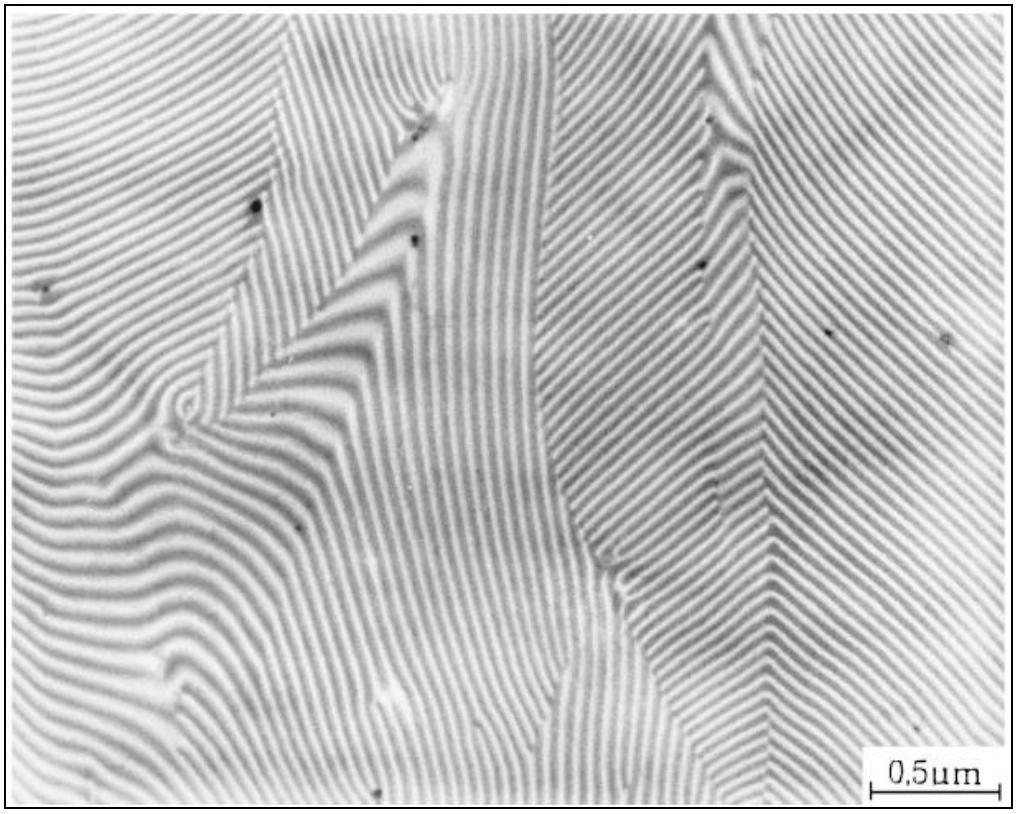

Fig 1.17: An example of the short range ordering of block copolymers as seen in a lamellar microphase morphology. [370]

Long range ordering of the microphase structure, and more importantly, control over this long range ordering, is necessary so as to optimise the use of these systems as templates for nanoparticle assembly. Such ordering can be attained by imposing additional forces on the block copolymer during the microphase separation process. One commonly used example is the implementation of a concentration gradient in a block copolymer that has been swelled with solvent in order to achieve thermodynamic equilibrium. Initially, the polymer is swollen with solvent such that the repulsion interaction between the blocks is negated. If the solvent is allowed to very slowly evaporate (the precise rate determining the final orientation of the microphases [371-372], the concentration of solvent at the surface is lowest, and a gradient in solvent concentration develops. Over time, the solvent concentration decreases and microphase separation occurs at the surface. Further evaporation leads to propagation of this ordering, which "grows" from the ordered morphology initiated at the surface and extends throughout the

polymer. [372-375] Temperature gradients can also be used in a similar way to achieve long range ordering of the microphase structure. [376]
This concept has also been applied to the use of selective solvents that form a eutectic mixture with a single block of a copolymer that typically packs into a crystalline structure. When swelled with solvent, the block copolymer is in a disordered state. As the solvent concentration decreases at the surface, the block /solvent solution undergoes a phase transition, which results in the formation of crystalline microphases. Continued solvent evaporation leads to growth of these crystalline phases further into the polymer with matching structural orientation. [377-381]

Another way by which external forces can be used to induce long range structural order is through taking advantage of the differing response of each polymer block to an external force. One example of this is the response of a block copolymer to an applied electric field. Polymer blocks with different dielectric constants will respond to an applied electric field to varying extents. The block with the highest dielectric constant interacts most strongly with the applied field and upon microphase separation, dominates the microphase structural ordering by forming microdomains that align with the applied field. [382-384] Mechanical flow fields have been used in a similar way to induce long range orientation of block copolymer microdomains, by taking advantage of viscosity differences between the blocks upon mechanical shear [385-388] or compression. [389-390]

A different approach to achieving long range order of microphase structures in a block copolymer (particularly in thin films) involves the use of interactions between the block copolymer and the substrate upon which it is cast. One example of this is the use of substrates where preferential wetting of the surface by one of the chemically distinct copolymer blocks occurs. This interaction nucleates microphase separation at this interface and upon cooling of the polymer or removal of the solvent, induces local ordering of the microphase structure, which subsequently propagates through the polymer. [391-393] Chemically patterned substrates have also been used in the same way to direct microphase structural orientation. [394-399] One illustration of

this is the use of parallel stripes of different chemical functionality to orient lamellar microphases perpendicular to the substrate. It is important to mention that this interaction between block copolymer and substrate can be mediated by the inclusion of nanoparticles into a particular block domain, as this can change that blocks surface energy. [400]

A further way by which long range microphase structural ordering may be imposed is by the introduction of spatial confinement of the block copolymer (between solid surfaces for example). Such confinement, particularly over length scales equivalent to tens of microphase periods or less, leads to structural orientation perpendicular to the axis of confinement, as short range ordering of the microphase structure is more difficult to achieve for other orientations (assuming no preferential interactions between the block copolymer and confining substrates). Both lateral confinement i.e. trenches and grooves [369, 401-402] as well as height confinement (thin films) has been performed. [403-409] Importantly, the spacing of the confined dimension must be considered, as confinement to anything but whole numbers of structural periods (or unit cells) can lead to the formation of new, strained morphologies [410-411] such as hexagonally packed spheres [412] or ellipsoidal microphases. [413]

1.3.3. Synthesis

One of the most important considerations regarding the formation of a microphase separated block copolymer is the synthetic method used in its fabrication. Although conceptually the synthesis of a block copolymer is simply a series of single block polymerisations (the formation of an initial block with subsequent extensions of this chain sequentially using different monomers), the method used needs to be carefully selected, as any given method is only applicable to a select range of monomers and chain configurations, must form polymers with active chain ends that can undergo chain extension, and in particular, should provide a high level of control over parameters such as block length (and consequently relative block volume fractions), with little variation between polymer chains. This is necessary if microphase separated block copolymers with well defined morphologies are to be obtained in a controlled fashion; a property that is crucial to the use of these materials as templates for the arrangement of nanoparticles into assemblies.

There exists a number of methods by which the synthesis of the individual polymer blocks can be performed, which can be broadly categorised as either step growth polymerisation or chain growth polymerisation.

Step Growth Polymerisation

In step growth polymerisation the monomer units are linked together by chemical bonds that are typically formed via a condensation reaction (such as that between a carboxylic acid and an alcohol to form an ester), usually with the concurrent release of small condensates such as water or methanol. [414] Such polymerisations are characterised by the systematic step-wise growth of the chains, as depicted in fig 1.18.

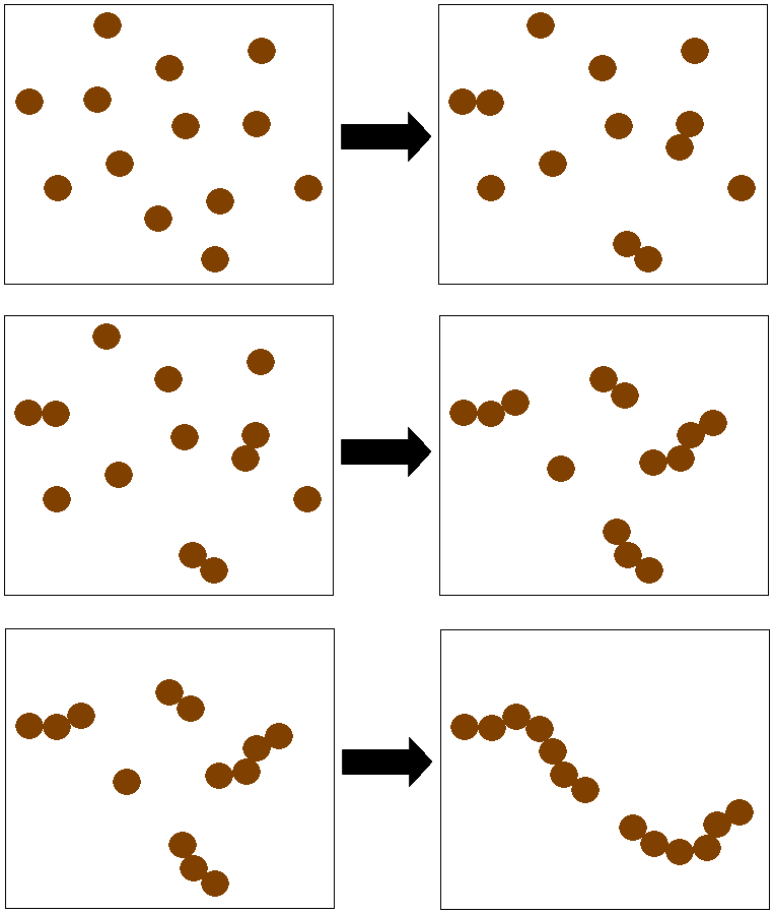

Fig 1.18: A depiction of the progress of a step growth polymerisation.

Initially, reactions between individual monomers dominate as they are the most common species present in the reaction mixture (fig 1.18 top). As the monomers are consumed, reactions between monomers and short chain oligomers, as well as between the oligomers themselves, become more prevalent (fig 1.18 middle). Eventually, reactions between the resulting long oligomer chains are most probable, leading to the formation of small numbers of very long polymer chains (fig 1.18 bottom). [415]

Chain Growth Polymerisation

In contrast to step growth polymerisation, chain growth polymerisation involves the covalent bonding of monomer units containing unsaturated bonds to a specific growth species, with no reactions taking place between the monomers themselves. This method of polymerisation occurs via the following steps: [416]

1) Initiation:

A small amount of a chemical known as an initiator (I), which breaks down to yield free radicals (species with unpaired electrons), is added to the reaction mixture which consists of monomers (M) in some solvent (S). Free radicals are highly reactive species that combine with the monomer, resulting in homolytic cleavage of one of the monomers unsaturated bonds, which in turn converts the monomer to a radical with an active site (the growth species). Ionic species can also be used as initiators, in which case the active site is no longer an unpaired electron, but a charge.

$$I_2 \leftrightarrow 2I^{\bullet}$$

$$I^{\bullet} + M \rightarrow I + M^{\bullet}$$

2) Propagation:

Following initiation of the polymerisation process, propagation occurs. This involves the monomer radical/ion formed from the initiation step combining with a monomer with no active site to form a dimer radical/ion. This process is repeated over time; with more monomers being added to form a polymer chain radical $R_r^{\bullet}$ or ion containing 'r' monomer units. This chain growth process results in a fast increase in polymer chain length, even at relatively low overall monomer consumption.

$$R_r^{\bullet} + M \rightarrow R_{r+1}^{\bullet}$$

3) Termination:

The polymerisation process terminates for a given polymer chain upon the event of one of a number of reactions that removes the chains ionic or radical functionality. One way by which this may occur is when two polymer chain radicals/ions $R_r^{\bullet}$ and $R_s^{\bullet}$ react with one another to either form a single

deactivated polymer chain P_{r+s} (chain combination) or two deactivated chains (disproportionation). The polymer radical/ion can also gain an electron from a monomer or solvent molecule (chain transfer), and so terminate.

Termination by combination:

$$R_r^{\bullet} + R_s^{\bullet} \rightarrow P_{r+s}$$

Termination by disproportionation:

$$R - CH_2^{\bullet} + R - CH_2^{\bullet} \rightarrow R = CH_2 + R - CH_3$$

Termination by chain transfer:

$$R_r^{\bullet} + M \rightarrow P_r + R_1^{\bullet}$$

$$R_r^{\bullet} + S \rightarrow P_r + S^{\bullet}$$

Living Polymerisation

The application of either chain growth or step growth polymerisation methods as described above to the synthesis of block copolymers is in reality rather problematic, principally owing to the lack of control that these methods offer over the very fast chain growth process.

For example, in the case of step growth polymerisation, the polymerisation mechanism is such that there is virtually no way to achieve and maintain a small range of chain lengths and efforts to extend a single block polymer chain with a second monomer can result in more than the desired number of blocks being formed (fig 1.19). [415] As this lack of control over chain growth is intrinsic to step growth polymerisation, it is clearly unsuitable to the formation of clearly defined domains in microphase separated block copolymers.

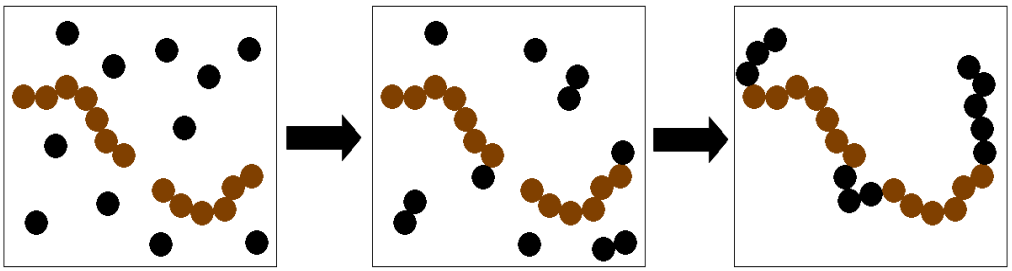

Fig 1.19: Example of step growth polymerisation applied to the extension of a single block to form a block copolymer.

In the case of chain growth polymerisation, a similar lack of control comes about as a result of termination reactions. Different polymer chains undergo termination at different times, resulting in some chains growing for longer periods of time than others and therefore, a range of polymer chain lengths results (fig 1.20). [417] The longer the chains (higher molecular weight), the greater this effect and the higher the probability of termination. This effect is further compounded by combination type termination reactions. Another consequence of these termination reactions is that the chains are no longer active, and so are not able to undergo further growth once terminated, thereby largely preventing the extension of these chains by the addition of a different type of monomer to form a block copolymer.

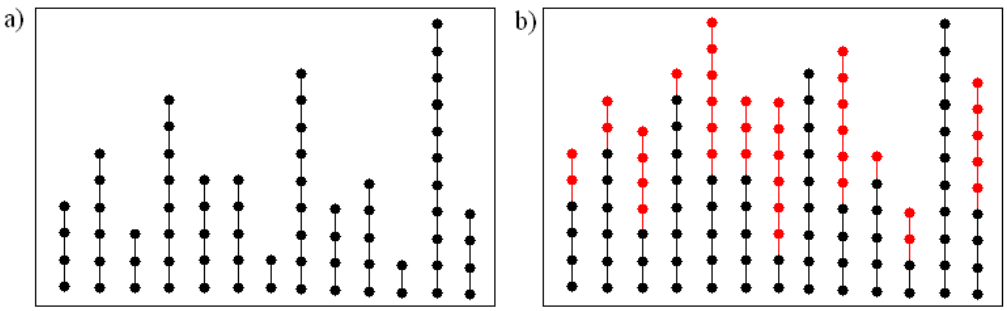

Fig 1.20: A depiction of (a) a homopolymer and (b) a diblock copolymer that result from variation in chain length.

However, as these termination reactions are not intrinsic to the chain growth polymerisation mechanism, it is possible for these reactions to be managed in order to prevent (or at least minimise) their occurrence. Termination by chain transfer (in the case of radical polymerisation) can be limited by strict control of the choice of solvent and reaction conditions such as temperature.

Termination by combination or disproportionation however, cannot be controlled in this way. [416] In order to minimise the occurrence of these other termination reactions, one must utilise so-called “living” polymerisation methods. Living polymerisation techniques employ one of two methods for eliminating termination reactions: a) using ions instead of radicals as the initiator, which results in polymer chains with charged ends that experience a mutual repulsion, thereby preventing termination by combination and inhibiting disproportionation or b) lowering the (instantaneous) concentration of growing polymer radicals, resulting in propagation being much more favourable than termination by combination or disproportionation (reaction between growing polymer chains). One common way by which this is achieved is by introducing a dormant species that exists predominantly over, and in equilibrium with, the growing radical species (fig 1.21). [416]

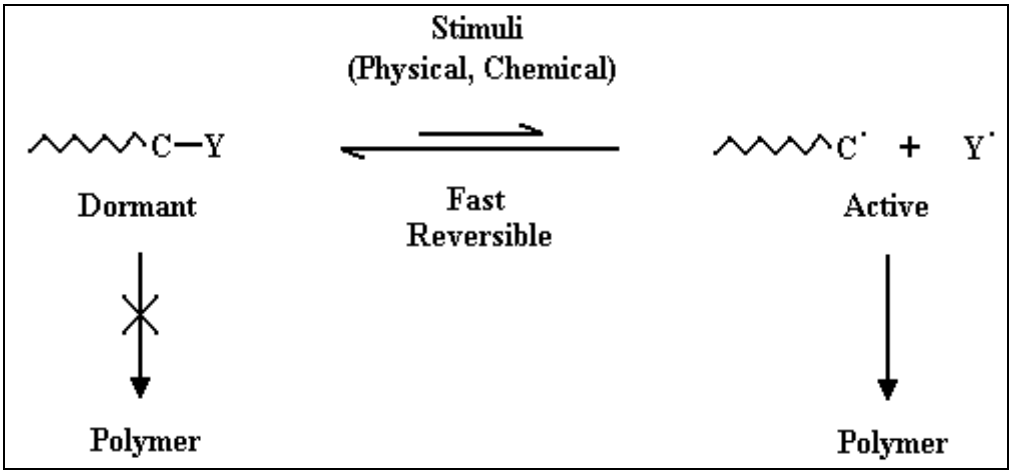

Fig 1.21: Reaction mechanism for a living radical polymerisation showing the equilibrium between an active polymer radical that can undergo propagation (right) and a dormant polymer chain that cannot undergo propagation (left). Note that the equilibrium favours the formation of the dormant species. [416]

Importantly, the reaction rate of this equilibrium must be greater than the rate of propagation (growth of the polymer chains), as this ensures that all the polymer chains have an equal opportunity to undergo propagation. [416] Some polymer chains will otherwise remain active for a long time (compared to the time for propagation to occur) and undergo many propagations, whereas other chains will remain dormant for a relatively long time and so undergo no

propagations (resulting in high polydispersity). [416] If these two conditions are satisfied (low concentration of active radicals that are activated/deactivated at a rate greater than propagation), the result is uniform growth of the chains with virtually no termination, and provided that the growth of all the chains is initiated near simultaneously, uniform chain lengths and molecular weight (a low polydispersity). ‡ Furthermore, at the end of the polymerisation, the vast majority of the polymer chains are in the stable dormant state, from which chain extension may readily occur.

There are four principal living polymerisation techniques that are used to synthesise block copolymers; all follow the previously outlined strategies. Each of these methods only varies in the precise mechanisms or chemical species that are employed to control the polymerisation. These methods include Atom Transfer Radical Polymerisation (ATRP), Nitroxide Mediated Radical Polymerisation (NMRP), Reversible Addition-Fragmentation chain Transfer (RAFT) polymerisation and ionic polymerisation. The first three polymerisation methods utilise a chemical equilibrium to prevent termination while the fourth method utilises mutual repulsion of charges. Note that there exist several other living polymerisation methods (group transfer [418], metathesis [419-420] and Ziegler-Natta catalysed polymerisation [421-423]) that are not examined here, as their application to block copolymerisation will not be relevant to the research undertaken in this thesis.

ATRP

In ATRP, equilibrium between dormant and active radical species occurs through a reversible redox process that is catalysed by a transition metal complex (fig 1.22).

‡ It is important to note that such an ideal system where termination reactions are nonexistent is never achieved in reality. At best, the number of termination reactions is significantly reduced. Thus, these methods of polymerisation are more accurately termed as controlled polymerisation. However, as they possess the characteristics of "living" systems, they will be referred to as living polymerisation in this thesis.

This complex (M_t^n-Y/Ligand) undergoes a one electron oxidation with an associative abstraction of a halogen atom (X) from a "dormant" species, a haloalkane (R-X), yielding a propagating radical species (R·) and modified complex (X- M_t^n-Y/Ligand). This radical species then undergoes propagation with monomers to form a polymer chain. [424] It is important to note that the oxidised transition metal complexes used in ATRP do not undergo reactions with like radicals and so exhibit no termination reactions, unlike the polymer radical species produced in conventional free radical polymerisation. [425]

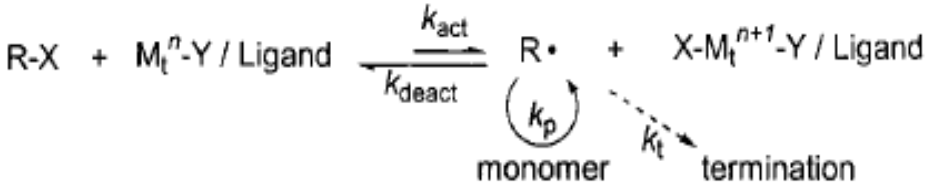

Fig 1.22: Reaction mechanism for ATRP. [424]

ATRP has a number of advantages. Firstly, a variety of chain topologies (linear, graft, star, hyperbranced) and monomer compositions (styrenes, acrylates, acrylamides and acrylonitriles) [424] can be synthesised over a wide range of temperatures (-20^{o}C – 130^{o}C) [426] and in both protic and aprotic media using this method. [427] Secondly, termination reactions are further limited by the so-called persistent radical effect, resulting in even lower polydispersity's. [425] However, ATRP also possesses some disadvantages. Being a multi component system, careful choice of the initiator, catalyst, solvent and reaction conditions is required for the conversion and yield to be optimised. [424] The presence of oxygen and other radical scavengers also needs to be avoided if a controlled polymerisation is to occur. [424] The requirement for unconventional initiating systems that are often incompatible with the polymerisation media is also a problem in using ATRP. [417] Purification of the resulting polymer is also required, to remove the transition metal complexes. [428]

In recent years, modifications to this method of controlled polymerisation have been developed that overcome many of these disadvantages. Chief among these is the development of ARGET (Activators Regenerated by

Electron Transfer) ATRP. In a typical ATRP reaction, the presence of radical scavengers (like oxygen) and a small number of termination reactions during polymerisation lead to the irreversible oxidation of some of the transition metal complex. As a result, a large amount of complex and high levels of reagent purification are required to achieve a well controlled polymerisation. ARGET ATRP utilises a reducing agent (such as tin 2-ethylhexanoate [429] or ascorbic acid [430] to reduce the oxidised complex back into its active form, thereby providing more tolerance for the presence of impurities and reducing the amount of catalyst required (and that consequently needs to be removed) (fig 1.23). [431-432]

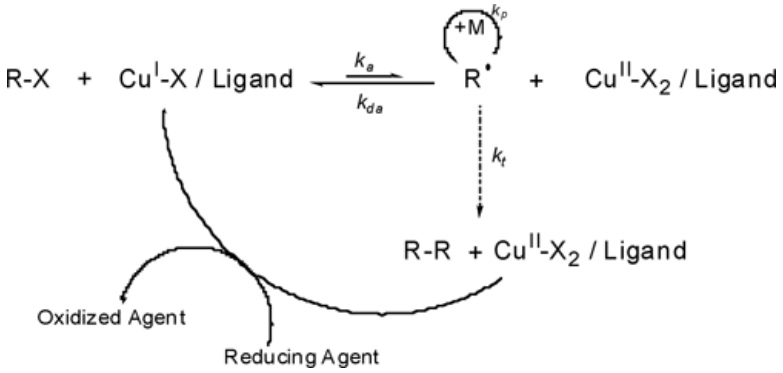

Fig 1.23: Reaction mechanism for ARGET ATRP.

Another advantage of ARGET ATRP is that catalyst induced side reactions are reduced to a significant degree, making it possible to drive an ATRP reaction to much higher conversion and prepare copolymers with much higher molecular weight [433-434] while retaining chain end functionality. [435] * The main disadvantage of this method however is the inclusion of an additional agent that needs to be removed from the polymer after synthesis.

NMRP

In NMRP, the equilibrium between dormant and active radical species is

* These are recent developments that were published after polymer synthesis was carried out in this research, and have only been demonstrated for a small range of monomers.

established by the reversible homolytic decomposition of a dormant alkoxyamine to form a polymer radical and a growth mediating nitroxide persistent radical (R•) (fig 1.24). This approach is similar to that of ATRP, with the main difference being that this method does not involve the use of a catalyst; it is instead a purely thermally activated process. [436]

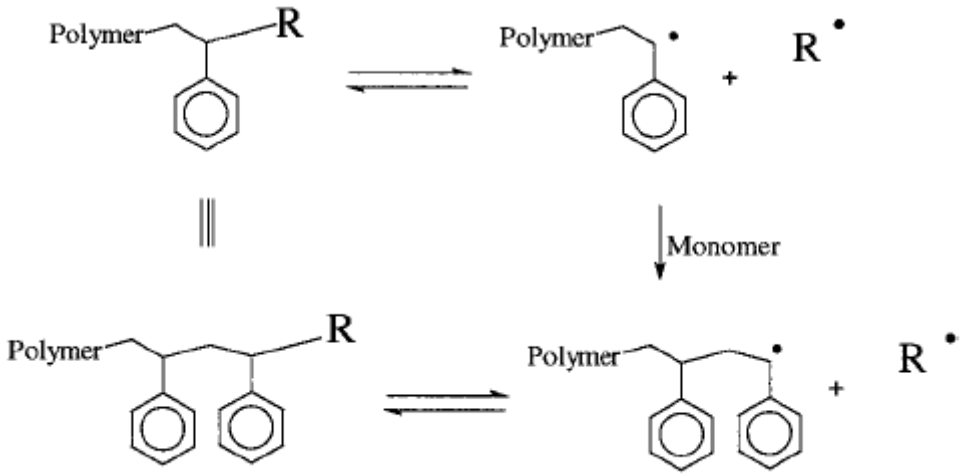

Fig 1.24: Reaction mechanism for NMRP, where R = mediating nitroxide species. [436]

NMRP has the advantages of (1) involving the use of persistent radicals, therefore leading to further reduced polydispersities through the persistent radical effect (2) being applicable to monomers with a wide variety of functional groups (there are few side reactions that will interfere with this simple control mechanism) and (3) being a high yield reaction with few side products which greatly simplifies the isolation and purification processes. [436] However, NMRP does require long reaction times or high reaction temperatures (>120^{o}C) to improve the reaction rate of these inherently slow reactions [426] and so is limited to the types of monomers which can handle these conditions. [417]

RAFT Polymerisation

In RAFT polymerisation, the equilibrium between the dormant and the active radical species occurs through a reversible chain transfer reaction involving a sequence of addition and fragmentation reactions (fig 1.25). [417] The

dormant species is a RAFT agent (fig 1.25 (2)) that is attached to the end of a polymer chain (fig 1.25 (3)). This species interacts with a propagating polymer chain radical (fig 1.25 (1)) to form an unstable intermediate (fig 1.25 (4)), which subsequently fragments to release the polymer that was previously attached to the RAFT agent as a radical. This radical then undergoes limited propagation before undergoing the same chain transfer process. The critical property of this reaction is that the initial chain transfer and subsequent chain equilibria favour fragmentations that result in the loss of the lower molecular weight group as a radical, which is critical if a low polydispersity is to be obtained.

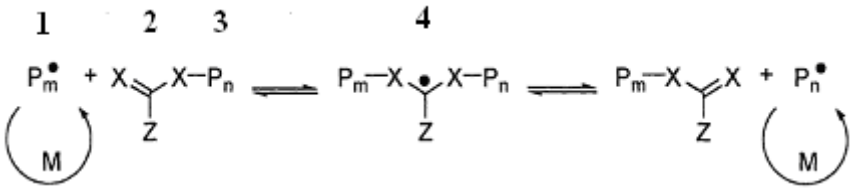

Fig 1.25: Reaction mechanism for RAFT. [437]

Any radically polymerisable monomer can be polymerised using RAFT. [426] A wide variety of chain architectures are also possible and the same initiators, solvents and temperatures are used as in conventional radical polymerisation. [417] The main disadvantages of RAFT are the formation of impurities that are hard to remove from the polymer and that each monomer generally polymerises best with a specific RAFT agent. [426]

Ionic Polymerisation

Ionic polymerisation involves initiation through the use of an alkyl-metal species that dissociates to form carbo-ionic species, resulting in a polymer chain that grows through the usual chain growth propagation process (fig 1.26). Termination by combination and disproportionation is essentially eliminated as a result of the mutual repulsion between the charged ends of the polymer chains. However, termination by chain transfer can still occur. [438]

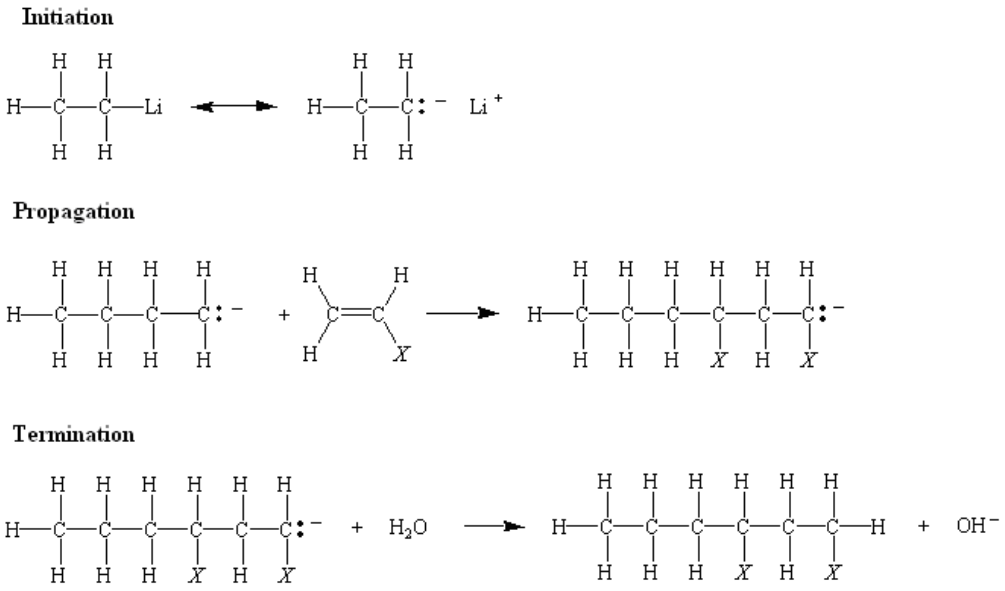

Fig 1.26: Reaction mechanism for ionic polymerisation (in this case anionic polymerisation).

Ionic polymerisation has numerous advantages over other living polymerisation methods. For example, the activation energy for initiation is much lower than for radical based polymerisation techniques. Therefore, much lower temperatures (-75^{o}C) can be used. [438] The polymer chains that are formed by this method have very low polydispersites and can potentially possess very high molecular weights (>10^{6} g/mol) [439] that are not accessible by other methods (as in other living polymerisations, termination by propagation and disproportionation still occur to a limited extent). In addition, this procedure can be applied to a wide range of monomers, with a variety of chain topologies being accessible. [428] However, to eliminate termination reactions, all species to which chain transfer can occur must be removed, requiring stringent purification of materials and polymerisation in a moisture and oxygen free environment. [428]

1.3.4. Template Directed Assembly

The idea behind the use of microphase separated block copolymers as nanoparticle assembly templates is to preferentially sequester metallic inclusions in a single highly selective microphase (by taking advantage of the unique chemical properties of each block), thereby causing the inclusions to be assembled into a structure that replicates that of the microphase separated block copolymer morphology.

Block copolymers possess numerous properties that are advantageous to their use as templates for nanoparticle assembly. For one, the size and separation of the microphases is on the order of the nanoscale (10-100 nm); a consequence of the polymer chains typically being of commensurate length. [440] Furthermore, the microphase separation is easy to achieve (being a self assembly process) and is moderately fast; ranging from minutes to several days depending on the morphology, polymer chain length and method used to achieve microphase separation. [366] The variety of monomer compositions that can comprise the block copolymer, afforded by the range of living polymerisation techniques available, means that these polymeric materials can possess numerous different physical properties that can be tailored for the particular application that the nanoparticle assembly is to be used in. Perhaps most importantly, the wide range of block copolymer types that can be formed with the available synthesis techniques, coupled with the variation in microphase separation due to factors such as relative block volume fraction, allows for the formation of a vast array of different microphase separation morphologies, the form of which can be precisely controlled.

As a result of these properties, there has been much work conducted in recent years with the aim of exploring the use of block copolymers as nanoparticle assembly templates. Such work can be classified as either (a) using the microphases as a template for directing the assembly of functionalised nanoparticles or (b) as a template to form a metallic nanoparticle assembly by in situ synthesis of the nanoparticles. [250]

In Situ Nanoparticle Formation:

A number of approaches have been investigated that use microphase separated block copolymers in forming nanoparticle assemblies via their in situ synthesis. One of the most common methods involves the selective removal of one of the copolymer microdomains (which takes advantage of the chemically distinct nature of the blocks and thus different responses to chemical or plasma etching treatments), with subsequent deposition of metal within the resulting voids. This has been performed by sputter coating [402, 441] as well as by reduction of metal species in the pores via electrochemical [442-449] and chemical means. [450-454] The most common microphase morphology that is utilised in this fashion is the hexagonally close packed cylinder microphase, owing to the accessibility of the created voids.

Other work has examined in situ nanoparticle formation by selectively loading one of the microphases with a metal precursor species. This is commonly achieved by tailoring the surface chemistry of the metallic species such that it is enthalpically favourable for it to preferentially associate with one of the copolymer blocks (which is possible as a result of the chemically distinct nature of the microphases). Although such sequestration results in a loss of entropy (due to ordering of the precursor species distribution within the block copolymer), the enthalpic drive for such sequestration typically outweighs this contribution. This species is then subsequently reduced, with the formation of nanoparticles that, with sufficient metal species loading, template the shape and spatial arrangement of the block copolymer microphase it is sequestered within. Most of the work performed using this technique differs in the loading method employed and, to a lesser extent, the means by which the metal species is reduced. Typically, the block copolymer is loaded with metallic species when in a disordered melt or solution prior to microphase separation taking place, with subsequent reduction by either chemical [455] or thermal means. [456] Selective loading is achieved through the selection of metal species and block copolymer compositions that yield a preferential attraction between the metal species and the desired microphase. Alternative loading methods include the utilization of copolymer blocks that possess functionality

that allows for the attachment of metal species to these polymer blocks by chemical means [457-459] and loading of block copolymers after microphase separation has taken place, such as by exposure to a vapour of the metal species. [460]

An extension of this means of in situ nanoparticle formation and therefore nanoparticle assembly is by the loading of block copolymer micelles, structures that form from block copolymers in a highly selective solvent, with the metal species in solution. The metal species is most often chemically reduced, and the resulting nanoparticle loaded miscelles are typically deposited onto a substrate to form a hexagonally close packed monolayer. [461-465] As with the loading of microphase separated block copolymers that form a solid matrix, loading of block copolymer micelles is most often performed by a preferentially attractive interaction between the micelles interior environment and the metal species, although binding of the metallic species to the polymer blocks by chemical means has also been utilised. [466]

The surface patterns that form as a result of block copolymer microphase separation have also been used to form nanoparticle assemblies by in situ synthesis. The dissimilar regions in such surface patterns exhibit a large difference in surface energy (a consequence of the repulsion interaction necessary for microphase separation to take place), which allows for selective wetting of the surface by different metals. A thin layer of metal is typically deposited onto the surface of a microphase separated block copolymer, and upon thermal annealing, the metal migrates, and is subsequently confined, to the regions of comparable surface energy. [467] By modifying the annealing conditions, one can retain the metal at the surface or (if the temperature is higher than the polymer's glass transition temperature but not so high that block repulsion is overcome) allow the metal atoms to migrate into the microdomain, upon which aggregation of the atoms into metal nanoparticles can be made to occur. [468-469]

Directed Nanoparticle Assembly: Theoretical Work

The microphase separation of block copolymers in the presence of ex-situ synthesized metallic nanoparticles provides yet another approach towards the formation of nanoparticle assemblies. In general, this approach facilitates better control of the structural characteristics of the sequestered component (such as size and shape), as the synthesis of the nanoparticles is not limited to the size and shape of the templating microdomains. This becomes important when applications rely on size- or shape-related nanoparticle properties. [354, 470]

This method relies on the same principle used to selectively load microphases with metallic growth species for in situ nanoparticle synthesis; that is functionalizing the nanoparticles to tailor their surface chemistry such that it is enthalpically favourable for the particles to preferentially associate with one of the copolymer blocks. However, the selective segregation of nanoparticles involves an additional complication in that their inclusion into a block copolymer results in a significant decrease in entropy originating from both localisation of the nanoparticles as well as the stretching of the polymer chains to accommodate the nanoparticles. In addition, the influence of the nanoparticles upon the polymer chain conformation and the effective block volume means that the presence of nanoparticles can in turn influence the microphase separation process as well as the equilibrium morphology of the block copolymer template.

As a result, much of the initial work in this direction is theoretical in nature, and was performed in an effort to understand what parameters control the microphase separation process in the presence of nanoparticles, and to determine the parameter space over which controlled segregation of nanoparticles to microphase separated block copolymer domains occurs. Many of the most significant contributions to this area were made by Balazs et al, who conducted simulations of microphase separation of a strongly segregated ($\chi N > 50$) A-B type diblock copolymer and studied the effect of the inclusion of hard spherical nanoparticles under a variety of conditions.

Among their most important findings is the elucidation of phase diagrams that illustrate the effect particle inclusions (that are coated with a layer of polymer corresponding to one of the copolymer blocks designated here as block A) upon the equilibrium microphase separated morphology. [471-472] The idea behind coating the nanoparticles is that this would make it more enthalpically favourable for the particles to interact preferentially with the corresponding polymer block.

These phase diagrams show that when a block copolymer is loaded with particles having diameters smaller than the A block polymer radius of gyration (the block that the functionalised particles are preferentially sequestered within), the pure polymer microphase separated morphology is retained when the volume fraction of particles is low, with the particles sequestering within the A block microdomains (fig 1.27). This is an important result, as it indicates that enthalpic considerations i.e. preferential nanoparticle segregation can outweigh entropic considerations while retaining the diblock copolymer morphology. As the nanoparticle volume fraction is increased, the block copolymer gradually transitions to a disordered morphology. This involves an initial macrophase separation into a pure microphase separated copolymer phase and a nanoparticle rich phase before finally transitioning to a completely disordered phase within which the particles are evenly distributed. This transition is much more sensitive to the nanoparticle volume fraction when the A block comprises a minority of the block copolymers volume ($f < 0.5$). In addition, it was found that this order-disorder transition is often preceded by a transition between different ordered microphase morphologies, a consequence of the effective increase in the volume of the A block microphases with increasing nanoparticle volume fraction. Importantly, these results are noted to be consistent with previous studies on the microphase separation of diblock copolymers incorporating highly selective solvents and homopolymers. [473]

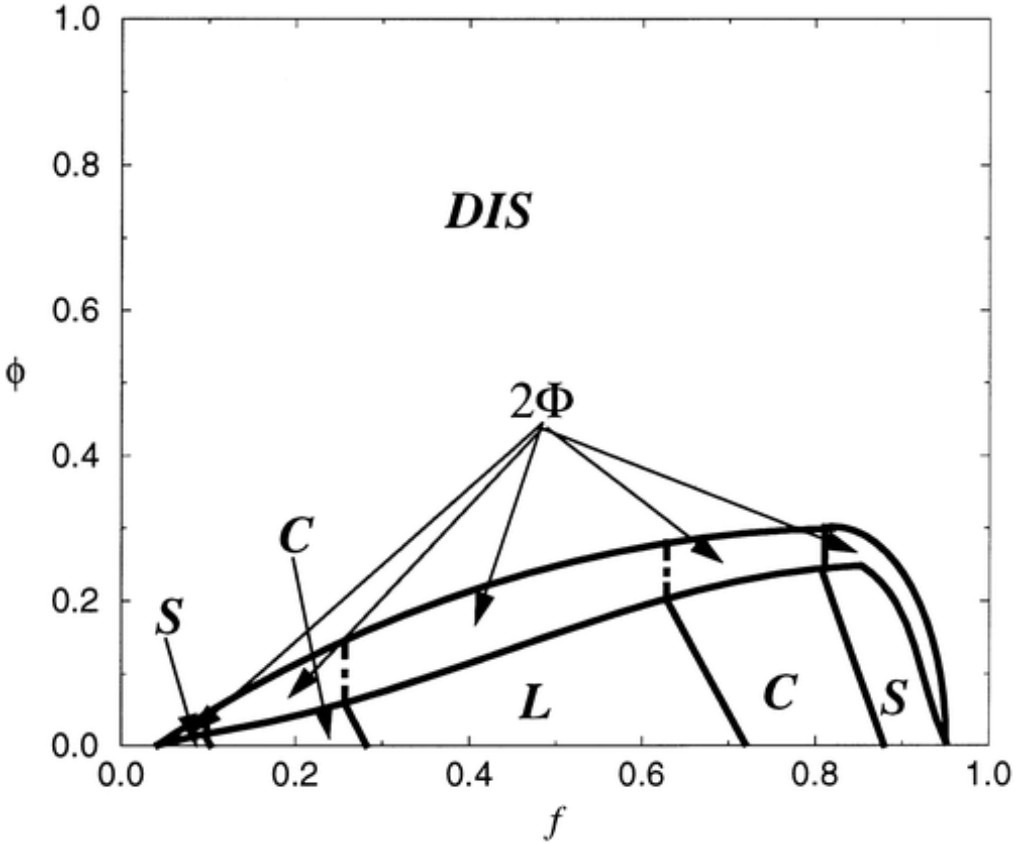

Fig 1.27: Computed phase diagram (as a function of volume fraction of block A (f) and nanoparticle volume fraction (Φ)) for a strongly segregated AB diblock copolymer containing nanoparticles with an enthalpically preferential interaction with the A block and diameter smaller than the A blocks radius of gyration. Regions S, C, L, DIS and 2Φ correspond to the spherical, cylindrical, lamellar, disordered and a 2 phase morphology region where both disordered and microphase separated regions are present in the polymer respectively at equilibrium. [471]

In the case of particles with diameters comparable to the A block polymers radius of gyration, a similar phase diagram applies (fig 1.28), but with some key differences. Firstly, macrophase separation occurs at higher nanoparticle volume fractions compared to the case of small nanoparticle inclusions, and the macrophase separated regime occurs over a broader range of particle filling fractions. The phase transition between microphase morphologies that occurs due to increased particle loading is also more gradual, involving an intermediate state in which both microphase morphologies are present. It was also noted that in the case of cylindrical and lamellar morphologies with moderate particle filling fractions, a new core-shell microphase separated morphology where the nanoparticles are located at the centre of the

microdomains forms. These changes in the phase diagram were generally ascribed to the greater entropic penalties associated with the polymer chain stretching necessary to accommodate these larger nanoparticles while forming an ordered block copolymer structure.

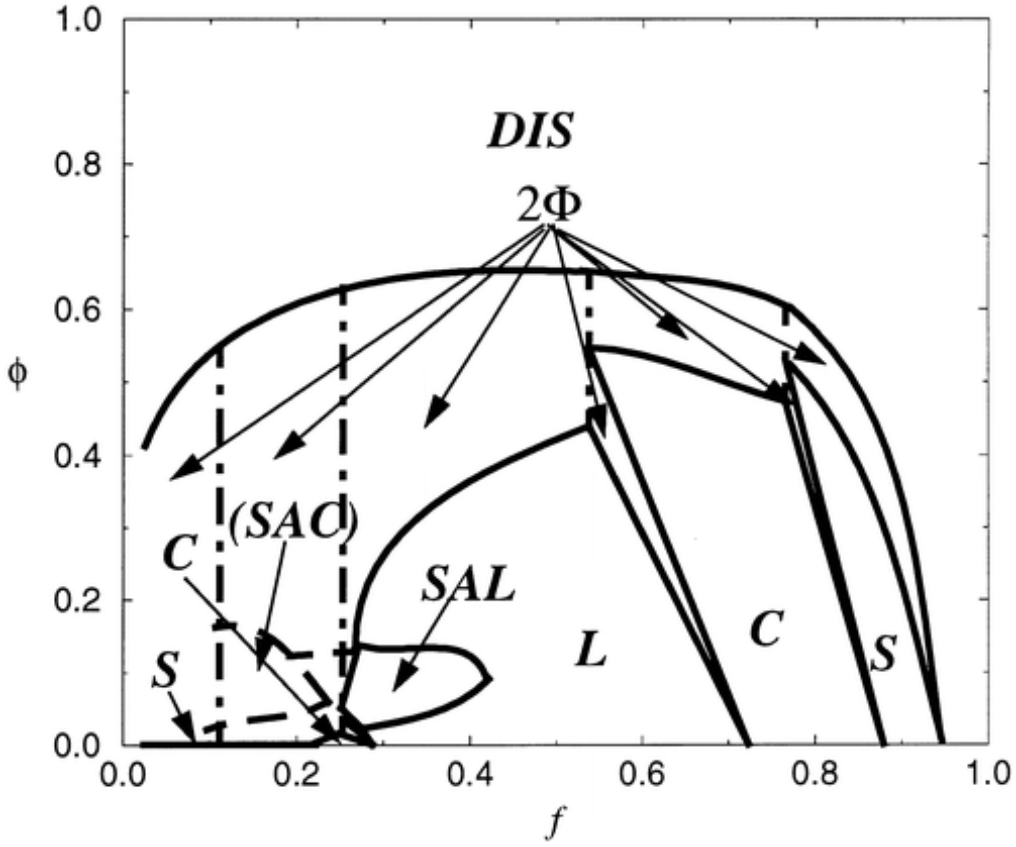

Fig 1.28: Computed phase diagram (as a function of volume fraction of block A (f) and nanoparticle volume fraction (Φ)) for a strongly segregated AB diblock copolymer containing nanoparticles with an enthalpically preferential interaction with the A block and diameter comparable to the A blocks radius of gyration. Regions S, C, L, DIS, SAC, SAL and 2Φ correspond to the spherical, cylindrical, lamellar, disordered, cylindrical core-shell, lamellar core-shell and a 2 phase morphology region where both disordered and microphase separated regions are present in the polymer respectively at equilibrium. [471]

Other work by Balazs et al further expanded upon these results. In one study, they found that a microphase separated block copolymer loaded with nanoparticles can be made to undergo a controlled phase transition between microphase morphologies by varying parameters such as particle size and the strength of interaction between the nanoparticles and the blocks. [474] Increasing the strength of this interaction makes the particles fill the

preferential domain to a greater extent, which will increase the effective volume occupied by that block and therefore, result in a different equilibrium morphology for sufficient particle filling fractions. Likewise, larger particles mean that such a transition may occur for smaller particle filling fractions, as each particle now occupies a greater volume.

In the case where the particles are non-selective (no preferential interaction with one of the polymer blocks), it was found that the particles tend to segregate at the interface between the microdomains. This was rationalised in terms of a reduction in the interfacial tension between the microphases by mediating the repulsive interaction between the two copolymer blocks (Note that this effect is sufficient to overcome the loss of translational entropy that results from the particles not being evenly distributed throughout the domains). Increases in particle size in this case can also lead to a change in equilibrium block copolymer morphology. As long as the diblock copolymer is asymmetric (one block occupies a greater volume than the other), the particles swell the minority phase to a greater extent than the majority phase, leading to a transition towards a lamellar morphology with increases in the particle size.

Further studies by the Balazs group examined the idea that the spatial distribution of nanoparticles in a block copolymer can be controlled by modulating enthalpic (strength and selectivity of the interactions between the nanoparticles and block copolymer) and entropic factors. [475] Here, it was determined that the interaction between nanoparticles and both A and B polymer blocks controls which domain the particles preferentially sequester within, whereas the size of the particles determines the spatial distribution of the particles within the domains in question. In the case of low volume fractions of particles that are large compared to the domains they are sequestered within, the particles are principally located in the centre of the sequestering domains. This was explained by considering that for large particles, the copolymer chains in the sequestering domain must stretch to get around the dispersed spheres, incurring a loss in the polymers conformational entropy. This stretching of the polymer chains is reduced by the segregation of

the particles into a central core where the chain ends are located. Although this also results in a loss of translational entropy (nanoparticles are less distributed), the increase in conformational entropy outweighs this contribution. On the other hand, for the same volume fractions of small particles, the stretching required by the polymers to circumvent the spheres is less significant. Hence, it is the translational entropy of the particles that dominates the behavior of the system. As more small particles are added to the system, the spheres are more uniformly dispersed and the entropic free energy per sequestering block increases.

The Balazs group also modelled the effect of nanoparticles on the microphase separation process itself. [476] They found that if the preferential interaction between the particles and one of the copolymer blocks (for example the A block) is relatively strong, then once the system segregates into A-rich and B-rich regions, the particles essentially become "bound" to the A block domains. The particles self-assemble into the A domains, swell these regions, and thereby modify the structure of the system. In the case of weak interactions between the particles and the A block, the majority of the particles are located in the A block domains, although some of the particles "jump" into the less preferred B block domains. To lower the free energy of the system, A domains eventually engulf the particles within the B block domains. This process has the effect of "cutting" the B-rich areas into separate regions (almost like an intermixing of the two block copolymer components). This result suggests that particle mobility is yet another factor that must be taken into account when microphase separating a block copolymer in the presence of nanoparticulate inclusions. When the particles are sufficiently mobile, they can "jump" over the interfaces and cause rearrangements to the domain morphology, so the overall structure becomes more disordered than in the absence of particles. When the mobility of the particles is suppressed, for example, by a strong-coupling interaction, which "anchors" the particles to one of the blocks, the particles serve to enhance the ordering.

Further work by the Balazs group examined the effect of spatial confinement of the block copolymer / nanoparticle mixture between two solid surfaces

upon microphase separation. [477] Here, the nanoparticles that are functionalised such that they are non-selective towards the blocks of a block copolymer (lamellar morphology) not only tended to concentrate at the interfaces between blocks as was shown previously, but that this resulted in organisation of the lamellar perpendicular to the substrate surfaces, indicating that loading of a block copolymer under spatial confinement with nanoparticles can influence microphase orientation as well as morphology.

Theoretical modelling of block copolymer microphase separation in the presence of nanoparticles by Sevink et al [478] found that the presence of relatively immobile nanoparticles (of comparable size to the equilibrium morphology domains in which they are to be sequestered within) serve to increase the rate of block copolymer microphase separation. This occurs as the nanoparticles limit the number of degrees of freedom for polymer chain orientation, due to the large amount of chain stretching that is required to accommodate the nanoparticles in the domains, as fewer degrees of freedom mean that less polymer rearrangement is necessary to facilitate microphase separation.

More recently, new simulation models for theoretical predictions of the interactions between nanoparticles and microphase separating block copolymers have been developed by Kim et al. [479] This model overcomes some of the limitations resulting from approximations used in the previous models, thereby yielding more accurate results. To date, this model has produced results that are in agreement with those obtained by both Balazs and Sevink. In addition, this model also promises to extend the range of scenarios that can be accurately covered by the theoretical studies of such systems.

Directed Nanoparticle Assembly: Experimental Work

Although the simulation and theoretical modelling of block copolymers microphase separated in the presence of nanoparticles yields important insights regarding the interplay of various factors on the resulting microphase morphology and nanoparticle distribution, such models are necessarily limited

to relatively simple, ideal cases. As such, many of the initial experimental studies have been performed on block copolymers containing nanoparticles in order to test the hypotheses set forth in the theoretical studies and then to expand upon this work by exploring regimes that are too difficult to simulate accurately.

The vast majority of such experimental work performed to date has been on diblock copolymers, where the nanoparticles are sequestered within a single copolymer domain. A number of these studies were initially performed to verify that selective segregation of appropriately functionalised nanoparticles into a single domain does indeed occur. [480-481] Some of the subsequent work verified a number of other theoretical predictions regarding the effect of nanoparticles on the microphase separation, such as the calculation that large volume fractions of nanoparticles disrupt the microphase separation process and lead to a disordered block copolymer morphology [482] and that an order-order microphase morphology transition may occur upon an increase in nanoparticle volume fraction. [483] Work in this direction also uncovered new phenomena that were not predicted in the theoretical models. For example, it was found that the presence of nanoparticles in a block copolymer undergoing microphase separation can stabilise the formation of short range ordered morphologies by concentrating at the "grain" boundaries between regions of different orientational order, thereby swelling these regions and relaxing the polymer chain stretching that results from such an orientational mismatch. [484]

Other studies were performed to experimentally investigate the spatial distribution of functionalised nanoparticles in a microphase separated diblock copolymer as a function of a range of parameters. The effect of particle size on nanoparticle distribution was the focus of some of the work carried out by Bockstaller et al. [354, 485] Their results compared favourably with the theoretical work; small particles tended to be distributed throughout the preferential domain (with concentrations near the domain interfaces) while large particles collected at the centre of the domains. Similarly, Kim et al

demonstrated that increases in nanoparticle volume fraction lead to the nanoparticles concentrating at the centre of the preferred microdomains. [486]

Other studies carried out by Kim et al [239], in addition to those by Tsutsumi et al [487-488], examined the effect of particle-polymer interactions upon nanoparticle spatial distribution. In one such study, Kim et al functionalised a nanoparticle with short polymer chains corresponding to one of the copolymer blocks, and found exclusive nanoparticle sequestration in that block. However, functionalising with a mixed monolayer consisting of polymer chains corresponding to both copolymer blocks lead to segregation of the nanoparticles at the interface between the block copolymer microphases, despite the large decrease in entropy (both due to the increase in chain stretching and localisation of the nanoparticles). [239] In a similar way, Tsutsumi et al also found that by functionalising the nanoparticles with short block copolymer chains matching the composition of the templating block copolymer matrix, the nanoparticles can be segregated at the interface between the microphases. [487] This interaction can also be modulated by varying the coverage of the nanoparticles with the short chain polymers. [488] At low coverages, interactions between the block copolymer and accessible portions of the bare metal nanoparticle surface dominate over interactions between the block copolymer and polymer ligands. At higher surface coverages, the polymer ligand-block copolymer interactions dominate.

Some studies have focused on investigating the affect of anisotropic nanoparticles (such as nanorods) upon the equilibrium microphase morphology. The inclusion of rod shaped particles into a block copolymer still results in microphase separation, and that the rods tend to orient themselves in an effort to minimise polymer chain stretching i.e. rods aligning parallel and in the centre of lamellar domains. [489] The effect of the presence of such anisotropic nanoparticles upon the microphase separation process has also been investigated. [490-491] Here, the inclusion of large surface area anisotropic nanoparticles dramatically sped up the kinetics of the microphase separation as a result of limiting the polymer chains configurational degrees of freedom; consistent with earlier theoretical studies.

More recent experimental work has been performed to investigate the applicability of block copolymers to the formation of useful nanoparticle assemblies, most of which has involved the templated assembly of such nanoparticles into patterned surface structures. One example of this is the use of substrates that are chemically patterned into stripes with different surface energies. [399] These stripes can direct the microphase separation of a lamellar diblock copolymer so that the domains are oriented perpendicular to the surface (through the preferential wetting of the stripes by a given block). Large nanoparticles that are functionalised to preferentially segregate in one of the lamellar domains are thereby directed to assemble into well defined rows, as the large particles preferentially sequester in the centre of the microphase. Another example is the loading of a block copolymer with a large volume fraction of metal particles, and subsequent pyrolysis of the block copolymer, leaving a metal structure that replicates the microphase structure within which the particles were sequestered. [492] Further examples involve the sequestration of nanoparticles on the surface of a microphase separated block copolymer. This is typically accomplished by utilizing the same enthalpy minimizing interactions used to sequester nanoparticles within a single microphase of a bulk copolymer. [467, 481, 493] However, it has also been demonstrated that one of the copolymer blocks may be chemically modified by treating with plasma, such that the surface of these microphases is electrically charged. This surface charge is then used to selectively sequester charged nanoparticles in these regions. [494]

Other work has examined the possibility of loading block copolymers with nanoparticles *after* microphase separation has been performed. This would thereby allow for the formation of templated nanoparticle assemblies with a wider range of nanoparticle compositions without subsequent changes in the block copolymer morphology (as the microphase morphology is effectively frozen due to a lack of polymer chain mobility), although at the expense of explicit control over nanoparticle spatial distribution and tailoring of the microphase morphology. For example, block copolymers that are decorated with nanoparticles at the air-polymer interface can be loaded with these

particles by thermal annealing above the polymers glass transition temperature, upon which the particles migrate into and sequester at the most enthalpically compatible block. [493] Saito et al accomplished selective loading of a block copolymer with nanoparticles following microphase separation by soaking the polymer in a water/1,4-dioxane solution containing silver nanoparticles. [495]

Although block copolymers containing nanoparticles are rather complex systems that have only recently begun to be understood, the use of block copolymers as templates for nanoparticle assembly holds much promise, owing to the multitude of beneficial properties that they possess in this regard. However, one anticipated shortfall in the use of block copolymers as templates for precisely assembling nanoparticles into structures is the lack of "network" type microphase morphologies; structures that would be particularly advantageous in the controlled arrangement of nanoparticles into corresponding networks rather than as arrays of isolated particles. This is considered to be significant as many of the most useful nanostructures have a network type structure.

1.4. Multisegment Nanorods

1.4.1. Introduction

One possible way by which network type assemblies of nanoparticles may be formed using block copolymers is to utilize anisotropic nanoparticles, such as nanorods (cylindrical nanoparticles with an aspect ratio of typically < 20), that are comprised of discrete surface regions that are each compatible with the different microphases inherent to the block copolymer (fig 1.29), thereby introducing an enthalpic driving force for "cross-phase" templating of the nanorods and allowing for the formation of network type structures (fig 1.30).

Fig 1.29: Depiction of a nanorod with discrete surface regions that are each compatible with different microphases of a block copolymer.

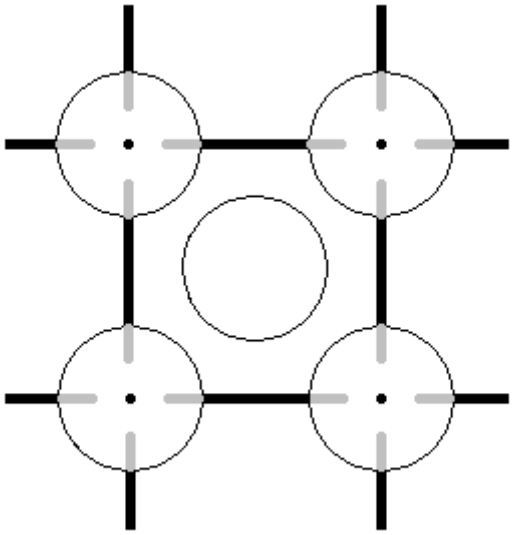

Fig 1.30: Example of a *possible* network type assembly of anisotropic nanoparticles in a BCC microphase separated block copolymer.

Such selective nanorod surfaces may be formed by making nanorods comprised of discrete metallic segments (known as segmented nanorods). By judiciously selecting the metallic composition of these segments, the surface chemistry of the nanorods can be varied along the nanorod length, thereby allowing different sections of such segmented nanorods to be selectively functionalized. [496] Functionalisation of these segments with short chain polymers corresponding to the block within which they are to be sequestered then yields the necessary selectivity.

1.4.2. Synthesis

As is the case with the synthesis of block copolymers, the conceptual simplicity of segmented nanorods is belied by the difficulties involved in forming nanorods with discrete metal segments in a controlled manner. Despite the wide range of synthetic procedures that have been developed towards the synthesis of metal nanoparticles, very few can be applied to the synthesis of rod-shaped metal nanoparticles comprised of discrete segments.

The only method that has so far been successfully applied to the synthesis of such particles is template electrodeposition; a technique that was first employed by Possin [497], and later developed by Giordano [498-499], to facilitate the controlled synthesis of single segment metal nanorods. More recent work by Martin [500-501] and Moskovits [502-503] further expanded this technique, eventually culminating in the synthesis of multisegment nanorods. [198, 303]

This method involves the use of a template (most commonly a membrane) that consists of an arrangement of open parallel pores, within which metal is reduced electrochemically (fig 1.31 a). This is accomplished by initially coating one side of the template in a layer of conductive material (most often a metal), which serves as the cathode upon which metal is to be electrochemically reduced (fig 1.31 b). A plating solution (containing the metal growth species) is then introduced into the pores (fig 1.31 c) and the metal is subsequently reduced at the cathode through the application of a

potential between the anode and the cathode (fig 1.31 d). The reduced metal templates the shape of the pores, thereby forming a rod shaped nanoparticle. As the nanoparticle growth is from the bottom of the template up, segmented nanorods can be formed by depositing the desired thickness of one metal, then depositing a second metal and so on (fig 1.31 e). This is usually accomplished by rinsing out the first plating solution and replacing with another, although it can be accomplished using a single plating solution under specific deposition conditions. [504-509] To obtain free nanorods, the conductive backing and template is removed (fig 1.31 f) and the suspension subjected to centrifugation in order to collect the nanorods.

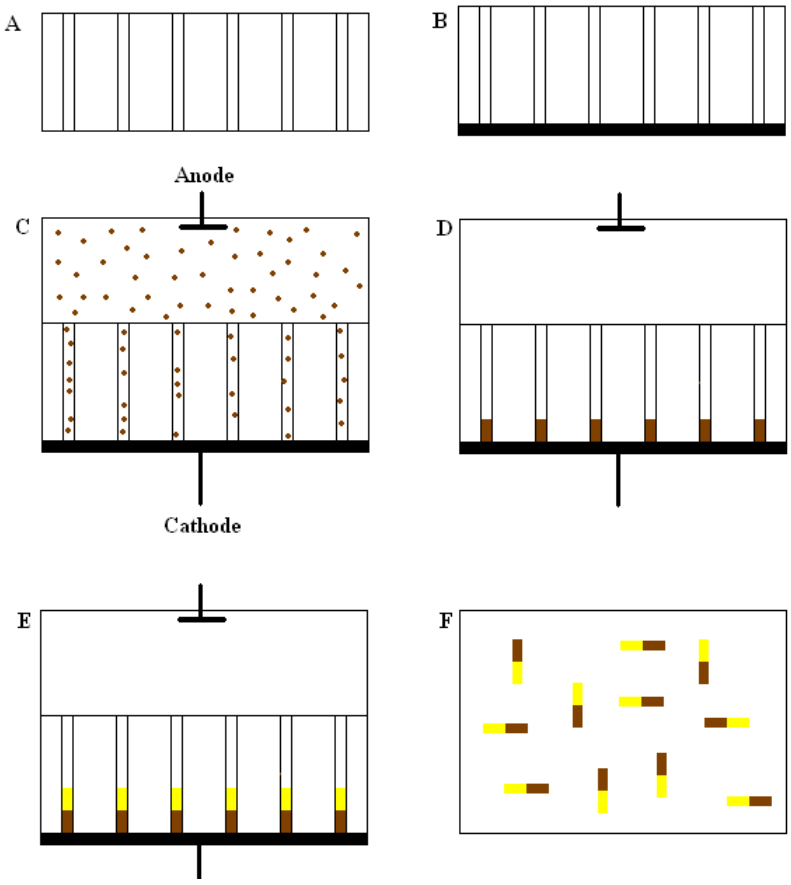

Fig 1.31: A typical template electrodeposition process, which involves a nanochannel template (A) being coated on one side with a layer of conductive material (B). This coating serves as a cathode during the application of a potential across the channels when a metal plating solution is introduced (C). This results in electrodeposition of material within the template pores (D). The plating solution is removed and electrodeposition repeated with a different plating solution to obtain segmented nanorods.(E). The conductive coating and template are then removed, yielding free nanorods (F).

This technique has numerous advantages; it only requires mild growth conditions (which also minimises undesirable competing chemical reactions and interdiffusion of the metal segments), it allows for rapid nanoparticle synthesis, nanoparticle growth can be accurately monitored and controlled by measuring the passed charge and this technique is low cost (both in required instrumentation and materials) [496, 510] Perhaps most importantly, this technique can be applied to a wide range of materials, including metals such as Au [198, 287, 303, 511-516], Ag [198, 516], Cu [517-520], Ni [287, 511, 517, 521-523], Co [521, 523-525], Pt [303, 500, 512, 524], Pb [518], Fe [522], Zn [526-527] and Bi [287], semiconductors such as Se [520], CdS [528], ZnO [529-530], CdSe [511, 531-533], CdTe [511] and Cadmium Chalcogenides [533], ceramics [534-535] and polymers. [536-540]

One of the most important considerations with this method is the template used, as this dictates the nanorod dimensions such as diameter and maximum length, yield of nanoparticles (pore density), reaction conditions and range of plating solution that can be used (chemical compatibility with the template). There exists a collection of templates that can be applied to this process (many of which have been previously reported in the literature for the synthesis of single segment nanorods using a variety of methods and material types) including; Zeolites [541-542], Nanochannel glass [176], Nanochannel mica [181, 497], Mesporous silica [543-549] and Block copolymers. [448, 550] In practice however, the most commonly used templates for synthesizing free segmented nanorods are the commercially available Porous Anodic Aluminium oxide (AAO) and Track etched Polycarbonate membranes [178], owing to their availability, cost and easy template removal without damaging the nanorods.

Aluminium oxide membranes consist of arrays of uniform, densely packed (10^{11} pores / cm^2) parallel cylindrical pores typically ranging between 10 – 250 nm in diameter, [551-552] although pores as small as 6 nm in diameter may be obtained by modifying the membrane. [553-555] These membranes are fabricated using a two step anodisation process established by Masuda et

al. [556] A thin sheet of high purity aluminium is annealed then subjected to an electropolishing solution to remove the uppermost aluminium oxide layer. The Aluminium is then anodized in an acidic electrolyte solution, which results in the formation of aluminium oxide on the surface in a repeating hexagonal pattern. The sheet is then placed into a chromate solution to etch the oxide layer. The sheet is anodized again in the same solution, with preferential alumina formation in previously etched pattern. The aluminium is then removed by etching to yield an array of cylindrical pores. The dimensions of the membrane can be readily modulated by varying different parameters. For example, longer anodisation time yields deeper alumina formation and therefore, thicker templates, while different acid solutions, concentrations, temperatures and anodisation voltages yield different pore diameters. [557]

This type of template has the advantages of good thermal resistance (which allows a range of conductive coating procedures to be used) and chemical resistance, high pore density and linearity as well as hydrophilic pore surfaces, making the pores relatively easy to fill with plating solutions. However, the high pore density means that the alumina surface area at the membrane faces is quite low, meaning that adhesion of the required conductive layer to the membrane is an issue. Furthermore, the brittle nature of these membranes means that they need to be relatively thick (60 μm) to provide mechanical strength.

Track etched polycarbonate membranes consist of a polycarbonate foil containing randomly arranged cylindrical pores with diameters between 10 – 2000 nm and a moderate pore density (10^9 pores / cm^2). These membranes are created using polymer foil that is bombarded with ions (normally α particles from radioactive material), which produce damage tracks as they pass through the polymer foil. These tracks are much more sensitive to chemical etching than the undamaged polycarbonate, therefore yielding pores upon such etching. The diameter of the pores is controlled principally by the etching time, although temperature and etching solution composition also have a role. [552, 557-558]

These membranes have the advantages of greater surface areas at the membrane faces, thereby improving adhesion of deposited conductive layers (although this is balanced by the relatively poor adhesion of metals to polycarbonate). These membranes are also easier to handle than AAO membranes as a result of the plasticity of the template material. The non-brittle nature of these membranes, along with the relatively lower pore density, also mean that these templates can be made much thinner than AAO membranes (6 μm), making mass transport of ions and gasses through the pores much easier. However, these membranes possess lower chemical and thermal stability compared to AAO, and the reduced pore density results in smaller yields of nanoparticles for a given template size. The pores in track etched polycarbonate are also not necessarily perpendicular to the surface, a result of the varying angles at which the track etching ions are emitted from the radioactive material, although the moderate pore density means that intersection of the pores is rare. Furthermore, the pores of these membranes are hydrophobic, making the introduction of plating solution to the pores difficult. However, this can be circumvented by applying a thin layer of hydrophilic poly(vinyl pyrrolidone) (PVP) to the surface of the pores.

Deposition Process:

The use of a template to confine the electrochemical reduction of a metal to a nanometric volume has important consequences for the electrodeposition process. To understand this, consider the steps involved in the electrochemical reduction.

Initially, the uncoated face of the template is exposed to a plating solution that contains a dissolved metal growth species. Mass transport of the dissolved species into the open pores occurs by a process known as diffusion, where a net migration of species from regions of high concentration to regions of low concentration takes place. This process is typically facilitated by pre-wetting the pores with a solvent identical to that of the plating solution (normally water). The flux of the dissolved species due to diffusion is governed by Fick's first law:

$$J_i = D\frac{dc_i}{dx}$$

Where J_i is the flux of the ith species in solution, D is the diffusion coefficient and dc_i/dx is the concentration gradient between two points for the ith species in solution.

The large initial concentration gradient between the base of the pores (cathode/solution interface) and the bulk solution leads to rather rapid diffusion towards the cathode. Once metal growth species in the solution has reached the base of the pores, some of the metallic species, which are surrounded by solvating molecules or ligands, become partially bound to the cathode surface as adions, which occurs through the rearrangement of ligands/water molecules to accommodate this adsorption. These adions may then be incorporated into the cathodes atomic lattice by diffusing across the surface until they encounter high energy growth sites, upon which further dehydration and/or desorption occurs concurrent with the reduction of the metal ions. This process continues until the metal ions are fully coordinated with other metal atoms on the surface and become part of the lattice. [559] This is a reversible process, which results in an equilibrium reaction between metal ions depositing onto the cathode surface and these ions going into solution. Typically, one of these processes is initially faster than the other, meaning that by the time equilibrium is established, a difference in charge between the solution and the surface occurs. This separation of charges takes the form of a diffuse double layer structure (fig 1.32), which consists of several regions. The inner Helmholtz plane (IHP) consists of dipolar solvent molecules (for example water) and specifically adsorbed ions (ions that have lost their waters of solvation and thus are more closely bound to the interface). The outer Helmholtz plane (OHP) consists of immobile and solvated ions of opposing charge to the electrode. Beyond this there exists the diffuse layer, which is made up of solution that contains an increased concentration of mobile ions, relative to the bulk solution. [560]

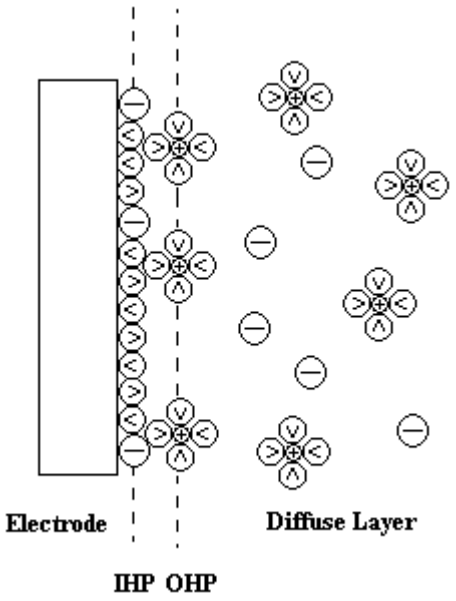

Fig 1.32: The diffuse double layer that forms at a metallic cathode. This consists of the inner Helmholtz plane (IHP), which is made up of specifically adsorbed ions, the outer hemlholtz plane (OHP), which is made up of solvated ions with charge opposing that of the electrode and the diffuse layer, which contains a mixture of ions/counter ions.

One consequence of this charge separation (and dipole alignment in the IHP) is the establishment of a potential difference between the metal cathode and the solution, which is known as the standard (half-cell) electrode potential. In order for there to be a net metal deposition onto the cathode surface, an external potential must be applied across the diffuse double layer that not only exceeds this equilibrium half cell potential (in order to make metal deposition faster than dissolution), but is also sufficient to overcome any resistance to the resulting current flow. The sum of these two excess potentials (known as the activation polarisation and ohmic polarisation) is called the overpotential. [559] Note that this potential is for the half cell reaction at the cathode surface ($M^{n+} + n\ e^- \rightarrow M^0$). To measure the potential difference over this interface, a second electrode surface is required to complete the circuit. However, this introduces a second interface and hence potential difference to the measurements, thus it only makes sense to discuss the *difference* between this potential and that due to a half cell reaction occurring at the second electrode.

An overpotential is then applied between the anode and cathode to induce reduction of the metal at the cathode. Growth of the resulting metal deposits generally occurs through two mechanisms; layer growth and crystallite growth. Layer growth involves outward growth of the deposit through the deposition of metal ions in a layer by layer fashion, while crystallite growth occurs by the nucleation of discrete crystallites on the metal surface, which grow outwards and coalesce into a complete layer. [510] These two mechanisms are in competition during electrodeposition and different plating solutions and conditions can influence the relative extents of each growth mechanism. This is reflected in the structure of the deposited metal i.e. layer growth results in larger grain sizes. The atomic structure of the cathode also plays an important role in determining the structure of the deposit, particularly over the nanometric volumes inside the pores. The crystal structure of the initial metal deposit can be characterised as that of an induction layer, with a crystal structure that is strongly influenced by that of the substrate. Further deposition yields deposits with a structure that undergoes a transition from that of the induction layer to that of the bulk metal, the structure of which is determined solely by the plating conditions. [510]

As deposition of the metal on the cathode continues, metal growth species near the cathode surface are depleted, and must be replaced from the bulk solution if deposition is to carry on. The rate of this consumption is determined by the overpotential used during the deposition. At very low overpotentials, the rate of metal growth species consumption is relatively low, and so mass transport to the diffuse double layer is sufficient to maintain equilibrium levels of the growth species. The resulting current due to the net reduction of metal onto the cathode at these external potentials (or more accurately the current per unit of electrode area or current density)[*] is therefore kinetically controlled by the rate of the reduction reaction (assuming no limitation at the anode). This is known as the Tafel region (region I in fig 1.33). [559]

[*] The current (charge passed per unit time) resulting from the application of an overpotential depends upon the volume of metal reduced at the cathode at any one instance, the amount of which is strongly dependant upon the cathode surface area. Therefore, it is more accurate to refer to the current density resulting from an applied overpotential.

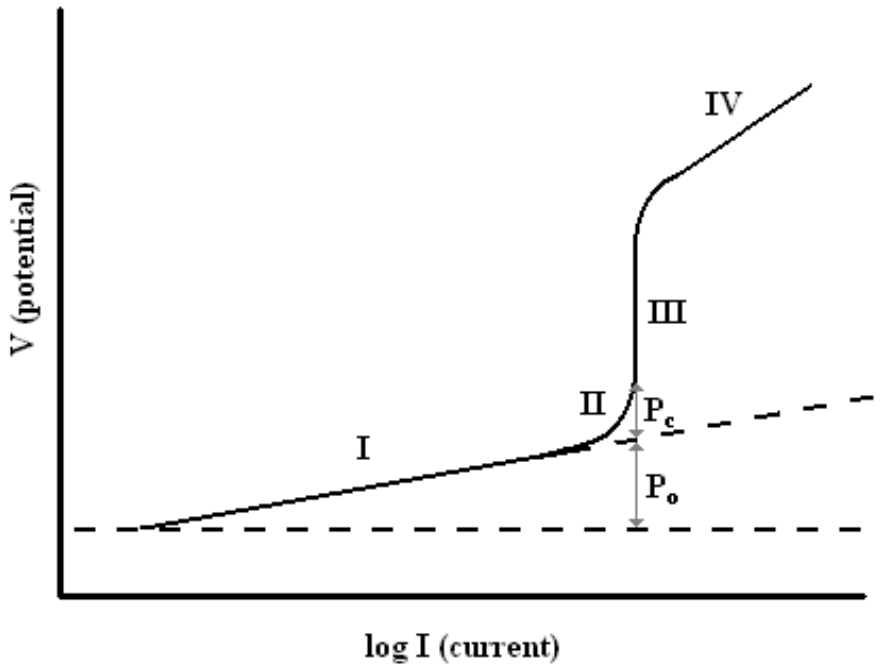

Fig 1.33: Graph showing the external potential required to obtain a specific current flow during an electrodeposition at a cathode. Several different system behaviours are shown; region I (Tafel region) exhibits kinetically controlled deposition characterised by an activation polarisation (P_o), region II exhibits kinetically controlled deposition characterised by a concentration polarisation (P_c), region III shows mass transport controlled deposition characterised by a limiting current, while region IV shows mass transport controlled depositon characterised by hydrogen evolution. The precise relationship between V and I will vary depending upon factors such as the plating solution used and the electrode area.

If higher overpotentials are used, the deposition rate, and therefore consumption of metal growth species, is correspondingly greater. At sufficiently high overpotentials, the diffuse double layer begins to be depleted of growth species faster than it is being replenished by mass transport from the bulk solution. This results in a concentration gradient between the growth species in the solution and the electrode surface, a region known as the diffusion layer (fig 1.34). [560] However, this drop in growth species concentration yields a consequent increase in the concentration gradient between the double layer and the bulk solution; thereby resulting in an increase in the diffusion rate of these species to the double layer.

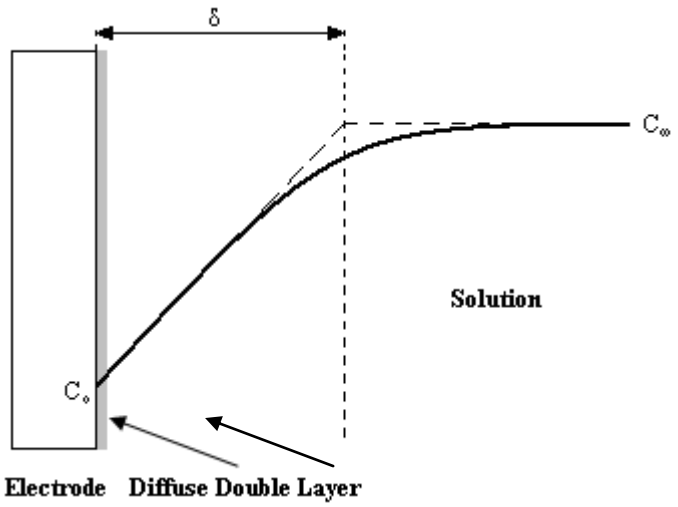

Fig 1.34: Graph of metal growth species concentration (C) as a function of distance from the cathode surface at high overpotentials. Bulk solution concentration (C_∞) decreases as one approaches the cathode surface (C_o), the distance over which this occurs being referred to as the diffusion layer (δ).

In the case of overpotentials that are marginally greater than the Tafel region (region II of fig 1.32), the depletion of metal growth species from the diffuse double layer can be matched by the increased diffusion rate, with the end result of a stable, smaller than equilibrium concentration of metal growth species in the diffuse double layer. This reduced concentration of growth species in the diffuse double layer leads to a concurrent change in the equilibrium half cell potential towards higher values, known as concentration polarisation, which needs to be accounted for in the applied overpotential if higher deposition rates are desired.

If even higher overpotentials are used (region III in fig 1.32), consumption of the growth species is greater than mass transport to the cathode, thereby depleting the diffuse double layer of metal growth species. The current that results from deposition at these potentials is therefore limited by mass transport to the cathode surface (the so called limiting current region), and so any increases in applied external potential do not result in an increase in deposition rate (and therefore cathodic current).

At yet higher overpotentials (region IV of fig 1.32), an increase in current may be observed, but this is not the result of faster metal deposition. Instead, it is

the result of undesirable side reactions occurring at the cathode, in particular evolution of hydrogen gas.

$$2H^{+} + 2e \rightarrow 2H_{adsorbed} \rightarrow H_{2\,(gas)}$$

The evolution of hydrogen can result in the formation of hydrates and hydroxides that may precipitate and occlude in the deposit. Such co-deposition usually influences the material properties. Furthermore, such bubbles may become trapped in the narrow pores of the membrane, preventing any further deposition in this pore (leading to nanorods with different segment lengths) and increasing the concentration polarisation in the remaining accessible pores. Very low overpotentials can also involve undesirable side reactions such as deposition of impurities from the plating solution along with the target metal; a result of the low current densities that occur at these potentials. [559] The occurrence of undesirable reduction reactions at the same time ensures that less of the passed charge contributes to the deposition of metal, which is referred to as a low current efficiency.

Importantly, the onset of concentration polarisation and limiting current behaviour may occur at very different potentials than normal for a given system when performing template electrodeposition; a consequence of both the restricted diffusion in such pores [561-562] and the additional mass transport mechanisms that come into play upon the application of an external potential. [563] One process, ion migration, involves the movement of ions as a direct result of the applied electric field i.e. positively charged ions migrating towards the negatively charged electrode and vica versa. This process essentially only influences charged species in the pores, as the motion of cations and anions in opposing directions results in little net viscous drag on the bulk solution (solvent and neutral species). Furthermore, this mechanism of transport is relatively slow due to resistance to motion of a given ion by the diffuse layer of counterions that surround all such ions in a solution, which are compelled to migrate in the opposite direction to the ion in question.

The second process, electroosmosis, occurs when the surface of the pores is charged, such that ions (primarily counterions) concentrate at and in the vicinity of the pore wall in order to balance charge. This results in the formation of a diffuse double layer. When an electric field is applied, ions within the diffuse double layer migrate towards the opposing charge electrode. Because the diffuse double layer has a net charge, there are more positive/negative ions moving in one direction than negative/positive respectively. This gives rise to viscous drag, which causes the rest of the solution to be pulled in the same direction. [564-565] Typically, higher surface charge densities yield a thicker diffuse double layer. [564, 566] The strength of ion migration and electroosmotic flow in the pores is controlled by the debye length, κ^{-1}, which is that characteristic length over which ionic interactions occur in solution. The debye length is inversely proportional to the ionic strength of the solution, which is defined by the following equation; [2]

$$i = \frac{1}{2}\sum_{B=1}^{n} C_B Z_B^2$$

where C_B is the concentration of the B^{th} ionic species and Z_B is the charge on the B^{th} ionic species. Therefore, if the solution contains high concentrations of ions with high charges, the ionic strength is high and therefore, the debye length is small. Conversely, a low concentration of ionic species with small charges would have a low ionic strength, yielding a large debye length. In the case of ion migration, a small debye length results in a small hydrodynamic radius for a given ion, as the diffuse layer of counterions surrounding the ion is quite thin. This in turn results in a smaller degree of resistance to movement through the fluid, yielding a greater velocity. With regards to electroosmotic flow, a large debye length (relative to the pore diameter) means that a greater cross-section of the pore is part of the pore wall diffuse double layer, leading to greater electroosmotic flow. [564]

Modifying factors

As a result of the number of steps involved in the electrodeposition process, there exists a wide range of vectors by which this process may be modified. For example, chemical additives are commonly included in metal plating solutions to enhance or alter the electrodeposition process through their presence in solution (electrolytes that improve solution conductivity and mediate debye lengths), by their adsorption to the electrode surface (levelling agents that promote even deposition over an electrode surface by adsorbing preferentially at the highest points and thereby inhibit deposition at these locations as well as grain refiners that promote or inhibit different growth mechanisms to change grain sizes) and by codeposition with the metal (brighteners that increase the reflectivity of the deposited metal). However, these additives must be selected carefully, as even additives that are not intended to be incorporated into the metal deposit often are, with consequent changes in the deposit properties. [510, 559]

Another example of how the deposition process may be modified is by introducing convection based mas transport, often accomplished by sonication. This serves to increase the mass transfer rate, thereby increasing the limiting current for the electrochemical reaction. The rate is increased by the formation and collapse of tiny bubbles in the fluid, creating high speed jets. The improved limiting current means higher current densities (faster deposition) before the onset of hydrogen evolution, improved metal adhesion to the cathode substrate as well as reduced porosity and stress due to defects in the deposits. [559]

1.4.3. Selective Functionalisation

Critical to the idea of sequestration of segmented nanorods across the microphase interfaces of block copolymers is the selective functionalisation of these nanoparticles. To date, this concept has been successfully demonstrated in the literature on numerous occasions, through the judicious selection of metals with distinct surface chemistry to comprise the individual segments. For example, it has been shown that thiol functional groups will selectively bind to gold segments while Heme IX porphyrin [567], carboxylic acids [568-571] and Histidine tagged proteins [572] preferentially bind to nickel in Ni-Au segmented nanorods. Another example is the selective functionalisation of thiols on gold and isocyanide on platinum. [303, 512, 569-571]

1.5. Research Aim

The principle aim of the work presented in this thesis is to investigate the possibility of using microphase separated block copolymers as templates to drive selectively functionalised segmented metal nanorods to align perpendicular to the interfaces between block copolymer microphases.

In carrying out this investigation, it is important to realise that although from an enthalpic viewpoint cross-phase templating of such nanoparticles is favourable, from an entropic point of view such templating is unfavourable, due to the resulting organised distribution and orientation of the nanorods and polymer chain stretching required to accommodate the nanorods in the microphases if ordered microphase separation is to be maintained. Therefore, in order to persue this investigation, an initial "proof of principle" experiment will be carried out under conditions that maximise the enthalpic drive towards cross-phase alignment, while minimising the associated penalty to the entropy of the system. This may be achieved (according to the literature) by implementing the following conditions:

- Segment functionalisation that is highly selective towards the targeted microphases.

- Small nanorod concentrations.

- Nanorod segment dimensions < microphase dimensions.

While the first two conditions are relatively easy to implement, achieving the third condition will be the principle challenge in this investigation. For example, although there are reports in the literature of very small nanorods formed by template electrodeposition, they typically involve only uniform compositions and are not collected from their synthesis templates. The literature involving free, segmented nanorods almost exclusively focuses on their applications in fluorescence based assays, and as such almost exclusively

involves the synthesis of large (> 100 nm diameter and/or > 1 μm long) nanorods where collection and control over segment dimensions and purity is readily achieved (this being harder to do as the segment dimensions are reduced). On the other hand, most literature on microphase separated block copolymers involves microdomains < 100 nm in diameter, as larger microphases typically require low polydispersity and very high molecular weight block copolymers that are consequently difficult to synthesise and process.

Given this gap in the literature, and the presumed requirement for nanorod segments with dimensions that are at least as small (and preferably smaller) than the dimensions of the sequestering microphases, much of the work presented in this dissertation involves expanding upon the current literature in order to access an overlap of these size regimes, before combining these materials to determine if (and under what conditions) templated cross-phase alignment of the nanoparticles occurs.

As such, the work presented in this dissertation is divided up into the following chapters. The next chapter (Chapter 2) deals with the preparation, specifically synthesis and microphase separation, of a series of block copolymers with properties appropriate for their use as templates in the cross phase alignment of segmented nanorods. A particular emphasis is made in this chapter on the acquisition of block copolymers with microphase dimensions at the upper limits of what has been achieved in the literature. Chapter 3 covers the preparation and characterisation of well defined, free single segment metal nanorods with dimensions (both diameter and length) at the lower limit of what has been obtained in the literature, which is extended to multi-segment nanorods with properties appropriate for use in cross-phase templating in Chapter 4. Finally, chapter 5 involves the investigation of the template directed alignment of these nanorods, first as a proof of principle experiment to determine if successful cross-phase template directed alignment of nanoparticles may be achieved in block copolymers under optimal conditions, and then under a variety of experimental conditions to explore this method of nanoparticle alignment. A schematic diagram of this work is provided below:

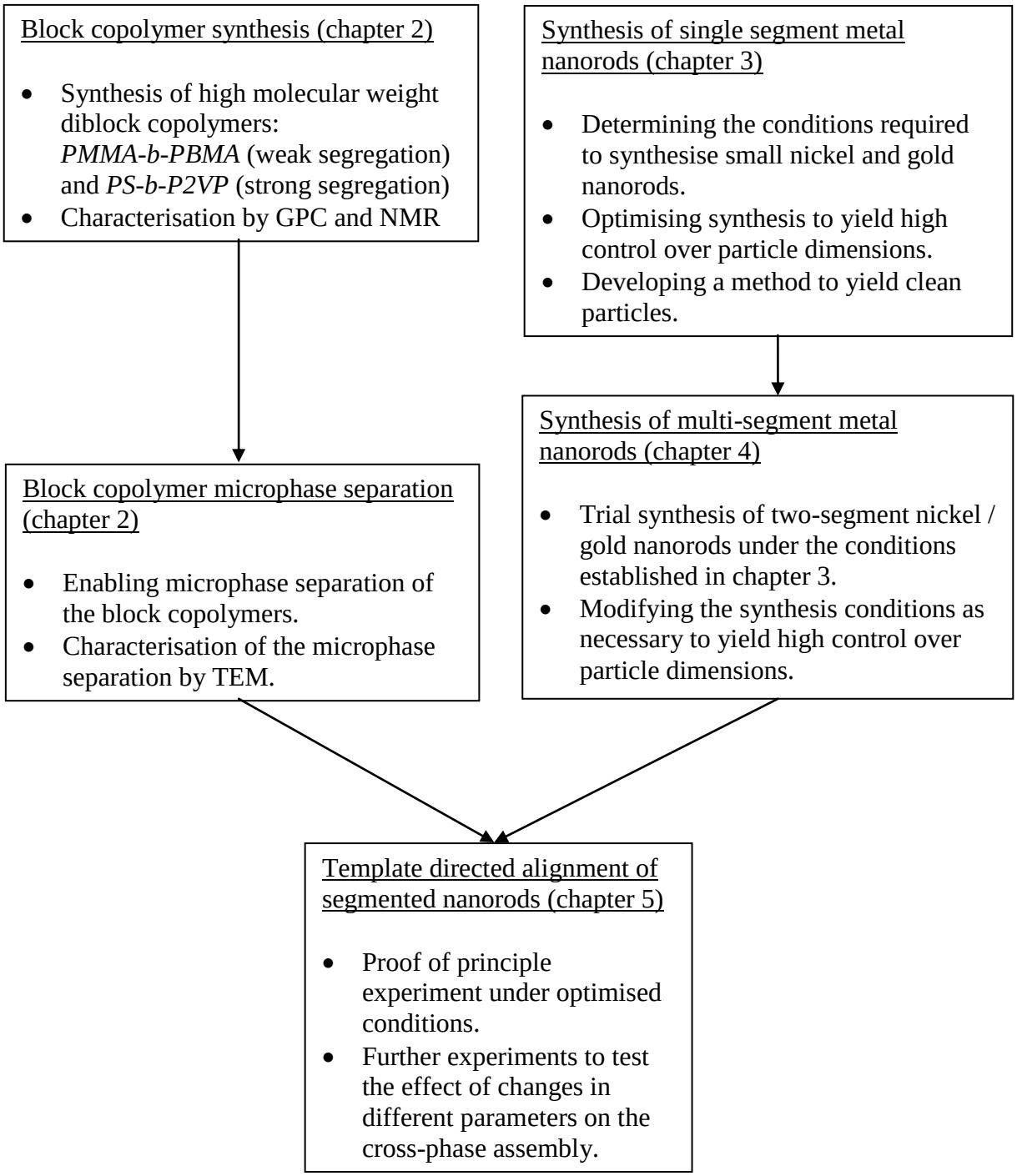
Block copolymer synthesis (chapter 2)
Synthesis of high molecular weight diblock copolymers: PMMA-b-PBMA (weak segregation) and PS-b-P2VP (strong segregation)
Characterisation by GPC and NMR
Synthesis of single segment metal nanorods (chapter 3)
Determining the conditions required to synthesise small nickel and gold nanorods.
Optimising synthesis to yield high control over particle dimensions.
Developing a method to yield clean particles.
Block copolymer microphase separation (chapter 2)
Enabling microphase separation of the block copolymers.
Characterisation of the microphase separation by TEM.
Synthesis of multi-segment metal nanorods (chapter 4)
Trial synthesis of two-segment nickel / gold nanorods under the conditions established in chapter 3.
Modifying the synthesis conditions as necessary to yield high control over particle dimensions.
Template directed alignment of segmented nanorods (chapter 5)
Proof of principle experiment under optimised conditions.
Further experiments to test the effect of changes in different parameters on the cross-phase assembly.

1.6. References

1. Klabunde, K.J., et al., *Nanoscale Materials in Chemistry*, ed. K.J. Klabunde. 2001, New York: John Wiley and Sons, inc. 292.
2. Atkins, P., de Paula, J., *Atkins' Physical Chemistry*. 7th ed. 2002, New York: Oxford University Press. 1149.
3. Rao, C.N.R., Kulkarni, G. U., Thomas, P. J., Edwards, P. P. Chemistry Society Reviews, 2000. **29**: p. 27.
4. Santhanam, V., Andres, R. P., *Metal Nanoparticles and Self-Assembly into Electronic Nanostructures*, in *Dekker Encyclopedia of Nanoscience and Nanotechnology*, J.A. Schwarz, Contescu, C. I., Putyera, K., Editor. 2004, CRC Press. p. 4014.
5. Ralph, D.C., Black, C. T., Tinkham, M. Physical Review Letters, 1997. **78**(21): p. 4087.
6. Aslam, M., Mulla, I. S., Vijayamohanan, K. Applied Physics Letters, 2001. **79**(5): p. 689.
7. Barner, J.B., Ruggiero, S. T. Physical Review Letters, 1987. **59**: p. 807.
8. Jakubovics, J.P., *Magnetism and Magnetic Materials*. 1987, Brookfield: The Institute of Metals.
9. Johnston, R.L., *Atomic and Molecular Clusters*. 2002: CRC Press. 236.
10. Majetich, S.A.S., M. Journal of Physics D: Applied Physics, 2006. **39**: p. R407.
11. Ida, N., *Engineering Electromagnetics*. 2nd ed. 2004: Springer.
12. Edelstein, A.S., Cammarata, R. C., *Nanoparticles: Synthesis, Properties and Applications*, ed. A.S.C. Edelstein, R. C. 1996, Bristol: Institute of Physics Publishing.
13. Chantrell, R.W., Wohlfarth, E. P. Journal of Magnetism and Magnetic Materials, 1983. **40**: p. 1.
14. Link, S., El-Sayed, M. A. Journal of Physical Chemistry B, 1999. **103**: p. 8410.
15. Noguez, C. Optical Materials, 2005. **27**: p. 1204.

16. Gonzalez, A.L., Noguez, C. Journal of Computational and Theoretical Nanoscience, 2007. **4**: p. 231.
17. El-Sayed, M.A. Accounts of Chemical Research, 2001. **34**: p. 257.
18. Ghosh, S.K., Pal, T. Chemical Reviews, 2007. **107**(11): p. 4797.
19. Murphy, C.J., Jana, N. R. Advanced Materials, 2002. **14**: p. 80.
20. Jin, R., Cao, Y., Mirkin, C. A., Kelly, K. L., Schatz, G. C., Zheng, J. G. Science, 2001. **294**: p. 1901.
21. Xia, Y., Yang, O., Sun, Y., Wu, Y., Mayers, B., Gates, B., Yin, Y., Kim, F., Yan, H. Advanced Materials, 2003. **15**(5): p. 353.
22. Hall, E., O. Proceedings of the Physics Society of London, B, 1951. **64**: p. 747.
23. Petch, N.J. Journal of the Iron and Steel Institute, 1953. **174**: p. 25.
24. Schaefer, D.M., Patil, A., Andres, R. P., Reifenberger, R. Applied Physics Letters, 1993. **63**(12): p. 1492.
25. Carlton, C., Ferreira, P. J. Materials Research Society Symposium Proceedings., 2007. **976**.
26. Nanda, K.K., Maisels, A., Kruis, F. E., Fissan, H., Stappert, S. Physical Review Letters, 2003. **91**(10): p. 106102.
27. Zhong, C.-J., Maye, M. M., Luo, J., Han, L., Kariuki, N., *Nanoparticles in Catalysis*, in *Nanoparticles: Building Blocks for Nanotechnology*, V.M. Rotello, Editor. 2004, Springer. p. 284.
28. Kolasinski, K.W., *Surface Science: Foundations of catalysis and nanoscience*. 2002, London: John Wiley and Sons, Ltd.
29. Berthier, Y., Delamare, F., Hondros, E., Huber, M., Marcus, P., Masson, A., Oudar, J., Rhead, G. E., Benard, J., *Adsorption on metal surfaces: an integrated approach*. Studies in surface science and analysis, ed. J. Benard. Vol. 13. 1983, Amsterdam: Elsevier.
30. Beach, D.B., Rondinone, A. J., Sumpter, B. G., Labinov, S. D., Richards, R. K. Journal of Energy Resources Technology, 2007. **129**(1): p. 29.
31. Haruta, M. The Chemical Record, 2003. **3**: p. 75.
32. Huber, H., McIntosh, D., Ozin, G. A. Inorganic Chemistry, 1977. **16**(5): p. 975.

33. Bamwenda, G.R., Tsubota, S., Nakamura, T., Haruta, M. Catalysis Letters, 1997. **44**: p. 83.
34. Bond, G.C., Thompson, D. T. Catalysis Reviews, 1999. **41**(3-4): p. 319.
35. Valden, M., Lai, X., Goodman, D. W. Science, 1998. **281**: p. 1647.
36. Gangopadhyay, S.H., G. C.; Dale, B.; Sorensen, C. M.; Klabunde, K. J.; Papaefthymiou, V.; Kostikas, A. Physical Review B, 1992. **45**: p. 9778.
37. Castro, T., Reifenberger, R., Choi, E., Andres, R. P. Physical Review B, 1990. **42**(13): p. 8548.
38. Cahn, R.W. Nature, 1986. **323**: p. 668.
39. Buffat, P., Borel, J-P. Physical Review A, 1976. **13**: p. 2287 - 2298.
40. Qi, W.H., Wang, M. P. Journal of Materials Science Letters, 2002. **21**: p. 1743.
41. Dick, K., Dhanasekaran, T., Zhang, Z., Meisel, D. Journal of the American Chemical Society, 2002. **124**(10): p. 2312.
42. Ahmadi, T.S., Wang, Z. L., Green, T. C., Henglein, A., El-Sayed, M. A. Science, 1996. **272**: p. 1924.
43. Felidj, N., Levi, G., Pantigny, J., Aubard, J. New Journal of Chemistry, 1998: p. 725.
44. Eckert, J., Holzer, J. C., Kril, C. E III., Johnson, W. L. Journal of Materials Research, 1992. **7**: p. 1751.
45. Koch, C.C. Nanostructured Materials, 1993. **2**: p. 109.
46. Hellstern, E., Fecht, H. J., Fu, Z., Johnson, W. L. Journal of Material Research, 1989. **4**: p. 1292.
47. Yamada, K., Koch, C. C. Journal of Material Research, 1993. **8**: p. 1317.
48. Yavari, A.R., Desre, P. J., Benameur, T. Physical Review Letters, 1992. **68**: p. 2235.
49. Gaffet, E., Louison, C., Harmelin, M., Faudet, F. Journal of Materials Science and Engineering, A, 1991. **134**: p. 1380.
50. Veltl, G., Scholz, B., Kunze, H. D. Journal of Materials Science and Engineering, A, 1991. **134**: p. 1410.

51. Fukanaga, T., Mori, M., Inou, K., Mizutani, U. Journal of Materials Science and Engineering, A, 1991. **134**: p. 863.
52. Gilman, P.S., Benjamin, J. S. Annual Review of Materials Science, 1983. **13**: p. 279.
53. Walsh, M., Hao, Y., Ross, C. A., Smith, H. I. Journal of Vacuum Science and Technology, B, 2000. **18**: p. 3539.
54. Vogeli, B., Smith, H. I., Castano, F. J., Hao, Y., Haratani, S., Ross, C. A. Journal of Vacuum Science and Technology, B, 2001. **19**: p. 2753.
55. Allpress, J.G., Sanders, J. V. Surface Science, 1967. **7**: p. 1.
56. Hagena, O. Surface Science, 1981. **106**: p. 101.
57. Fenn, J.B. Applied Atomic Collision Physics, 1982. **5**: p. 349.
58. Campargue, R. Journal of Physical Chemistry, 1984. **88**: p. 4466.
59. McCay, T.D., Price, L. L. Physics of Fluids, 1983. **26**: p. 2115.
60. Kappes, M.M., Kunz, R. W., Schumacher, E. Chemical Physics Letters, 1982. **91**: p. 413.
61. Martin, T.P. Angewandte Chemie International Edition in English, 1986. **25**: p. 197.
62. Cohen, M., Chou, M. Y., Knight, W. D., de Heer, W. A. Journal of Physical Chemistry, 1987. **91**: p. 3141.
63. Phillips, J.C. Chemical Reviews, 1986. **86**: p. 619.
64. Sattler, K., Muhlbach, J., Pfau, P., Recknagel, E. Physical Letters, 1982. **87A**: p. 418.
65. Gohlich, H., Lange, T., Bergmann, T., Martin, T. P. Physical Review Letters, 1990. **65**: p. 748.
66. Martin, T.P., Bergmann, T., Gohlich, H., Lange, T. Chemical Physics Letters, 1991. **176**: p. 343.
67. Dietz, T., Duncan, M., Liverman, M., Smalley, R. Journal of Chemical Physics, 1980. **73**: p. 4816.
68. Dietz, T., Duncan, M., Powers, D., Smalley, R. Journal of Chemical Physics, 1981. **74**: p. 6511.
69. Smalley, R.E. Laser Chemistry, 1983. **2**: p. 167.
70. Powers, D.E., Hansen, S. G., Geusic, M. E., Puiu, A. C., Hopkins, J. B., Dietz, T. G., Duncan, M. A., Langridge-Smith, P. R. R., Smalley, R. E. Journal of Physical Chemistry, 1982. **86**: p. 2556.

71. Powers, D.E., Hansen, S. G., Geusic, M. E., Michalopoulos, D. L., Smalley, R. E. Journal of Physical Chemistry, 1983. **78**: p. 2866.
72. Heath, J.R., Liu, Y., O'Brien, S. C., Zhang, Q-L., Curl, R. F., Tittel, F. K., Smalley, R. E. Journal of Chemical Physics, 1985. **83**: p. 5520.
73. Cox, D.M., Trevor, D. J., Whetten, R. L., Kaldor, A. J. Journal of Physical Chemistry, 1988. **92**: p. 421.
74. Whetten, R.L., Cox, D. M., Trevor, D. J., Kaldor, A. Surface Science, 1985. **156**: p. 8.
75. Loh, S.K., Hales, D. A., Armentrout, P. B. Chemical Physics Letters, 1986. **129**: p. 527.
76. Rohlfing, E.A., Cox, D. M., Kaldor, A. Journal of Chemical Physics, 1984. **81**: p. 3322.
77. Bloomfield, L.A., Freeman, R. R., Brown, W. L. Physical Review Letters, 1985. **54**: p. 2246.
78. Lai-Hing, K., Wheeler, R. G., Wilson, W. L., Duncan, M. A. Journal of Chemical Physics, 1987. **87**: p. 3401.
79. Wheeler, R.G., Lai-Hing, K., Wlison, W. L., Duncan, M. A. Chemical Physics Letters, 1986. **131**(8).
80. Tang, Z.X., Nafis, S., Sorensen, C. M., Hadjipanayis, G. C., Klabunde, K. J. Journal of Magnetism and Magnetic Materials, 1989. **80**: p. 285.
81. Pfund, A.H. Physical Review, 1930. **35**: p. 1434.
82. Harris, L., Jeffries, D., Siegel, B. M. Journal of Applied Physics, 1948. **19**: p. 791.
83. Uyeda, R.J. Crystal Growth and Design, 1974. **24**: p. 69.
84. Tasaki, A., Tomiyana, S., Lida, S. Japanese Journal of Applied Physics, 1965. **4**: p. 707.
85. Hayashi, C. Journal of Vacuum Science and Technology, A, 1987. **5**: p. 1375.
86. Granqvist, C.G., Buhrman, R. A. Journal of Applied Physics, 1976. **47**: p. 2200.
87. Du, Y., W., Wu, J., Lu, H., Wang, T., Hiu, Z. Q., Tang, H., Walker, J. C. Journal of Applied Physics, 1987. **61**: p. 3314.

88. Andres, R.P., Bielefeld, J. D., Henderson, J. J., Janes, D. B., Kolagunta, V. R., Kubiak, C. P., Mahoney, W. J., Osifchin, R. G. Science, 1996. **273**: p. 1690.
89. Berthet, A., Thomann, A. L., Aires, F. J. C. S., Brun, M., Deranlot, C., Bertolini, J. C., Rozenbaum, J. P., Brault, P., Andrezza, P. Journal of Catalysis, 2000. **190**: p. 49.
90. Hahn, H., Averback, R. S. Journal of Applied Physics, 1990. **67**: p. 1113.
91. CXiao, G., Chien, C. L. Journal of Applied Physics, 1987. **61**: p. 3308.
92. Xiao, G., Chien, C. L. Journal of Applied Physics, 1987. **61**: p. 1280.
93. Xiao, G., Liou, S. H., Levy, A., Taylor, J. N., Chien, C. L. Physical Review, B, 1986. **34**: p. 7573.
94. Edelstein, A.S., Das, B. N., Holtz, R. L., Koon, N. C., Rubinstein, M., Wolt, S. A., Kihlsran, K. E. Journal of Applied Physics, 1987. **61**: p. 3320.
95. Chow, G.W., Pattnaik, A., Schlesinger, T. E., Cammarata, R. C., Twigg, M. E., Edelstein, A. S. Journal of Material Research, 1991. **6**: p. 737.
96. Jensen, T.R., Schatz, G. C., Van Duyne, R. P. Journal of Physical Chemistry, B, 1999. **103**: p. 2394.
97. Hulteen, J.C., Treichel, D. A., Smith, M. T., Duval, M. L., Jensen, T. R., Van Duyne, R. P. Journal of Physical Chemistry, B, 1999. **103**: p. 3854.
98. Mandich, M.L., Bondybey, V. E., Reents, W. D. Journal of Chemical Physics, 1987. **86**: p. 4245.
99. Chumanov, G., Sokolov, K., Gregory, B. W., Cotton, T. M. Journal of Physical Chemistry, 1995. **99**: p. 9466.
100. Berkowitz, A.E., Walter, J. L. Journal of Material Research, 1987. **2**: p. 227.
101. Berkowitz, A.E., Walter, J. L., Wall, K. F. Physical Review Letters, 1981. **46**: p. 1484.
102. Slade, S.B., Berkowitz, A. E., Parker, F. T. Journal of Applied Physics, 1991. **69**: p. 5127.
103. Hung, C.H., Katz, J. L. Journal of Material Research, 1992. **7**: p. 1861.

104. Skandan, G., Kear, B. H., Chang, W., Hanh, H., *Apparatus for making nanostructured ceramic powders and whiskers. US Patent: 5,514,350*. 1996, Rutgers University: USA.
105. Tompa, G.S., Skandan, G., Glumac, N., Kear, B. H. American Ceramic Society Bulletin, 1999. **78**(10): p. 70.
106. Van Wonterghem, J., Morup, S., Charles, S. W., Wells, S., Villadsen, J. Physical Review Letters, 1985. **55**: p. 410.
107. Gates, B.C., Lamb, H. H. Journal of Molecular Catalysis, 1989. **52**: p. 1.
108. Ichikawa, M. Advances in Catalysis, 1992. **38**: p. 283.
109. Iwasawa, Y. Catalysis Today, 1993. **18**: p. 21.
110. Gates, B.C. Journal of Molecular Catalysis, 1994. **86**: p. 96.
111. Zhang, Y., Dai, H. Applied Physics Letters, 2000. **77**: p. 3015.
112. Kapon, E., Kash, K., Clausen Jr, E. M., Hwang, D. M., Colas, E. Applied Physics Letters, 1992. **60**: p. 477.
113. Walther, M., Kaplon, E., Christen, J., Hwang, D. M., Bhat, R. Applied Physics Letters, 1992. **60**: p. 521.
114. Jorritsma, J., Gijs, M. A. M., Kerkhof, J. M., Stienen, J. G. H. Nanotechnology, 1996. **7**: p. 263.
115. Olson, E., Spalding, G. C., Goldman, A. M., Rooks, M. Applied Physics Letters, 1994. **65**: p. 2740.
116. Gates, B.C., *Supported Nanostructured Catalysts: Metal Complexes and Metal Clusters*, in *Nanostructured Materials*, J.Y. Ying, Editor. 2001, Academic Press: San Diego.
117. Ross, C.A., Haratani, S., Castano, F. J., Hao, Y., Hwang, M., Shima, M., Cheng, J. Y., Vogeli, B., Farhoud, M., Walsh, M., Smith, H. I. J. Journal of Applied Physics, 2002. **91**(10): p. 6848.
118. LaMer, V.K., Dinegar, R. H. Journal of the American Chemical Society, 1950. **72**(11): p. 4847.
119. Burkin, A.R., Richardson, F. D. Powder Metallurgy, 1967. **10**: p. 32.
120. Van Wonterghem, J., Morup, S., Koch, C. J. W., Charles, S. W., Wells, S. Nature, 1986. **322**: p. 622.
121. Inoue, A., Saida, J., Masumoto, T. Metallurgical Transactions, A, 1988. **19**: p. 2315.

122. Shen, J., Hu, Z., Hsia, Y., Chen, Y. Applied Physics Letters, 1991. **59**: p. 2510.
123. Chow, G.M., Ambrose, T., Xiao, J. Q., Twigg, M. A., Baral, S., Ervin, A. M., Qadri, S. B., Feng, C. R. Nanostructured Materials, 1991. **1**: p. 361.
124. Chow, G.M., Ambrose, T., Xiao, J. Q., Kaatz, F., Ervin, A. Nanostructured materials, 1993. **2**: p. 131.
125. Bonnemann, H., Brijoux, W., Joussen, T. Angewandte Chemie International Edition in English, 1990. **29**: p. 273.
126. Bonnemann, H., Brijoux, W., Brinkmann, R., Dinjus, E., Jouben, T., Koraff, B. Angewandte Chemie International Edition in English, 1990. **30**: p. 1312.
127. Zeng, D., Hampden-Smith, M. J. Chemistry of Materials, 1993. **5**: p. 681.
128. Riecke, R.D. Science, 1986. **246**: p. 1260.
129. Tsai, K., Dye, J. L. Chemistry of Materials, 1993. **5**: p. 540.
130. Lu, D.-L., Tanaka, K. Journal of Physical Chemistry, 1996. **100**: p. 1833.
131. Gilbert, S.E., Cavalleri, O., Kern, K. Journal of Physical Chemistry, 1996. **100**: p. 12123.
132. Kind, H., Bittner, A. M., Cavalleri, O., Kern, K. Journal of Physical Chemistry, B, 1998. **102**: p. 7582.
133. Suslick, K.S., Fang, M., Hyeon, T., Cichowlas, A. A. Materials Research Society Symposium Proceedings., 1994. **351**: p. 443.
134. Suslick, K.S., Fang, M., Hyeon, T., Mdleleni, M. M., *Applications of sonochemistry to materials synthesis*, in *Sonochemistry and Sonoluminescence*, I.A. Crum, Mason, T. J., Reisse, J., Suslick, K. S., Editor. 1999, Kluwer Publishers: Dordrecht.
135. Smith, T.W., Wychick, D. Journal of Physical Chemistry, 1980. **84**: p. 1621.
136. Ishikawa, T., Matijevic, E. Langmuir, 1988. **4**: p. 26.
137. Kim, F., Song, J. H., Yang, P. Journal of the American Chemical Society, 2002. **124**(48): p. 14316.

138. Bronstein, L.M., Mirzoeva, E. Sh., Valetsky, P. M., Solodovnikov, S. P., Register, R. A. Journal of Materials Chemistry, 1995. **5**: p. 1197.
139. Turkevich, J., Stevenson, P. C., Hiller, J. Discussions of the Faraday Society, 1951. **11**: p. 55.
140. Yee, C., Scotti, M., Ulman, A., White, H., Rafailovich, M., Sokolov, J. Langmuir, 1999. **15**: p. 4314.
141. Teranishi, T., Hosoe, M., Tanaka, T., Miyake, M. Journal of Physical Chemistry, 1999. **103**: p. 3818.
142. Cassagneau, T., Fendler, J. H. Journal of Physical Chemistry, B, 1999. **103**: p. 1789.
143. Bright, R.M., Musick, M. D., Natan, M. J. Langmuir, 1998. **14**: p. 5695.
144. Turkevich, J., Kim, G. Science, 1970. **169**: p. 873.
145. Rampino, L.D., Nord, F. F. Journal of the American Chemical Society, 1941. **63**: p. 2745.
146. Gao, Y., Jiang, P., Liu, D. F., Yuan, H. J., Yan, X. Q., Zhou, Z. P., Wang, J. X., Song, L., Liu, L. F., Zhou, W. Y., Wang, G., Wang, C. Y., Xie, S. S. Chemical Physics Letters, 2003. **380**(1-2): p. 146.
147. Jin, C.G., Jiang, G. W., Liu, W. F., Cai, W. L., Yao, L. Z., Yao, Z., Li, X. G. Journal of Materials Chemistry, 2003. **13**: p. 1743.
148. Yen, M.-Y., Chiu, C-W., Hsia, C-H., Chen, F-R., Kai, J-J., Lee, C-Y., Chiu, H-T. Advanced Materials, 2003. **15**(3): p. 235.
149. Zach, M.P., Ng, K. H., Penner, R. M. Science, 2000. **290**: p. 2120.
150. Luborsky, F.E. Journal of Applied Physics, 1961. **32**: p. 1715.
151. Yiping, L., Hadjipanayis, G. C., Sorensen, C. M., Klabunde, K. J. Journal of Magnetism and Magnetic Materials, 1989. **79**: p. 321.
152. Schmid, G. Chemical Reviews, 1992. **92**: p. 1709.
153. Toshima, N., Yonezawa, T. New Journal of Chemistry, 1998. **11**: p. 1179.
154. Keating, C.D., Kovaleski, K. K., Natan, M. J. Journal of Physical Chemistry, B, 1998. **102**: p. 9404.
155. Mann, S., Hannington, J. P., Williams, R. J. P. Nature, 1986. **324**: p. 565.

156. Bhandarkar, S., Bose, A. J. Colloid and Interface Science, 1990. **135**: p. 531.
157. Bhandarkar, S., Yaacob, I., Bose, A. Materials Research Society Symposium Proceedings., 1990. **180**: p. 637.
158. Markowitz, M.A., Chow, G. M., Singh, A. Langmuir, 1994. **10**: p. 4095.
159. Li, T., Moon, J., Morrone, A. A., Mecholsky, J. J., Talham, D. R., Adatr, J. H. Langmuir, 1999. **15**: p. 5328.
160. Lisiecki, I., Pileni, M. P. Journal of the American Chemical Society, 1993. **115**: p. 3887.
161. Antonietti, M., Heinz, S. Nachrichten Aus Chemie Technik Und Laboratorium, 1992. **40**: p. 308.
162. Mayer, A.B.R., Mark, J. E. Polymer Preprints, 1996. **74**: p. 459.
163. Spatz, J.P., Roescher, A., Moller, M. Advanced Materials, 1996. **8**: p. 337.
164. Bates, F.S., Fredrickson, G. H. Physics Today, 1999. **52**: p. 32.
165. Kurihara, K., Fendler, J. H. Abstracts of the American Chemical Society, 1983. **186**: p. 41.
166. Braun, E., Eichen, Y., Sivan, U., Ben-Yoseph, G. Nature, 1998. **391**: p. 775.
167. Moser, W.R., Find, J., Emerson, S. C., Krausz, I. M., *Engineered Synthesis of Nanostructured Materials and Catalysts*, in *Nanostructured Materials*, J.Y. Ying, Editor. 2001, Academic Press: San Diego.
168. Clark, T.D., Ghadiri, M. R. Journal of the American Chemical Society, 1995. **117**: p. 12364.
169. Zhao, M., Crooks, R. M. Advanced Materials, 1999. **11**: p. 217.
170. Zhao, M., Crooks, R. M. Angewandte Chemie Internation Edition in English, 1999. **38**: p. 364.
171. Zhao, M., Sun, L., Crooks, R. M. Journal of the American Chemical Society, 1998. **120**: p. 4877.
172. Balogh, L., Tomalia, D. A. Journal of the American Chemical Society, 1998. **120**: p. 7355.

173. Keller, F., Hunter, M. S., Robinson, D. L. Journal of the Electrochemical Society, 1953. **100**: p. 411.
174. Masuda, H., Yamada, H., Satoh, M., Asoh, H., Nakao, M., Tamamura, T. Applied Physics Letters, 1997. **71**: p. 2772.
175. Li, A.P., Muller, F., Birner, A., Neilsch, K., Gosele, U. Journal of Applied Physics, 1998. **84**: p. 6023.
176. Tonucci, R.J., Justus, B. J., Campillo, A. J., Ford, C. E. Science, 1992. **258**: p. 783.
177. Huber, C.A., Huber, T. E., Sadoqi, M., Lubin, J. A., Manalis, S., Prater, C. B. Science, 1994. **263**: p. 800.
178. Martin, C.R. Science, 1994. **266**: p. 1961.
179. Blondel, A., Meier, J. P., Doudin, B., Ansermet, J-Ph. Applied Physics Letters, 1994. **65**: p. 3019.
180. Liu, K., Chien, C. L., Searson, P. C. Physical Review, B, 1998. **58**: p. 14681.
181. Sun, L., Searson, P. C., Chien, C. L. Applied Physics Letters, 1999. **74**: p. 2803.
182. Jacobs, P.A. Studies in Surface Science and Catalysis, 1984. **29**: p. 357.
183. Stucky, G.D., MacDougall, J. E. Science, 1990. **247**: p. 669.
184. Karge, H.G., Beyer, H. K. Studies in Surface Science and Catalysis, 1991. **69**: p. 43.
185. Gellens, L.R., Mortier, W. J., Schoonheydt, R. A., Uytterhoeven, J. Journal of Physical Chemistry, 1981. **85**: p. 2783.
186. Ding, J.H., Gin, D. L. Chemistry of Materials, 2000. **12**: p. 22.
187. Bharathi, S., Lev, O. Chemical Communications, 1997: p. 2302.
188. Yanagi, H., Ohno, T. Langmuir, 1999. **15**: p. 4773.
189. Zubimendi, J.L., et al. Journal of Physical Chemistry, 1993. **97**: p. 5095.
190. Cho, A.Y. (1995) Materials Research Society Bulletin.
191. Fasol, G. Science, 1998. **280**: p. 545.
192. Zhang, Y., Franklin, N. W., Chen, R. J., Dai, H. Chemical Physics Letters, 2000. **331**: p. 35.
193. Ajayan, P.M.S., O., Redlich, P., Colliex, C. Nature, 1995. **375**: p. 564.

194. Song, J.H., Wu, Y., Messer, B., Kind, H., Yang, P. Journal of the American Chemical Society, 2001. **123**: p. 10397.
195. Sun, Y., Mayers, B. T., Xia, Y. Nano Letters, 2002. **2**: p. 481.
196. Wen, X., Yang, S. Nano Letters, 2002. **2**: p. 451.
197. Puntes, V.F., Krishnan, K. M., Alivastos, A. P. Science, 2001. **291**: p. 2115.
198. Nicewarner-Pena, S.R., Freeman, R. G., Reiss, B. D., He, L., Pena, D. J., Walton, I. D., Cromer, R., Keating, C. D., Natan, M. J. Science, 2001. **294**: p. 137.
199. Filankembo, A., Pileni, M. P. Journal of Physical Chemistry, B, 2000. **104**: p. 5865.
200. Johnson, C.J., Dujardin, E., Davis, S. A., Murphy, C. J., Mann, S. Journal of Materials Chemistry, 2002. **12**: p. 1765.
201. Sun, Y., Gates, B., Mayers, B., Xia, Y. Nano Letters, 2002. **2**: p. 165.
202. Sun, Y., Xia, Y. Advanced Materials, 2002. **14**: p. 833.
203. Sun, Y., Yin, Y., Mayers, B. T., Herricks, T., Xia, Y. Chemistry of Materials, 2002. **14**: p. 4736.
204. Curtis, A.C., Duff, D. G., Edwards, P. P., Jefferson, D. A., Johnson, B. F. G., Kirkland, A. I., Wallace, A. S. Angewandte Chemie Internation Edition in English, 1988. **27**: p. 1531.
205. Bradley, J.S., Tesche, B., Busser, W., Maase, M., Reetz, M. T. Journal of the American Chemical Society, 2000. **122**: p. 4631.
206. Cordente, N., Respaud, M., Senocq, M-J., Amiens, C., Chaudret, B. Nano Letters, 2001. **1**(10): p. 565.
207. Park, S.-J., Kim, S., Lee, S., Khim, Z. G., Char, K., Hyeon, T. Journal of the American Chemical Society, 2000. **122**: p. 8581.
208. Everett, D.H., *Basic Principles of Colloid Science*. 1988, London: Royal Society of Chemistry.
209. Hunter, R.J., *Introduction to Modern Colloid Science*. 1993: Oxford University Press.
210. Rozenberg, B.A., Tenne, R. Progress in Polymer Science, 2008. **33**(1): p. 40.

211. Brust, M., Walker, M., Bethell, D., Schiffrin, D., Whyman, R. Journal of the Chemical Society, Chemical Communications, 1994. **1994**: p. 801.
212. Brown, L.O., Hutchison, J. E. Journal of Physical Chemistry, B, 2001. **105**: p. 8911.
213. Schmid, G. Structure and Bonding, 1985. **62**: p. 51.
214. Schmid, G. Inorganic Synthesis, 1990. **27**: p. 214.
215. Badia, A., Singh, S., Demers, L., Cuccia, L., Brown, G. R., Lennox, R. B. Chemistry, A European Journal, 1996. **2**: p. 359.
216. Daniel, M.C., Astruc, D. Chemical Reviews, 2004. **104**: p. 293.
217. Sandhyarani, N., Pradeep, T. International Reviews in Physical Chemistry, 2003. **22**: p. 221.
218. Hostetler, M.J., Templeton, A. C., Murray, R. W. Langmuir, 1999. **15**: p. 3782.
219. Peschel, S., Schmid, G. Angewandte Chemie Internation Edition in English, 1995. **34**: p. 1442.
220. Collier, C.P., Vossmeyer, T., Heath, J. R. Annual Review of Physical Chemistry, 1998. **49**: p. 371.
221. Henglein, A., Giersig, M. Journal of Physical Chemistry, B, 1999. **103**: p. 9355.
222. Porter Jr, L.A., Ji, D., Westcott, S. L., Graupe, M., Czernuszewics, R. S., Halas, N. J., Lee, T. R. Langmuir, 1998. **14**: p. 7378.
223. Fink, J., Kiely, C. J., Bethell, D., Schiffrin, D. J. Chemistry of Materials, 1998. **10**: p. 922.
224. Lowe, A.B., Sumerlin, B. S., Donovan, M. S., McCormick, C. L. Journal of the American Chemical Society, 2002. **124**: p. 11562.
225. Teranishi, T., Kiyokawa, I., Miyake, M. Advanced Materials, 1998. **10**: p. 596.
226. Teranishi, T., Hosoe, M., Miyake, M. Advanced Materials, 1997. **9**: p. 65.
227. Wuelfing, W.P., Gross, S. M., Miles, D. T., Murray, R. W. Journal of the American Chemical Society, 2998. **120**: p. 12696.

228. Marinakos, S.M., Novak, J. P., Brousseau III, L. C., House, A. B., Edeki, E. M., Feldhaus, J. C., Feldheim, D. L. Journal of the American Chemical Society, 1999. **121**: p. 8518.
229. Watson, K.J., Zhu, J., Nguyen, S. T., Mirkin, C. A. Journal of the American Chemical Society, 1999. **121**: p. 462.
230. Wang, R., Yang, J., Zheng, Z., Carducci, M. D., Jiao, J., Seraphin, S. Angewandte Chemie Internation Edition in English, 2001. **40**: p. 549.
231. Frankamp, B.L., Boal, A. K., Rotello, V. M. Journal of the American Chemical Society, 2002. **124**: p. 15146.
232. Tom, R.T., Nair, A. S., Singh, N., Aslam, M., Nagendra, C. L., Philip, R., Vijayamohanan, K., Pradeep, T. Langmuir, 2003. **19**: p. 3439.
233. Liz-Marzan, L.M., Giersig, M., Mulvaney, P. Langmuir, 1996. **12**: p. 4329.
234. Tunc, I., Suzer, S., Correa-Duarte, M. A., Liz-Marzan, L. M. Journal of Physical Chemistry, B, 2005. **109**: p. 7597.
235. Woehrle, G.E., Brown, L. O., Hutchison, J. E. Journal of the American Chemical Society, 2005. **127**: p. 2172.
236. Matrab, T., Chehimi, M. M., Perruchot, C., Adenier, A., Guillez, A., Save, M., Charleux, B., Cabet-Deliry, E., Pinson, J. Langmuir, 2005. **21**: p. 4686.
237. Xu, F.J., Cai, Q. J., Kang, E. T., Neoh, K. G. Langmuir, 2005. **21**: p. 3221.
238. Ostmark, E., Macakova, L., Auletta, T., Malkoch, M., Malmstrom, E., Blomberg, E. Langmuir, 2005. **21**: p. 4512.
239. Chiu, J.J., Kim, B. J., Kramer, E. J., Pine, D. J. Journal of the American Chemical Society, 2005. **127**: p. 5036.
240. Kell, A.J., Donkers, R. L., Workentin, M. S. Langmuir, 2005. **21**: p. 735.
241. Schmitt, H., Badia, A., Dickinson, L., Reven, L., Lennox, R. B. Advanced Materials, 1998. **10**: p. 475.
242. Boal, A.K., Rotello, V. M. Journal of the American Chemical Society, 2002. **124**: p. 5019.
243. Labande, A., Ruiz, J., Astruc, D. Journal of the American Chemical Society, 2002. **124**: p. 1782.

244. Kreibig, U., Genzel, L. Surface Science, 1985. **156**: p. 678.
245. Mulvaney, P. Langmuir, 1996. **12**: p. 788.
246. Osuna, J., de Caro, D., Amiens, C., Chaudret, B., Snoeck, E., Respaud, M., Broto, J-M., Fert, A. Journal of Physical Chemistry, 1996. **100**: p. 14571.
247. De, M., Ghosh, P. S., Rotello, V. M. Advanced Materials, 2008. **20**(22): p. 4225.
248. Liu, W.-T. Journal of Bioscience and Bioengineering, 2006. **102**(1): p. 1.
249. Baker, C.C., Pradhan, A., Shah, S. I, *Metal Nanoparticles*, in *Encyclopedia of Nanoscience and Nanotechnology*, H.S. Nalwa, Editor. 2004. p. 449.
250. Lazzari, M.,Lopez-Quintela, M.A. Advanced Materials, 2003. **15**(19): p. 1583.
251. Shouheng, S., et al. Science, 2000. **287**: p. 1989.
252. Reiss, G.H., A. Nature Materials, 2005. **4**: p. 725.
253. Park, C., Yoon, J.,Thomas, E.L. Polymer, 2003. **44**: p. 6725.
254. Markovich, G., Collier, C. P., Henrichs, S. E., Remacle, F., Levine, R. D., Heath, J. R. Accounts of Chemical Research, 1999. **32**: p. 415.
255. Feldheim, D.L., Grabar, K. C., Natan, M. J., Mallouk, T. E. Journal of the American Chemical Society, 1996. **118**(32): p. 7640.
256. Collier, C.P., Saykally, R. J., Shiang, J. J., Henrichs, S. E., Heath, J. R. Science, 1997. **277**: p. 1978.
257. Stafford, C.A., Das Sarma, S. Physical Review Letters, 1994. **72**(22): p. 3590.
258. Schmid, G., *Nanoparticles: From Theory to Application*. 2004: Wiley-VCH.
259. Livermore, C., Crouch, C. H., Westervelt, R. M., Campman, K. L., Gossard, A. C. Science, 1996. **274**(5291): p. 1332.
260. Chen, S. Analytica Chimica Acta, 2003. **496**: p. 29.
261. Grabar, K.C., Allison, K. J., Baker, B. E., Bright, R. M., Brown, K. R., Freeman, R. G., Fox, A. P., Keating, C. D., Musick, M. D., Natan, M. J. Langmuir, 1996. **12**: p. 2353.

262. Novak, J.P., Feldheim, D. L. Journal of the American Chemical Society, 2000. **122**: p. 3979.
263. Jensen, T., Kelly, L., Lazarides, A., Schatz, G. C. Journal of Cluster Science, 1999. **10**(2): p. 295.
264. Boal, A.K., Frankamp, B. L., Uzun, O., Tuominen, M. T., Rotello, V. M. Chemistry of Materials, 2004. **16**(17): p. 3252.
265. Jonsson, T., Nordblad, P., Svedlindh, P. Physical Review, B, 1998. **57**: p. 497.
266. Russier, V., Petit, C., Pileni, M. P. Journal of Applied Physics, 2003. **93**: p. 10001.
267. Brown, E.R., Joannopoulos, J. D., Fan, S., Villeneuve, P. R., McMahon, O. B., *Metallodielectric Photonic Crystal*, USPTO, Editor. 1996: USA.
268. Ward, A.J., Pendry, J. B., Stewart, W. J. Journal of Physics: Condensed Matter, 1995. **7**: p. 2217.
269. Lin, X.M., Sorensen, C. M., Klabunde, K. J. Chemistry of Materials, 1999. **11**: p. 198.
270. Wuelfing, W.P., Murray, R. W. Journal of Physical Chemistry, B, 2002. **106**: p. 3139.
271. Evans, S.D., Johnson, S. R., Cheng, Y. L., Shen, T. Journal of Materials Chemistry, 2000. **10**: p. 183.
272. Snow, A.W., Wohltjen, H. Chemistry of Materials, 1998. **10**: p. 947.
273. Bowden, N., Terfort, A., Carbeck, J., Whitesides, G. M. Science, 1997. **276**: p. 233.
274. Kiely, C.J., Fink, J., Brust, M., Bethell, D., Schiffrin, D. J. Nature, 1998. **396**: p. 444.
275. Lisiecki, I., Albouy, P. A., Pileni, M. P. Advanced Materials, 2003. **15**: p. 712.
276. Sun, S., Murray, C. B., Weller, D., Folks, L., Moser, A. Science, 2000. **287**: p. 1989.
277. Yang, H., Ogawa, T., Hasegawa, D., Takahashi, M. Journal of Applied Physics, 2008. **103**: p. 07D526.
278. Hermanson, K.D., Lumsdon, S. O., Williams, J. P., Kaler, E. W., Velev, O. D. Science, 2001. **294**: p. 1082.

279. Evoy, S., Dilello, N., Deshpande, V., Narayanan, A., Liu, H., Riegelman, M., Martin, B. R., Hailer, B., Bradley, J-C., Weiss, W., Mayer, T. S., Gogotsi, Y., Bau, H. H., Mallouk, T. E., Raman, S. Microelectronic Engineering, 2004. **75**: p. 31.

280. Papadakis, S.J., Gu, Z., Gracias, D. H. Applied Physics Letters, 2006. **88**: p. 233118.

281. Giersig, M., Mulvaney, P. Langmuir, 1993. **9**: p. 3408.

282. Ozturk, B., Blackledge, C., Flanders, B. N., Grischowsky, D. R. Applied Physics Letters, 2006. **88**: p. 073108.

283. Smith, P.A., Nordquist, C. D., Jackson, T. N., Mayer, T. S., Martin, B. R., Mbindyo, J., Mallouk, T. E. Applied Physics Letters, 2000. **77**: p. 1399.

284. Chen, M., Pica, T., Jiang, Y-B., Li, P., Yano, K., Liu, J. P., Datye, A. K., Fan, H. Journal of the American Chemical Society, 2007. **129**: p. 6348.

285. Tanase, M., Bauer, L. A., Hultgren, A., Silevitch, D. M., Sun, L., Reich, D. H., Searson, P. C., Meyer, G. J. Nano Letters, 2001. **1**: p. 155.

286. Gu, Z., Ye, H., Gracias, D. H. Transactions on Nanotechnology, 2006. **5**(1): p. 62.

287. Hangarter, C.M., Myung, M. V. Chemistry of Materials, 2005. **17**: p. 1320.

288. Kim, F., Kwan, S., Akana, J., Yang, P. Journal of the American Chemical Society, 2001. **123**: p. 4360.

289. Yang, P., Kim, F. ChemPhysChem, 2002. **3**: p. 503.

290. Chung, S.-W., Markovich, G., Heath, J. R. Journal of Physical Chemistry, B, 1999. **102**: p. 6685.

291. Cassagneau, T., Mallouk, T. E., Fendler, J. H. Journal of the American Chemical Society, 1998. **120**: p. 7848.

292. Paul, S., Pearson, C., Molloy, A., Cousins, M. A., Green, M., Kolliopoulou, S., Dimitrakis, P., Normand, P., Tsoukalas, D., Petty, M. C. Nano Letters, 2003. **3**(4): p. 533.

293. Yang, P. Nature, 2003. **425**: p. 243.

294. Whang, D., Jin, S., Wu, Y., Lieber, C. M. Nano Letters, 2003. **3**: p. 1255.

295. Silly, F., Gusev, A. O., Taleb, A., Pileni, M-P., Charra, F. Material Science and Engineering, C, 2002. **19**(1-2): p. 193.

296. Yang, G., Tan, L., Yang, Y., Chen, S., Liu, G-Y. Surface Science, 2005. **589**(1-3): p. 129.

297. Velev, O.D. Science, 2006. **312**(5772): p. 376.

298. Eldridge, M.D., Madden, P. A., Frenkel, D. Nature, 1993. **365**: p. 35.

299. Bartlett, P., Ottewill, R. H., Pusey, P. N. Physical Review Letters, 1992. **68**: p. 3801.

300. Shevchenko, E.V., Talapin, D. V., Kotov, N. A., O'Brien, S., Murray, C. B. Nature, 2006. **439**: p. 55.

301. Decher, G., Hong, J-D., Schmitt, J. Thin Solid Films, 1992. **210/211**: p. 831.

302. Schmitt, J., Decher, G., Dressick, W. J., Brandow, S. L., Geer, R. E., Shashidhar, R., Calvert, J. M. Advanced Materials, 197. **9**(1): p. 61.

303. Martin, B.R., Dermody, D. J., Reiss, B. D., Fang, M., Lyon, A. L., Natan, M. J., Mallouk, T. E. Advanced Materials, 1999. **11**(12): p. 1021.

304. Cozzoli, P.D., Pellegrino, T., Manna, L. Chemical Society Reviews, 2006. **35**: p. 1195.

305. Felton, E.J., Reich, D. H., *Biomedical Applications of Multifunctional Magnetic Nanowires*, in *Biomedical Applications of Nanotechnology*, V. Labhasetwar, Leslie-Pelecky, D. L., Editor. 2007, Wiley-Interscience.

306. Love, C.J., Urbach, A. R., Prentiss, M. G., Whitesides, G. M. Journal of the American Chemical Society, 2003. **125**: p. 12696.

307. Brousseau III, L.C., Novak, J. P., Marinakos, S. M., Feldheim, D. L. Advanced Materials, 1999. **11**: p. 447.

308. Thomas, K.G., Barazzouk, S., Ipe, B. I., Joseph, S. T. S., Kamat, P. V. Journal of Physical Chemistry, B, 2004. **108**: p. 13066.

309. Sato, T., Ahmed, H. Applied Physics Letters, 1997. **70**: p. 2759.

310. Brust, M., Bethell, D., Schiffrin, D. J., Kiely, C. J. Advanced Materials, 1995. **7**: p. 795.

311. Clark, T.D., Tien, J., Duffy, D. C., Paul, K. E., Whitesides, G. M. Journal of the American Chemical Society, 2001. **123**: p. 7677.
312. Syms, R.R.A., Yeatman, E. M., Bright, V. M., Whitesides, G. M. Journal of Microelectromechanical Systems, 2003. **12**(4): p. 387.
313. Li, M., Schnablegger, H., Mann, S. Nature, 1999. **402**: p. 393.
314. Mirkin, C.A. Inorganic Chemistry, 2000. **39**: p. 2258.
315. Mucic, R.C., Storhoff, J. L., Mirkin, C. A., Letsinger, R. L. Journal of the American Chemical Society, 1998. **120**: p. 12674.
316. Alivastos, A.P., Johnsson, K. P., Peng, X., Wilson, T. E., Loweth, C. J., Bruchez Jr, M. P., Schultz, P. G. Nature, 1996. **382**: p. 609.
317. Loweth, C.J., Caldwell, W. B., Peng, X., Alivastos, A. P., Schultz, P. G. Angewandte Chemie Internation Edition in English, 1999. **38**: p. 1808.
318. Shenton, W., Davis, S. A., Mann, S. Advanced Materials, 1999. **11**: p. 449.
319. Mattoussi, H., Mauro, M. J., Goldman, E. R., Anderson, G. P., Sundar, V. C., Mikulec, F. V., Bawendi, M. G. Journal of the American Chemical Society, 2000. **122**: p. 12142.
320. Caswell, K.K., Wilson, J. N., Bunz, U. H. F., Murphy, C. J. Journal of the American Chemical Society, 2003. **125**: p. 13914.
321. Li, M., Wong, K. K. W., Mann, S. Chemistry of Materials, 1999. **11**: p. 23.
322. Jacobs, H.O., Campbell, S. A., Steward, M. G. Advanced Materials, 2002. **14**: p. 1553.
323. Grzybowski, B.A., Winkleman, A., Wiles, J. A., Brumer, Y., Whitesides, G. M. Nature Materials, 2003. **2**: p. 241.
324. Martin, B.R., St Angelo, S. K., Mallouk, T. E. Advanced Functional Materials, 2002. **12**: p. 759.
325. Zhu, T., Fu, X. Y., Mu, T., Wang, J., Liu, Z. F. Langmuir, 1999. **15**: p. 5197.
326. Schmitt, J., Machtle, P., Eck, D., Mohwald, H., Helm, C. A. Langmuir, 1999. **15**: p. 3256.
327. Mayya, K.S., Sastry, M. Langmuir, 1999. **15**: p. 1902.

328. Henderson, J.L., Feng, S., Ferrence, G. M., Bein, T., Kubiak, C. P. Inorganica Chimica Acta, 1996. **242**: p. 115.

329. Antonietti, M., Goltner, C. Angewandte Chemie Internation Edition in English, 1997. **109**: p. 944.

330. Westcott, S.L., Oldenburg, S. J., Lee, T. R., Halas, N. J. Langmuir, 1998. **14**: p. 5396.

331. Mirkin, C.A., Letsinger, R. L., Mucic, R. C., Storkoff, J. J. Nature, 1996. **382**: p. 607.

332. Mbindyo, J.K.N., Reiss, B. D., Martin, B. R., Keating, C. D., Natan, M. J., Mallouk, T. E. Advanced Materials, 2001. **13**: p. 249.

333. Salem, A.K., Chao, J., Leong, K. W., Searson, P. C. Advanced Materials, 2004. **16**: p. 268.

334. Firestone, M.A., Williams, D. E., Seifert, S., Csencsits, R. Nano Letters, 2001. **1**(3): p. 129.

335. Marinakos, S.M., Brousseau III, L. C., Jones, A., Feldheim, D. C. Chemistry of Materials, 1998. **10**: p. 1214.

336. Hornyak, G.L., Kroll, M., Pugin, R., Sawitowski, T., Schmid, G., Bovin, J-O., Karrson, G., Hofmeister, H., Hopfe, S. Chemistry, A European Journal, 1997. **3**: p. 1951.

337. Messer, B., Song, J. H., Yang, P. Journal of the American Chemical Society, 2000. **122**: p. 10232.

338. Melosh, N.A., Boukai, A., Diana, F., Gerardot, B., Badolato, A.,Petroff, P. M., Heath, J. R. Science, 2003. **300**: p. 112.

339. Schnider, G., Krenn, J. R., Gotschy, W., Lamprecht, B., Ditlbacher, H., Leitner, A., Aussenegg, F. R. Journal of Applied Physics, 2001. **90**: p. 3825.

340. Dieluweit, S., Pum, D., Sleytr, U. B. Supramolecular Science, 1998. **5**: p. 15.

341. Shenton, W., Pum, D., Sleytr, U. B., Mann, S. Nature, 1998. **389**: p. 585.

342. Davis, S.A., Burkett, S. L., Mendelson, N. H., Mann, S. Nature, 1997. **385**: p. 420.

343. Beveridge, T.J. Current Opinion in Structural Biology, 1994. **4**: p. 202.

344. Walter, E.C., Zach, M. P., Favier, F., Murray, B. J., Inazu, K., Hemminger, J. C., Penner, R. M. ChemPhysChem, 2003. **4**(2): p. 131.
345. Hampden-Smith, P.W., Kodas, T. T. Chemical Vapor Deposition, 1995. **1**: p. 8.
346. Wu, P.W., Cheng, W., Martini, I. B., Dunn, B., Schwartz, B. J., Yablonovich, E. Advanced Materials, 2000. **12**: p. 1438.
347. Deng, T., Arias, F., Ismagilov, R. F., Kenis, P. J. A., Whitesides, G. M. Analytical Chemistry, 2000. **72**: p. 645.
348. Stellacci, F., Bauer, C. A., Meyer-Friedrichsen, T., Wenseleers, W., Alain, V., Kuebler, S. M., Pond, S. J. K., Zhang, Y., Marder, S. R., Perry, J. W. Advanced Materials, 2002. **14**: p. 194.
349. Gates, B.D., et al. Chemical Reviews, 2005. **105**: p. 1171.
350. Xia, Y., Whitesides, G. M. Annual Review of Materials Science, 1998. **28**: p. 153.
351. Whitesides, G.M., Love, J. C., *The Art of Building Small*, in *Scientific American*. 2001. p. 39.
352. Chou, S.Y., Krauss, P. R., Renstrom, P. J. Applied Physics Letters, 1995. **67**: p. 3114.
353. Knez, M., et al. Nano Letters, 2003. **3**(8): p. 1079.
354. Bockstaller, M.R., Kolb, R., Thomas, E. L. Advanced Materials, 2001. **13**(23): p. 1783.
355. Lodge, T.P. Macromolecular Chemistry and Physics, 2003. **204**: p. 265.
356. Hamley, I.W., *Developments in Block Copolymer Science and Technology*. 2004: John Wiley & Sons, Ltd.
357. Liebler, L. Macromolecules, 1980. **13**: p. 1602.
358. Wu, M.W., *Progress in block copolymer lithography*, in *Physics*. 2005, Princeton University.
359. Bates, F.S. Annual Review of Physical Chemistry, 1990. **41**: p. 525.
360. Shull, K.R., Mayes, A. M., Russell, T. P. Macromolecules, 1993. **26**: p. 3929.
361. Canevarolo, S.V., *Properties and Uses of Triblock Copolymers*, in *Handbook of Polymer Science and Technology: Performance*

Properties of Plastics and Elastomers, N.P. Cheremisinoff, Editor. 1989, Marcel Dekker Inc.: New York.

362. Shull, K.R. Macromolecules, 1992. **25**: p. 2122.
363. Vavasour, J.D., Mhitmore, M. D. Macromolecules, 1992. **25**: p. 5477.
364. Hashimoto, T., Shibayama, M., Kawai, H. Macromolecules, 1980. **13**: p. 1237.
365. Hashimoto, T., Shibayama, M., Kawai, H. Macromolecules, 1980. **13**: p. 1660.
366. Cavicchi, K.A., Lodge, T. P. Journal of Polymer Science, B: Polymer Physics, 2003. **41**: p. 715.
367. Ho, R.-M., Tseng, W-H., Fan, H-W., Chiang, Y-W., Lin, C-C., Ko, B-T., Huang, B-H. Polymer, 2005. **46**(22): p. 9362.
368. Cheng, J.Y., Ross, C. A., Thomas, E. L., Smith, H. I., Vancso, G. J. Applied Physics Letters, 2002. **81**(19): p. 3657.
369. Cheng, J.Y., Ross, C. A., Thomas, E. L., Smith, H. I., Vancso, G. J. Advanced Materials, 2003. **15**(19): p. 1599.
370. Weidisch, R., Michler, G. H., Arnold, M., Fischer, H. Journal of Material Science, 2000. **35**: p. 1257.
371. Kim, G., Libera, M. Macromolecules, 1998. **31**: p. 2569.
372. Fukunaga, K., Elbs, H., Magerle, R., Krausch, G. Macromolecules, 2000. **33**: p. 947.
373. Lin, Z., Kim, D. H., Wu, X., Boosahda, L., Stone, D., LaRose, L., Russell, T. P. Advanced Materials, 2002. **12**: p. 1373.
374. Hwang, J., Huh, J., Jung, B., Hong, J-M., Park, M., Park, C. Polymer, 2005. **46**: p. 9133.
375. Lazzari, M., Liu, G., Lecommandoux, S., *Block Copolymers in Nanoscience*. 2006, Weinhei: Wiley-VCH.
376. Bodycomb, J., Funaki, Y., Kimishima, K., Hashimoto, T. Macromolecules, 1999. **32**: p. 2075.
377. De Rosa, C., Park, C., Lodz, B., Wittmann, J-C., Fetters, L. J., Thomas, E. L. Macromolecules, 2000. **33**: p. 4871.
378. De Rosa, C., Park, C., Thomas, E. L., Lodz, B. Nature, 2000. **405**: p. 433.

379. Park, C., Cheng, J. Y., Fasolka, M. J., Mayes, A. M., Ross, C. A., Thomas, E. L., De Rosa, C. Applied Physics Letters, 2001. **79**: p. 848.
380. Park, C., De Rosa, C., Fetters, L. J., Lodz, C. B., Thomas, E. L. Advanced Materials, 2001. **13**: p. 724.
381. Park, C., De Rosa, C., Thomas, E. L. Macromolecules, 2001. **34**: p. 2602.
382. Morkved, T.L., Lu, M., Urbas, A. M., Ehrichs, E. E., Jaeger, H. M., Mansky, P., Russell, T. P. Science, 1996. **273**: p. 931.
383. Thurn-Albrecht, T., DeRouchey, J., Russell, T. P., Jaeger, H. M. Macromolecules, 2000. **33**: p. 3250.
384. Boker, A., Knoll, A., Elbs, H., Abetz, V., Muller, A. H. E., Krausch, G. Macromolecules, 2002. **35**: p. 1319.
385. Keller, A., Pedemonte, E., Wilmouth, F. M. Nature, 1970. **225**: p. 538.
386. Albalak, R.J., Thomas, E. L. Journal of Polymer Science, B: Polymer Physics, 1993. **31**: p. 37.
387. Maring, D., Wiesner, U. Macromolecules, 1997. **30**: p. 660.
388. Pinheiro, B.S., Winey, K. I. Macromolecules, 1998. **31**: p. 4447.
389. Pakula, T., Saijo, K., Kawai, H., Hashimoto, T. Macromolecules, 1985. **18**: p. 1294.
390. Ymaoka, I., Kimura, M. Polymer, 1993. **34**: p. 4399.
391. Kim, G., Libera, M. Macromolecules, 1998. **31**: p. 2569.
392. Kim, G., Libera, M. Macromolecules, 1998. **31**: p. 2670.
393. Hamley, I.W. Nanotechnology, 2003. **14**: p. R39.
394. Heier, J., Genzer, J., Kramer, E. J., Bates, F. S., Walheim, S., Krausch, G. Journal of Physical Chemistry, 1999. **111**: p. 11101.
395. Yang, X.M., Peters, R. D., Nealey, P. F., Solak, H. H., Cerrina, F. Macromolecules, 2000. **33**: p. 9575.
396. Rockford, L., Mochrie, S. G. J., Russell, T. P. Macromolecules, 2001. **34**: p. 1487.
397. Rockford, L., Yiu, Y., Mansky, P., Russel, T. P. Physical Review Letters, 1999. **82**: p. 2602.
398. Peters, R.D., Yang, X. M., Wang, Q., de Pablo, J. J., Nealey, P. F. Journal of Vacuum Science and Technology, B, 2000. **18**: p. 3530.

399. Kang, H., Detcheverry, F. A., Mangham, A. N., Stoykovich, M. P., Daoulas, K. Ch., Hamers, R. J., Muller, M., de Pablo, J. J., Nealey, P. F. Physical Review Letters, 2008. **100**: p. 148303.

400. Lin, Y., Boker, A., He, J., Sill, K., Xiang, H., Abetz, C., Li, X., Wang, J., Emrick, T., Long, S., Wang, Q., Balazs, A., Russell, T. P. Nature, 2005. **434**: p. 55.

401. Segalman, R., Yokohama, H., Kramer, E. J. Advanced Materials, 2001. **13**: p. 1152.

402. Xiao, S., Yang, X. M., Edwards, E. W., La, Y-H., Nealey, P. F. Nanotechnology, 2005. **16**(7): p. S324.

403. Lambooy, P., Russell, T. P., Kellogg, G. J., Mayes, A. M., Gallagher, P. D., Satija, S. K. Physical Review Letters, 1994. **72**: p. 2899.

404. Koneripalli, N., Singh, N., Levicky, R., Bates, F. S., Gallagher, P. D., Satija, S. K. Macromolecules, 1995. **28**: p. 2897.

405. Koneripalli, N., Levicky, R., Bates, F. S., Ankner, J., Kaiser, H., Satija, S. K. Langmuir, 1996. **12**: p. 6681.

406. Mansky, P., Liu, Y., Huang, E., Russell, T., Hawker, C. Science, 1997. **275**: p. 1458.

407. Huang, E., Russell, T., Harrison, C., Chaikin, P., Register, R., Hawker, C., Mays, J. Macromolecules, 1998. **31**: p. 7641.

408. Kellogg, G., Walton, D., Mayes, A., Lambooy, P., Russell, T., Gallagher, P., Satja, S. Physical Review Letters, 1996. **76**: p. 2503.

409. Huang, E., Pruzinsky, S., Russell, T. Macromolecules, 1999. **32**: p. 5299.

410. Fasolka, M.J., Mays, A. M. Annual Review of Materials Research, 2001. **31**: p. 323.

411. Krausch, G., Magerle, R. Advanced Materials, 2002. **14**: p. 1579.

412. Stein, G.E., Cochran, E., Fredrickson, G. E., Kramer, E. J., Li, X., Wang, J. in *American Physical Society*. 2006.

413. Pereira, G.G. Macromolecules, 2004. **37**: p. 1611.

414. Flory, P.J., *Principles of Polymer Chemistry*. 15th ed. 1992: Cornell University Press.

415. Painter, P.C., Coleman, M. M., *Fundamentals of Polymer Science: An Introductory Text*. 2nd ed. 1997: CRC Press.

416. Kamigaito, M., Ando, T., Sawamoto, M. Chemical Reviews, 2001. **101**: p. 3689.
417. Moad, G., Rizzardo, E., Thang, S. H. Australian Journal of Chemistry, 2005. **58**: p. 379.
418. Webster, O., Hertler, W. R., Sogah, D. Y., Farnham, W. B., Rajan-Babu, T. V. Journal of the American Chemical Society, 1983. **105**: p. 5706.
419. Grubbs, R.H., Tuman, W. Science, 1989. **243**: p. 907.
420. Schrock, R.R. Accounts of Chemical Research, 1990. **23**: p. 158.
421. Killian, C.M., Tempel, D. J., Johnson, L. K., Brookhart, M. K. Journal of the American Chemical Society, 1996. **118**: p. 11664.
422. Scollard, J.D., McConville, D. M. Journal of the American Chemical Society, 1996. **118**: p. 10008.
423. Baumann, R., Davis, W. M., Schrock, R. R. Journal of the American Chemical Society, 1997. **119**: p. 3830.
424. Matyjaszewski, K., Xia, J. Chemical Reviews, 2001. **101**: p. 2921.
425. Fischer, H. Journal of Polymer Science, A: Polymer Chemistry, 1999. **37**: p. 1885.
426. Wieland, P.C., Raether, B., Nuyken, O. Macromolecular Rapid Communications, 2001. **22**: p. 700.
427. Tsarevsky, N.V., Braunecker, W. A., Brooks, S. J., Matyjaszewski, K. Macromolecules, 2006. **39**: p. 6817.
428. Guerro-Sanchez, C., Abeln, C., Schubert, U. S. Journal of Polymer Science, A: Polymer Chemistry, 2005. **43**: p. 4151.
429. Jakubowski, W., Matyjaszewski, K. Macromolecules, 2005. **38**: p. 4139.
430. Min, K., Gao, H., Matyjaszewski, K. Journal of the American Chemical Society, 2005. **127**: p. 3825.
431. Jakubowski, W., Min, K., Matyjaszewski, K. Macromolecules, 2006. **39**: p. 39.
432. Braunecker, W.A., Matyjaszewski, K. Progress in Polymer Science, 2007. **32**: p. 93.
433. Pietrasik, J., Dong, H.,Matyjaszewski, K. Macromolecules, 2006. **39**: p. 6384.

434. Dong, H., Tang, W.,Matyjaszewski, K. Macromolecules, 2007. **40**: p. 2974.

435. Mueller, L., et al. Macromolecules, 2007. **40**: p. 6464.

436. Hawker, C.J., Bosman, A. W., Harth, E. Chemical Reviews, 2001. **101**: p. 3661.

437. Moad, G., Mayadunne, R. T. A., Rizzardo, E., Skidmore, M., Thang, S. H. Macromolecular Symposia, 2003. **192**: p. 1.

438. Billmeyer Jr, F.W., *Textbook of Polymer Science*. 2nd ed. 1971: John Wiley & Sons.

439. Appelt, B., Meyerhoff, G. Macromolecules, 1980. **13**: p. 657.

440. Yeh, S.-W., Wei, K-H. Macromolecules, 2005. **38**: p. 6559.

441. Choi, D.-G., Jeong, J-R., w, K-Y., Jung, H-T., Shin, S-C., Yang, S-M. Nanotechnology, 2004. **15**: p. 970.

442. Blondel, A., Meier, J. P., Doudin, B., Ansermet, J-P., Attenborough, K., Evans, P., hart, R., Nabiyouni, G., Schwarzacher, W. Journal of Magnetism and Magnetic Materials, 1995. **148**: p. 317.

443. Dubois, S., Michel, A., Eymery, J. P., Duvail, J. L., Piraux, L. Journal of Material Research, 1999. **14**: p. 665.

444. Bantu, A.K.M., Rivas, J., Zaragoza, G., Lopez-Quintela, M. A., Blanco, C. J. Non-Crystalline Solids, 2001. **287**: p. 5.

445. Molares, M.E.T., Buschmann, V., Dobrev, D., Neumann, R., Scholz, R., Schubert, I. U., Vetter, J. Advanced Materials, 2001. **13**: p. 62.

446. Bantu, A.K.M., Rivas, J., Zaragoza, G., Lopez-Quintela, M. A., Blanco, M. C. Journal of Applied Physics, 2001. **89**: p. 3393.

447. Rivas, J., Bantu, A. K. M., Zaragoza, G., Blanco, M. C., Lopez-Quintela, M. A. Journal of Magnetism and Magnetic Materials, 2002. **249**: p. 220.

448. Thurn-Albrecht, T., Schotter, J., Kastle, G. A., Emley, N., Shibauchi, T., Krusin-Elbaum, L., Guarini, K. W., Black, C. T., Tuominen, M. T., Russel, T. P. Science, 2000. **290**: p. 2126.

449. Bal, M., Ursache, A., Tuominen, M., Goldbach, J. T., Russell, T. P. Applied Physics Letters, 2002. **81**: p. 3479.

450. Brumlik, C.J., Menon, V. P., Martin, C. R. Journal of Material Research, 1994. **9**: p. 1174.

451. Demoustier-Champagne, S., Delvaux, M. Materials Science and Engineering, C, 2001. **15**: p. 269.
452. Martin, C.R., Nishizawa, M., Jirage, K., Kang, M. S., Lee, S. B. Advanced Materials, 2001. **13**: p. 1351.
453. Barbic, M., Mock, J. J., Smith, D. R., Schultz, S. Journal of Applied Physics, 2002. **91**: p. 9341.
454. Wirtz, M., parker, M., Kobayashi, Y., martin, C. R. Chemistry, A European Journal, 2002. **8**: p. 3573.
455. Hashimoto, T., Harada, M., Sakamoto, N. Macromolecules, 1999. **32**: p. 6867.
456. Abes, J.I., Cohen, R. E., Ross, C. A. Chemistry of Materials, 2003. **15**: p. 1125.
457. Chan, Y.N.C., Schrock, R. P., Cohen, R. E. Chemistry of Materials, 1992. **4**: p. 24.
458. Chan, Y.N.C., Crig, G. S. W., Schrock, R. P., Cohen, R. E. Chemistry of Materials, 1992. **4**: p. 885.
459. Sohn, B.H., Cohen, R. E. Journal of Applied Polymer Science, 1997. **65**: p. 723.
460. Horiuchi, S., Sarwar, M. I., Nakao, Y. Advanced Materials, 2000. **12**: p. 1507.
461. Lu, J., Yi, S. S., Kopley, T., Qian, C., Liu, J., Gulari, E. Journal of Physical Chemistry, B, 2006. **110**(13): p. 6655.
462. Spatz, J.P., Mossmer, S., hartmann, C., Moller, M., Herzog, T., Krieger, M., Boyen, H-G., Ziemann, P., Kabius, B. Langmuir, 2000. **16**: p. 407.
463. Boontongkong, Y., Cohen, R. E. Macromolecules, 2002. **35**: p. 3647.
464. Spatz, J.P., Herzog, T., Mobmer, S., Ziemann, P., Moller, M. Advanced Materials, 1999. **11**(2): p. 149.
465. Haupt, M., Miller, S., Glass, R., Arnold, M., Sauer, R., Thonke, K., Moller, M., Spatz, J. P. Advanced Materials, 2003. **15**(10): p. 829.
466. Forster, S., Antonietti, M. Advanced Materials, 1998. **10**: p. 195.
467. Morkved, T.L., Wiltzius, P., Jaeger, H. M., Grier, D. G., Witten, T. A. Applied Physics Letters, 1994. **64**: p. 422.
468. Lopes, W.A., Jaeger, H. M. Nature, 2001. **414**: p. 735.

469. Lopes, W.A. Physical Review, E, 2002. **65**: p. 031606.
470. Hamdoun, B., Ausserre, D., Gabuil, V., Gallot, Y., Clinard, C., Joly, S. Journal de Physique II, 1996. **4**: p. 493.
471. Huh, J., Ginzburg, V. V., Balazs, A. C. Macromolecules, 2000. **33**: p. 8085.
472. Thompson, R.B., Ginzburg, V. V., Matsen, M. W., Balazs, A. C. Macromolecules, 2002. **35**: p. 1060.
473. Huang, C.-I., Lodge, T. P. Macromolecules, 1998. **31**: p. 3556.
474. Lee, J.Y., Thompson, R. B., Jasnow, D., Balazs, A. C. Macromolecules, 2002. **35**: p. 4855.
475. Thompson, R.B., Ginzburg, V. V., Matsen, M. W., Balazs, A. C. Science, 2001. **292**: p. 2469.
476. Ginzburg, V.V., Gibbons, C., Qiu, F., Peng, G., Balazs, A. C. Macromolecules, 2000. **33**: p. 6140.
477. Lee, J.Y., Shou, Z., Balazs, A. C. Physical Review Letters, 2003. **91**: p. 136103.
478. Sevink, G.J.A., Zvelindovsky, A. V., van Vlimmeren, B. A. C., Maurits, N. M., Fraaije, J. G. E. M. Journal of Chemical Physics, 1999. **110**: p. 2250.
479. Sides, S.W., Kim, B. J., Kramer, E. J., Fredrickson, G. H. Physical Review Letters, 2006. **96**: p. 250601.
480. Sohn, B.H., Choi, J. M., Yoo, S., Yun, S. H., Zin, W. C., Jung, J. C., Kanehara, M., Hirata, T., Teranishi, T. Journal of the American Chemical Society, 2003. **125**(21): p. 6368.
481. Zehner, R.W., Lopes, W. A., Morkved, T. L., Jaeger, H., Sita, L. R. Langmuir, 1998. **14**: p. 241.
482. Ribbe, A.E., Okumura, A., Matsushige, K., Hashimoto, T. Macromolecules, 2001. **34**: p. 8239.
483. Kim, B.J., Chiu, J. J., Yi, G-R., Pine, D. J., Kramer, E. J. Advanced Materials, 2005. **17**: p. 2618.
484. Listak, J., Bockstaller, M. R. Macromolecules, 2006. **39**: p. 5820.
485. Bockstaller, M.R., Lapetnikov, Y., Margel, S., Thomas, E. L. Journal of the American Chemical Society, 2003. **125**: p. 5276.

486. Chiu, J.J., Kim, B. J., Yi, G-R., Bang, J., Kramer, E. J., Pine, D. J. Macromolecules, 2007. **40**: p. 3361.

487. Tsutsumi, K., Funaki, Y., Hirokawa, Y., Hashimoto, T. Langmuir, 1999. **15**: p. 5200.

488. Kim, B.J., Bang, J., Hawker, C. J., Kramer, E. J. Macromolecules, 2006. **39**: p. 4108.

489. Deshmukh, R.D., Liu, Y., Composto, R. J. Nano Letters, 2007. **7**(12): p. 3662.

490. Krishnamoorti, R., Silva, A. S., Mitchell, C. A. Journal of Chemical Physics, 2001. **115**: p. 7175.

491. Silva, S., Mitchell, C. A., Tse, M. F., Wang, H-C., Krishnamoorti, R. Journal of Chemical Physics, 2001. **115**: p. 7166.

492. Warren, S.C., Messina, L. C., Slaughter, L. S., Kamperman, M., Zhou, Q., Gruner, S. M., DiSalvo, F. J., Weisner, U. Science, 2008. **320**(5884): p. 1748.

493. Lin, B.H., Morkved, T. L., Meron, M., Huang, Z. Q., Viccaro, P. J., Jaeger, H. M., Williams, S. M., Schlossman, M. L. Journal of Applied Physics, 1999. **85**: p. 3180.

494. Niu, S., Saraf, R. F. Nanotechnology, 2007. **18**: p. 125607.

495. Saito, R., Okamura, S., Ishizu, K. Polymer, 1992. **33**: p. 1099.

496. Hurst, S.J., Payne, E. K., Qin, L., Mirkin, C. A. Angewandte Chemie Internation Edition in English, 2006. **45**: p. 2672.

497. Possin, G.R. Review of Scientific Instruments, 1970. **41**: p. 772.

498. Williams, W.D., Giordano, N. Review of Scientific Instruments, 1984. **55**: p. 410.

499. Madsen, J.T., Giordano, N. Physical Review, B, 1985. **31**: p. 6395.

500. Penner, R.M., Martin, C. M. Analytical Chemistry, 1987. **59**: p. 2625.

501. Martin, C.R. Advanced Materials, 1991. **3**: p. 457.

502. Preston, C.K., Moskovits, M. J. Journal of Physical Chemistry, 1993. **97**: p. 8495.

503. Al-Malawi, D., Liu, C. Z., Moskovits, M. J. Journal of Material Research, 1994. **9**: p. 1014.

504. Yahalom, J., Zadok, O. Journal of Materials Science, 1987. **22**: p. 1573.

505. Dubois, S., Marchal, C., Beuken, J. M., Piraux, L., Duvail, J. L., Fert, A., George, J. M., Maurice, J. L. Applied Physics Letters, 1997. **70**: p. 396.
506. Chen, M., Searson, P. C., Chien, C. L. Journal of Applied Physics, 2003. **93**: p. 8253.
507. Liu, K., Nagodawithana, K., Searson, P. C., Chien, C. L. Physical Review, B, 1995. **51**: p. 7381.
508. Evans, P.R., Yi, G., Schwarzacher, W. Applied Physics Letters, 2000. **76**: p. 481.
509. Choi, J.-R., Oh, S. J., Ju, H., Cheon, J. Nano Letters, 2005. **5**: p. 2197.
510. Bicelli, L.P., Bozzini, B., Mele, C., D'Urzo, L. International Journal of Electrochemical Science, 2008. **356**: p. 408.
511. Pena, D., Razavi, B., Smith, P. A., Mbindyo, J. K. M., Natan, M. J., Mayer, T. S., Mallouk, T. E., Keating, C. D. Materials Research Society Symposium Proceedings., 2001. **636**: p. D4.6.1.
512. Kovtyukhova, N.I., Mallouk, T. E. Chemistry, A European Journal, 2002. **8**: p. 4354.
513. Brumlik, C.J., Martin, C. R., Tokuda, K. Analytical Chemistry, 1992. **64**: p. 1201.
514. Foss, C.A., Hornyak, G. L., Stockert, J. A., Martin, C. R. Journal of Physical Chemistry, 1992. **96**: p. 7497.
515. Brumlik, C.J., Martin, C. R. Journal of the American Chemical Society, 1991. **113**: p. 3174.
516. Cepak, V.M., martin, C. R. Journal of Physical Chemistry, B, 1998. **102**: p. 9985.
517. Guo, Y.-G., Wan, L-J., Gong, J-R., Bai, C-L. Physical Chemistry Chemical Physics, 2002. **4**: p. 3422.
518. de Menten de Horne, F., Piraux, L., Michotte, S. Applied Physics Letters, 2005. **86**: p. 152510.
519. Gao, T., Meng, G., Zhang, J., Sun, S., Zhang, L. Applied Physics, A: Materials Science Proceedings, 2002. **74**(3): p. 403.
520. Chakarvarti, S.K., Vetter, J. J. Micromechanics and Microengineering, 1993. **3**: p. 57.

521. Whitney, T.M., Jiang, J. S., Searson, P. C., Chien, C. L. Science, 1993. **261**: p. 1316.
522. Xue, D.S., Shi, H. G., Si, M. S. Journal of Physics: Condensed Matter, 2003. **16**: p. 8775.
523. Searson, P.C., Cammarata, R. C., Chien, C. L. Journal of Electronic Materials, 1995. **24**(8): p. 955.
524. Su, Y.-K., Qin, D-H., Zhang, H-L., Li, H., Li, H-L. Chemical Physics Letters, 2004. **388**: p. 406.
525. Schwanbeck, H., Schmidt, U. Electrochimica Acta, 2000. **45**: p. 4389.
526. Li, Y., Meng, G. W., Zhang, L. D. Applied Physics Letters, 2000. **76**: p. 2011.
527. Wang, J.-G., Tian, M-L., Kumar, N., Mallouk, T. E. Nano Letters, 2005. **5**: p. 1247.
528. Routkevitch, D., Bigioni, T., Moskovits, M., Xu, J. M. Journal of Physical Chemistry, 1996. **100**: p. 14037.
529. Zheng, M.J., Zhang, L. D., Li, G. H., Shen, W. Z. Chemical Physics Letters, 2002. **363**: p. 123.
530. Wang, Q., Wang, G., Xu, B., Jie, J., Han, X., Li, G., Li, Q., Hou, J. G. Material Letters, 2005. **59**: p. 1378.
531. Xu, D.S., Xu, Y. J., Chen, D. P., Guo, G. L., Gui, L. L., Tang, Y. Q. Chemical Physics Letters, 2000. **325**: p. 340.
532. Kressin, A.M., Doan, V. V., Klein, J. D., Sailor, M. J. Chemistry of Materials, 1991. **3**: p. 1015.
533. Klein, J.D., Herrick II, R. D., Palmer, D., Sailor, M. J., Brumlik, C. J., Martin, C. R. Chemistry of Materials, 1993. **5**: p. 902.
534. Zheng, M., Zhang, L., Zhang, X., Zhang, J., Li, G. Chemical Physics Letters, 2001. **334**: p. 298.
535. Hoyer, P. Langmuir, 1996. **12**: p. 1411.
536. Cai, Z., Lei, J., Liang, W., Menon, V., Martin, C. R. Chemistry of Materials, 1991. **3**: p. 960.
537. Sapp, S.A., Mitchell, D. T., martin, C. R. Chemistry of Materials, 1999. **11**: p. 1183.
538. VanDyke, L.S., martin, C. R. Langmuir, 1990. **6**: p. 1118.

539. Martin, C.R., Parthasarathy, R., Menon, V. Synthetic Metals, 1993. **55-57**: p. 1165.
540. Burford, R.P., Tongtam, T. Journal of Material Science, 1991. **26**(12): p. 3264.
541. Wu, C.-G., Bein, T. Science, 1994. **264**: p. 1757.
542. Beck, J.S., Vartuli, J. C., Roth, W. J., Leonowicz, M. E., Kresge, C. T., Schmitt, K. D., Chu, C. T. W., Olson, D. H., Sheppard, E. W., McCullen, S. B., Higgins, J. B., Schlenker, J. L. Journal of the American Chemical Society, 1992. **114**: p. 10834.
543. Yang, C.-M., Sheu, H-S., Chao, K. J. Advanced Functional Materials, 2002. **12**: p. 143.
544. Lee, K.-B., Lee, S-M., Cheon, J. Advanced Materials, 2001. **13**: p. 517.
545. Hong, B.H., Bae, S. C., Lee, C., Jeong, S., Kim, K. S. Science, 2001. **294**: p. 348.
546. Huang, M.H., Choudrey, A., Yang, P. Chemical Communications, 2000: p. 1063.
547. Han, Y.-J., Kim, J. M., Stucky, G. D. Chemistry of Materials, 2000. **12**: p. 2068.
548. Battacharyya, S., Saha, S. K., Chakravorty, D. Applied Physics Letters, 2000. **77**: p. 3770.
549. kang, H., Jun, Y-W., Park, J-I., Lee, K. B., Cheon, J. Chemistry of Materials, 2000. **12**: p. 3530.
550. Thurn-Albrecht, T., Steiner, R., DeRouchey, J., Stafford, C. M., Huang, E., Bal, M., Tuominen, M., Hawker, C. J., Russel, T. P. Advanced Materials, 2000. **12**: p. 787.
551. Despic, A., Parkhutik, V. P., in *Modern Aspects of Electrochemistry*, J.O. Bockris, White, R. E., Conway, B. E., Editor. 1989, Plenum Press: New York.
552. Davis, D.M., *Electrodeposition of Magnetic Nanowires and Nanotubes*, in *Chemistry*. 2005, Texas Tech University.
553. Lu, Q., Feng, G., Komarneni, S., Mallouk, T. E. Journal of the American Chemical Society, 2004. **126**: p. 8650.

554. Wu, Y., Cheng, G., Katsov, K., Sides, S. W., Wang, J., Tiang, J., Fredrickson, G. H., Moskovits, M., Stucky, G. D. Nature Materials, 2004. **3**: p. 816.
555. Wu, Y., Livneh, T., Zhang, Y. X., Cheng, G., Wang, J., Tang, J., Moskovits, M., Stucky, G. D. Nano Letters, 2004. **4**: p. 2337.
556. Masuda, H., Fukuda, K. Science, 1995. **268**: p. 1466.
557. Wade, T.L., Wegrowe, J-E. European Journal of Applied Physics, 2005. **8**: p. 3.
558. Fleicher, R.L., Price, P. B., Walker, R. M., *Nuclear Tracks in Solids*. 1975, Berkley: University of California Press.
559. Schwartz, M., *Deposition from Aqueous Solutions: An Overview*, in *Handbook of Deposition Technologies for Films and Coatings*, R.F. Bunshah, Editor. 1994, William Andrew.
560. Brett, C.M.A., Brett, A. M. O., *Electrochemistry: Principles, Methods and Applications*. 1993, New York: Oxford Science Publications.
561. Szymczyk, A., Labbez, C., Fievet, P., Vidonne, A., Foissy, A., Pagetti, J. Advances in Colloid and Interface Science, 2003. **103**: p. 77.
562. Kastening, B., Heins, M. Electrochimica Acta, 2005. **50**(12): p. 2487.
563. Bath, B.D., White, H. S., Scott, E. R. Analytical Chemistry, 2000. **72**: p. 433.
564. Kuo, T.-C., Sloan, L. A., Sweedler, J. V., Bohn, P. W. Langmuir, 2001. **17**: p. 6298.
565. Faibish, R.S., Elimelech, M., Cohen, Y. Journal of Colloid and Interface Science, 1998. **204**: p. 77.
566. Bluhm, E.A., Bauer, E., Chamberlin, R. M., Abney, K. D., Young, J. S., Jarvinen, G. D. Langmuir, 1999. **15**: p. 8668.
567. Bauer, L.A., Reich, D. H., Meyer, G. J. Langmuir, 2003. **19**: p. 7043.
568. Birenbaum, N.S., Lai, B. T., Chen, C. S., Reich, D. H., Meyer, G. J. Langmuir, 2003. **19**: p. 9580.
569. Salem, A.K., Chen, M., Hayden, J., Leong, K. W., Searson, P. C. Nano Letters, 2004. **4**: p. 1163.
570. Chen, M., Guo, L., Ravi, R., Searson, P. C. Journal of Physical Chemistry, B, 2006. **110**: p. 211.
571. Chen, M., Searson, P. C. Advanced Materials, 2005. **17**: p. 2765.

572. Lee, K.-B., Park, S., Mirkin, C. A. Angewandte Chemie Internation Edition in English, 2004. **43**: p. 3048.